1982

Remote sensing of land resources: application of LANDSAT satellite imagery

Jahanshir Golchin
Iowa State University

INFORMATION TO USERS

This was produced from a copy of a document sent to us for microfilming. While the most advanced technological means to photograph and reproduce this document have been used, the quality is heavily dependent upon the quality of the material submitted.

The following explanation of techniques is provided to help you understand markings or notations which may appear on this reproduction.

1. The sign or "target" for pages apparently lacking from the document photographed is "Missing Page(s)". If it was possible to obtain the missing page(s) or section, they are spliced into the film along with adjacent pages. This may have necessitated cutting through an image and duplicating adjacent pages to assure you of complete continuity.

2. When an image on the film is obliterated with a round black mark it is an indication that the film inspector noticed either blurred copy because of movement during exposure, or duplicate copy. Unless we meant to delete copyrighted materials that should not have been filmed, you will find a good image of the page in the adjacent frame. If copyrighted materials were deleted you will find a target note listing the pages in the adjacent frame.

3. When a map, drawing or chart, etc., is part of the material being photographed the photographer has followed a definite method in "sectioning" the material. It is customary to begin filming at the upper left hand corner of a large sheet and to continue from left to right in equal sections with small overlaps. If necessary, sectioning is continued again—beginning below the first row and continuing on until complete.

4. For any illustrations that cannot be reproduced satisfactorily by xerography, photographic prints can be purchased at additional cost and tipped into your xerographic copy. Requests can be made to our Dissertations Customer Services Department.

5. Some pages in any document may have indistinct print. In all cases we have filmed the best available copy.

University
Microfilms
International

300 N. ZEEB RD., ANN ARBOR, MI 48106

Golchin, Jahanshir

REMOTE SENSING OF LAND RESOURCES: APPLICATION OF LANDSAT SATELLITE IMAGERY

Iowa State University PH.D. 1982

PLEASE NOTE:

In all cases this material has been filmed in the best possible way from the available copy. Problems encountered with this document have been identified here with a check mark ✓.

1. Glossy photographs or pages ✓
2. Colored illustrations, paper or print ✓
3. Photographs with dark background ✓
4. Illustrations are poor copy _____
5. Pages with black marks, not original copy _____
6. Print shows through as there is text on both sides of page _____
7. Indistinct, broken or small print on several pages _____
8. Print exceeds margin requirements _____
9. Tightly bound copy with print lost in spine _____
10. Computer printout pages with indistinct print _____
11. Page(s) _____ lacking when material received, and not available from school or author.
12. Page(s) _____ seem to be missing in numbering only as text follows.
13. Two pages numbered _____. Text follows.
14. Curling and wrinkled pages _____
15. Other _____

Remote sensing of land resources:

Application of LANDSAT satellite imagery

by

Jahanshir Golchin

A Dissertation Submitted to the

Graduate Faculty in Partial Fulfillment of the

Requirements for the Degree of

DOCTOR OF PHILOSOPHY

Department: Civil Engineering
Major: Water Resources

Approved:

Signature was redacted for privacy.

In Charge of Major Work

Signature was redacted for privacy.

For the Major Department

Signature was redacted for privacy.

For the Graduate College

Iowa State University
Ames, Iowa

1982

TABLE OF CONTENTS

INTRODUCTION

Remote sensing is a tool which can be used to solve some of the problems facing man and his environment. Since early in the 1960s, when the term "remote sensing" appeared in scientific literature, it has advanced so much that it can be applied to almost any area of terrestrial science. It has been a useful tool in agriculture, water resources, forestry, land management, urban planning, geology, social and economical development, military planning and many other areas.

The aim of this study is to demonstrate the advantages of using remote sensing in monitoring changes in farmland use and, where possible, to determine whether those lands are under irrigation. Irrigation, because of both the large volumes of water withdrawn and consumed, is a water use category of key interest to the Iowa Natural Resources Council (INRC). Collecting accurate, up-to-date information of irrigated land in Iowa has been challenging due to the absence of legal authority to collect this information. The methods introduced here are the least complex and have minimum requirements for material and equipment, so they can be easily applied whenever needed. Small environmental organizations and local agencies, with limited budgets and legal power, have potential uses of such information obtained by remote sensing that would otherwise be hard and costly for them to obtain.

The tools of remote sensing used in this research were basically LANDSAT satellite black and white (single band) and false color composite images as well as low altitude color near-infrared oblique pictures taken from a low level airplane. This thesis is composed of two parts. The

first part is a review and discussion of the principles of remote sensing by satellite. This part includes discussions of the following subjects:

physical processes in remote sensing;

fundamentals of image interpretation;

system and operation of LANDSAT satellites; and

water resources application.

The second part is devoted to the study of three interrelated subjects in west-central Iowa. These are monitoring changes in:

soil moisture;

irrigated lands; and

crop types.

In this study, sophisticated techniques of data processing were avoided where possible. The intention is to determine if remote sensing procedures can be made useful to all people concerned with the subject of natural resource preservation.

FUNDAMENTALS OF SATELLITE REMOTE SENSING

Theory of Physical Processes in Remote Sensing

Radiation physics

A review of the physics of light is fundamental to develop a basis for understanding the processes in remote sensing. Electromagnetic theory provides much of the information used in this field. All objects having a temperature greater than absolute zero (zero degrees Kelvin or -273°C) emit electromagnetic radiation. The temperature of a matter is a determining factor in the amount of radiation energy emitted by that matter. For a given temperature, the maximum amount of this emitted energy is called blackbody radiation. A blackbody, in other words, can be defined as a body (matter) that emits the maximum possible rate of energy at a given temperature for every wavelength. The ratio of the actual energy radiated from a matter to that for a blackbody under the same condition is called emissivity. The Stefan-Boltzmann radiation law can be used to compute the amount of energy emitted by a blackbody:

$$W = \sigma T^4 \tag{1}$$

where

W = total radiant emittance, Watts/m^2;

σ = Stefan-Boltzmann constant, 0.2897 cm°K; and

T = absolute temperature, °K.

Electromagnetic energy is propagated as waves. The wavelength of electromagnetic radiation is given by the basic relation:

$$\lambda = \frac{c}{f} \tag{2}$$

where

λ = wavelength, m;

c = speed of light, 3×10^8 m/sec; and

f = frequency, numbers of wavelengths, cycles/sec.

The wavelength of maximum emittance (blackbody) for a specified temperature is given by Wien's displacement law:

$$\lambda m = \frac{0.2897}{T} \qquad (3)$$

where

λm = wavelength of maximum emittance, cm; and

T = absolute temperature, ^{o}K.

This equation explains mathematically that the wavelength of maximum emittance is inversely related to the temperature of the object. The sun's surface temperature is estimated to be 6000 ^{o}K, so that solar energy is most intense at a wavelength of about 0.5 micrometer. The wavelength of maximum spectral emittance of all terrestrial matter is commonly between 10 and 12 micrometers, which is in the thermal infrared range. These points will be discussed later in more detail.

The range of electromagnetic frequencies is called electromagnetic spectrum. It is the order of the radiation according to frequency, wavelength or energy. The wavelength range starts with the gamma rays ($3x10^{-6}$ to $3x10^{-5}$ micrometers) and continues to the very large wavelengths of radio or very-low-frequency (VLF) waves ($8x10^{5}$ to $3x10^{12}$ micrometers) (Figure 1). As it appears in the spectrum, the smaller wavelengths have larger frequencies and vice versa (Equation 2).

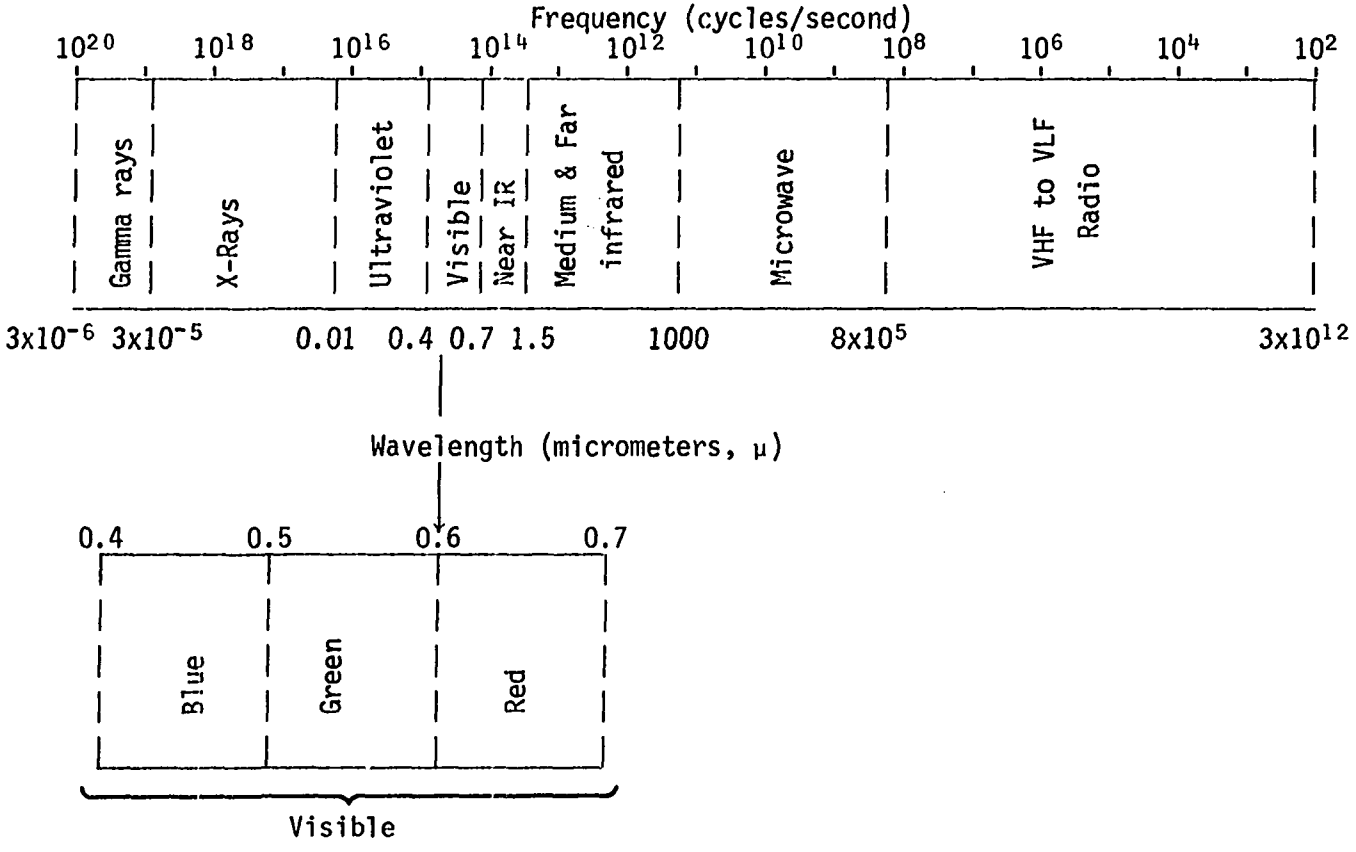

Figure 1. Spectrum of electromagnetic energy on logarithmic scale

The larger the frequency (shorter wavelength), the greater the energy of radiation. This is shown through the particle concept of electromagnetic radiation introduced by Plank. Magnetic radiation consists of a stream of flow of particles or quanta, where each quanta has an energy content, E, given by:

$$E = hf \tag{4}$$

where

E = quantum energy, erg;

h = Plank's constant, 6.625×10^{-27} erg. sec; and

f = frequency, sec^{-1}.

Objects and light energy The absorptivity of a matter is defined as the ratio of the amount of radiant energy absorbed to the total amount incident upon that matter. An object that absorbs a large amount of radiation energy also emits a large amount of energy. This can be shown by an equality relation:

$$\alpha = \varepsilon$$

where α represents the absorptivity and ε the emissivity of the matter. For a blackbody, then, $\alpha = \varepsilon = 1$ and, for a whitebody, $\alpha = \varepsilon = 0$. Note that α and ε are unitless parameters and in nature range between less than 1 and 0.

Another important light characteristic is reflectivity. Reflectivity is the ratio of radiant energy reflected, E_r, to the total that incident upon the surface, E_i:

$$r = \frac{E_r}{E_i} \tag{5}$$

where

r = reflection coefficient.

A blackbody absorbs and emits all the radiation incident on it. Thus, it reflects no energy. In contrast, snow, which is a poor absorber of visible part of spectrum, also is a poor emitter of energy in this range, but is a good reflector of the visible light.

Natural bodies are not perfect absorbers or emitters. Earth, in general, is considered as a "gray body," but in certain wavelength bands, such as 8 to 14 micrometers, it behaves as a "black body." Examples of this are wet soil and vegetation which have emissivities of 0.97 to 0.99. Kirchoff's law states that the absorptivity of an object for radiation of a specific wavelength is equal to its emissivity for the same wavelength, or:

$$\alpha(\lambda) = \varepsilon(\lambda).$$

Whatever energy, if any, that is not absorbed or reflected will be transmitted through the body of the matter (medium). Transmissivity is the ratio of transmitted radiation, E_t, to the total radiation incident upon the matter, E_i:

$$t = \frac{E_t}{E_i} \tag{6}$$

where

t = transmission coefficient.

The sum of absorptivity (or emissivity), reflectivity, and transmissivity for a specific wavelength λ must be equal to unity, but each one is less than unity:

$$\alpha(\lambda) + r(\lambda) + t(\lambda) = 1.$$

Introducing Plank's expression (Equation 4) for the energy radiated (or emitted) per unit wavelength per unit area of a blackbody, W_λ, the spectral distribution of energy radiated (or emitted) by that blackbody at various temperatures can be constructed (Figure 2):

$$W_\lambda = \frac{2\pi hc^2}{\lambda^5}\left(\frac{1}{e^{hc/\lambda KT}-1}\right) \tag{7}$$

where

W_λ = radiated energy for a wavelength: Watts/m^2/Angstrum;

π = 3.14;

h = 6.625 x 10^{-34} Jule-Sec (Plank's constant);

c = speed of light, 3 x 10^8 m/sec;

λ = wavelength, m;

e = natural logarithm base, 2.71828;

K = Boltzmann's constant, 1.38 x 10^{-23} Jule/degree; and

T = absolute temperature, $^\circ$K.

From Wien's displacement law (Equation 3) the wavelength of maximum emission, λ_{max}, can be calculated. For example, the sun may be considered as a blackbody with surface temperature of about 6000°K, and from Wien's equation, the wavelength of maximum emission (peak of the 6000°K curve in Figure 2) is:

$$\lambda_{max}(\text{sun}) = \frac{0.2898\ \text{cm}^\circ\text{K}}{6000^\circ\text{K}} = 4.83 \times 10^{-5}_{\text{cm}} = 0.483 \text{ micrometers.}$$

For the earth, which is a near blackbody with a mean surface temperature

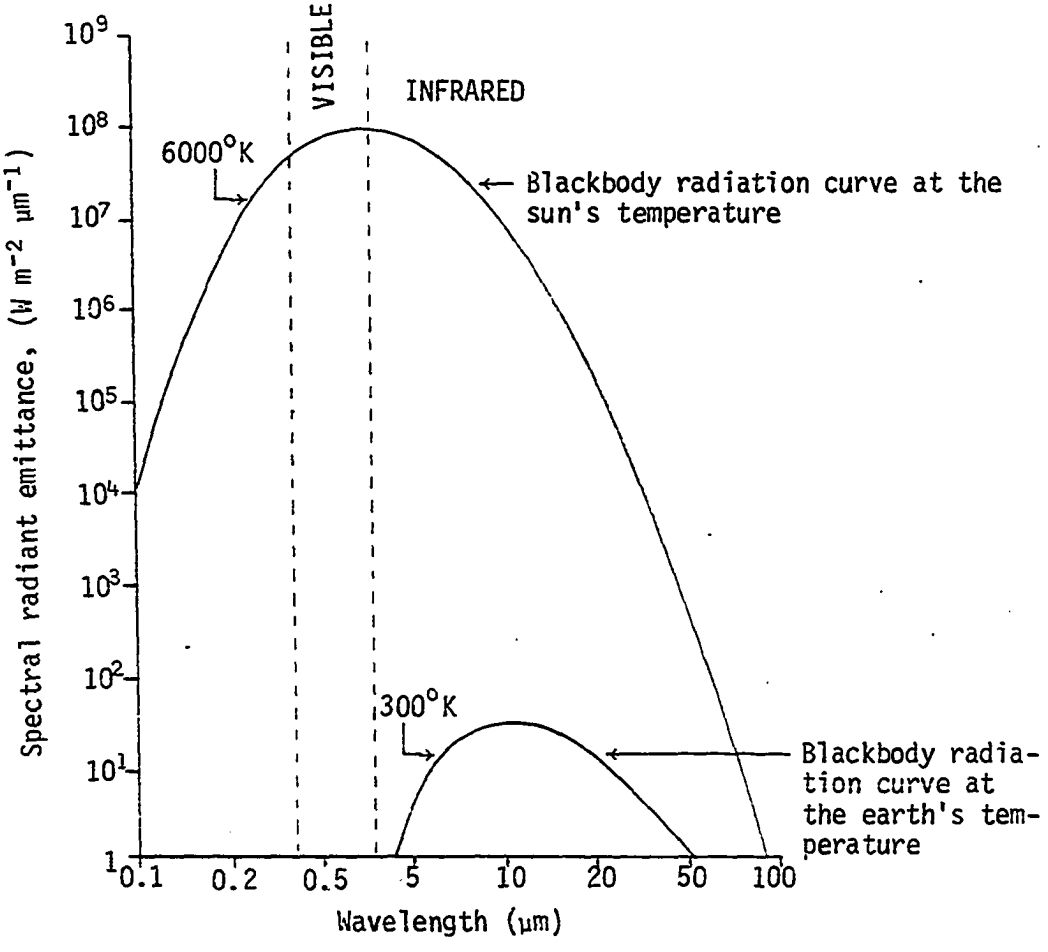

Figure 2. Energy distribution of a blackbody at the sun's and earth's temperature in different wavelength (Lapp and Andrews, 1954)

of about 300°K, this maximum emission wavelength is:

$$\lambda_{max}(\text{earth}) = \frac{0.2898\ \text{cm}^{\circ}\text{K}}{300^{\circ}\text{K}} = 9.66 \times 10^{-4}\text{cm} = 9.66\ \text{micrometers},$$

which is the peak of 300°K curve in Figure 2.

The theoretical and actual spectra of solar radiation at the top of the atmosphere and the actual spectrum at earth's surface are shown in Figure 3(A). The earth's radiation is shown in Figure 3(B). As is evident in these figures, the solar and the earth's spectra do not overlap. The range of solar radiation is between 0.14 and 4.0 micrometers and the range of earth's spectrum is between 3 and 80 micrometers. Thus, while the solar spectrum covers mostly visible and near infrared part of light spectrum, the earth's spectrum ranges mostly in medium and far infrared. This explains why thermal infrared photography at night is useful in determining heat losses and other factors.

Atmospheric effects on radiation Due to existance of gases and aerosol particles in the air surrounding the earth, not all, but only a few, parts of electromagnetic spectrum can be used in remote sensing. Part of the energy emanating from terrestrial sources is absorbed by certain atmospheric constraints, notably water vapor (H_2O) and carbon dioxide (CO_2). Portions of the spectrum that are transparent to terrestrial back radiation and can be used in remote sensing are called "windows" (see Figure 3B).

As stated before, the earth is the main source of radiant energy of higher wavelengths. These higher wavelengths, 3 micrometers and greater, are the energy source for infrared photography. In this higher range, the

Figure 3. A. Spectral energy of sun before and after passing through the atmosphere. Atmospheric absorption by different gases and vapors is shown (Valley, 1965)

Figure 3. B. Earth's radiation energy measured from a satellite. Smooth curves represent blackbody radiation at different earth temperatures (Kunde et al., 1974)

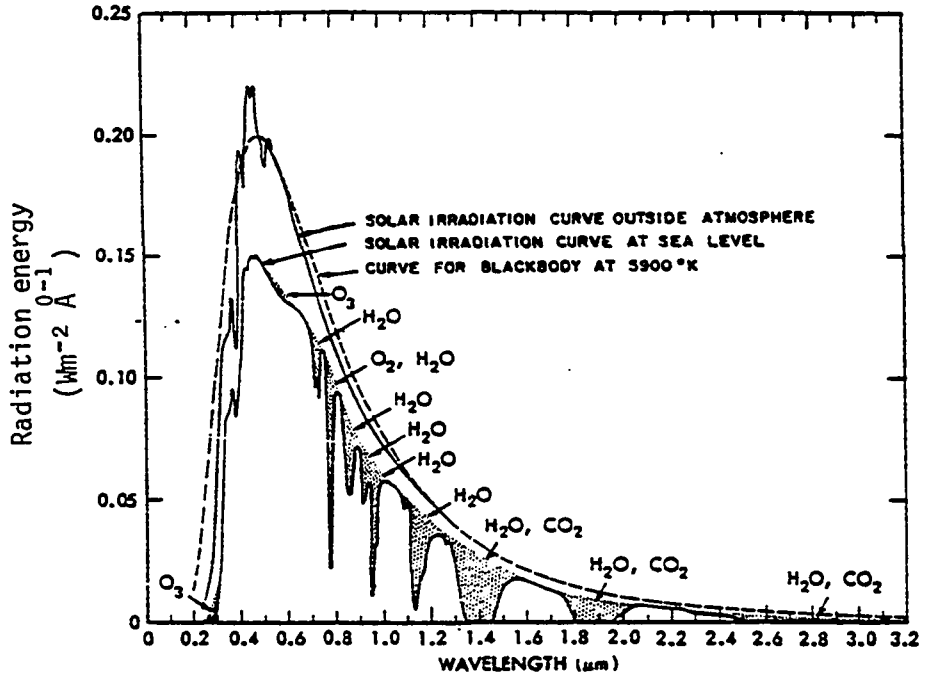
Radiation energy
(Wm⁻² Δ⁻¹)
SOLAR IRRADIATION CURVE OUTSIDE ATMOSPHERE
SOLAR IRRADIATION CURVE AT SEA LEVEL
CURVE FOR BLACKBODY AT 5900 °K
O3
H2O
O2, H2O
H2O
H2O
H2O
H2O
H2O, CO2
H2O, CO2
H2O, CO2
O3
0.25
0.20
0.15
0.10
0.05
0
0 0.2 0.4 0.6 0.8 1.0 1.2 1.4 1.6 1.8 2.0 2.2 2.4 2.6 2.8 3.0 3.2
WAVELENGTH (μm)

A

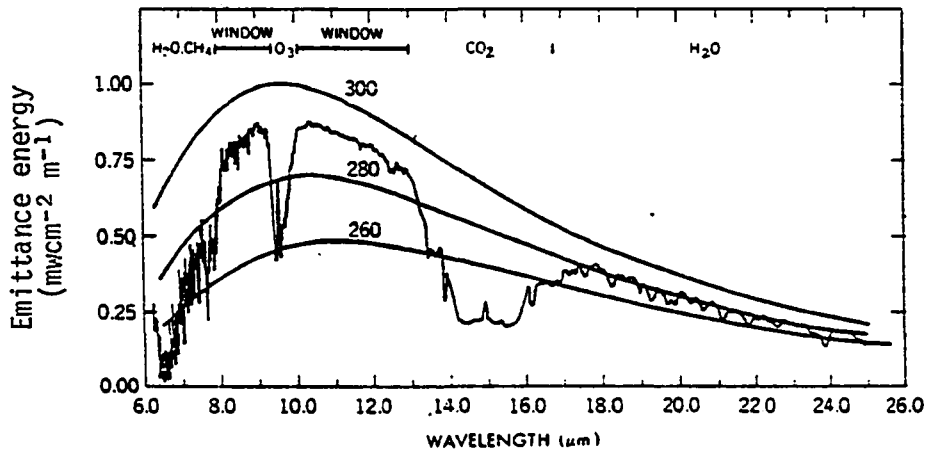
Emittance energy
(mWcm⁻² m⁻¹)
WINDOW
WINDOW
H2O.CH4
O3
CO2
H2O
300
280
260
1.00
0.75
0.50
0.25
0.00
6.0 8.0 10.0 12.0 14.0 16.0 18.0 20.0 22.0 24.0 26.0
WAVELENGTH (μm)

B

two major windows are between 8 to 9.5 and 10.5 to 13.5 micrometers. Table 1 lists the principal windows available for satellite remote sensing. This table provides information to chose the best bands to be used in satellite sensing.

Table 1. Principal atmospheric windows in electromagnetic spectrum (Lintz and Simonett, 1976)

Radiation Type	Wavelength, micrometer	
	Less clear window	More clear window
Ultraviolet and visible		0.30 - 0.75
Near infrared		0.77 - 0.91
	1.00 - 1.12	
	1.19 - 1.34	
		1.55 - 1.75
		2.05 - 2.40
Mid infrared	3.50 - 4.16	
	4.50 - 5.00	
Thermal infrared		8.00 - 9.20
(THIR)		10.20 - 12.40
	17.00 - 22.00	

The use of these windows in remote sensing will be discussed in more detail under the LANDSAT System section of this thesis.

Infrared light

The earth receives radiation from the sun in the wavelengths extending from very high-frequency gamma rays to very low-frequency (VLF) long radio waves. Most of the electromagnetic radiation, about 99 percent, occurs in the wavelengths greater than 0.70 micrometers or in the invisible part of spectrum. In nature, most plants are adapted to reflect a high percentage of the radiation in the infrared region in order to prevent them from becoming too warm during the day (Pettry et al., 1974). This characteristic of the plants and the reflective and emissive properties of other bodies and objects nearby have led to the use of remote sensing in natural resources. Even though the development of infrared film and thermal scanners are an important part of remote sensing, the value of conventional photography should not be overlooked in research on the environment.

Transformation of invisible light into the visible The spectral reflectance of fresh vegetation would begin at about 0.4 micrometers. It shows a low level of reflectivity in the violet to blue color range (0.5 to 0.6 micrometers), and decreases through the orange to red range (0.6 to 0.7 micrometers). In other words, a plant looks green to the eye because of the combination of various wavelengths. Considering only the visible range (0.4 to 0.7 micrometers), a plot of the spectral "signatures" for a large variety of plants would show a great deal of similarity since they would appear, with rather subtle differences, essentially green. Ordinary color photography, designed to reproduce the colors seen by the eye, records these similarities.

Given a sensor that is able to record reflected energy in the near infrared range, that is from 0.7 to about 0.9 micrometers, a much different look will appear. Figure 4 shows spectral signatures for several plant classifications, and also compares the spectral reflectances for vegetation, soil, and water. The similarities of these signatures are in the visible range, while, in the near-infrared region, differences between signatures increases. Figure 5 is an aerial color photo side-by-side with an aerial near infrared photo, taken simultaneously of the same scene. This figure gives an opportunity to observe the differences between these two portions of the spectrum for the same scene.

Color film is made of three emulsion layers that respond to the blue, green, and red ranges of the spectrum, so that the final print exhibits colors similar to those in nature. Color infrared film is made to respond to green, red, and near-infrared light, but recorded as blue, green and red, respectively. Since there is possibility of blue light intrusion, when using color infrared, a filter should be used to prevent such intrusion. Such a filter eliminates all light of wavelengths shorter than 0.5 micrometers. The result is an image in which the colors are shifted so that blue is unseen, green appears blue, red appears green, and near-infrared appears red. Thus, on color infrared photo, vegetation assumes colors ranging from low intensity red (pale) to bright red often mixed with greens and browns, depending on species, season, and stress conditions. Figure 5 is a color near-infrared aerial picture taken over a central Iowa farm, which, at the time of the photography, was planted to corn, soybeans, and hay. Crop recognition and moisture stress condition are easily detectable from this picture. At the time of photography

Figure 4. A. Typical spectral reflectance curves for various vegetation (Fritz, 1968)

Figure 4. B. Typical spectral reflectance curves for vegetation, soil, and water (Swain and Davis, 1978)

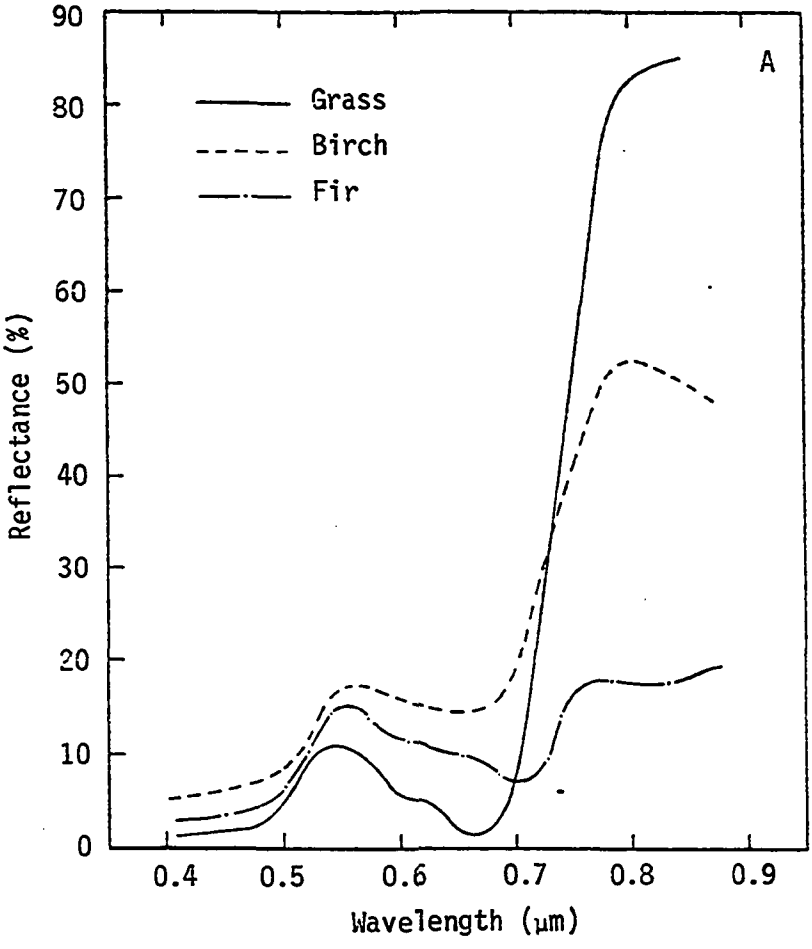
A
Grass
Birch
Fir
Reflectance (%)
Wavelength (μm)
0
10
20
30
40
50
60
70
80
90
0.4
0.5
0.6
0.7
0.8
0.9

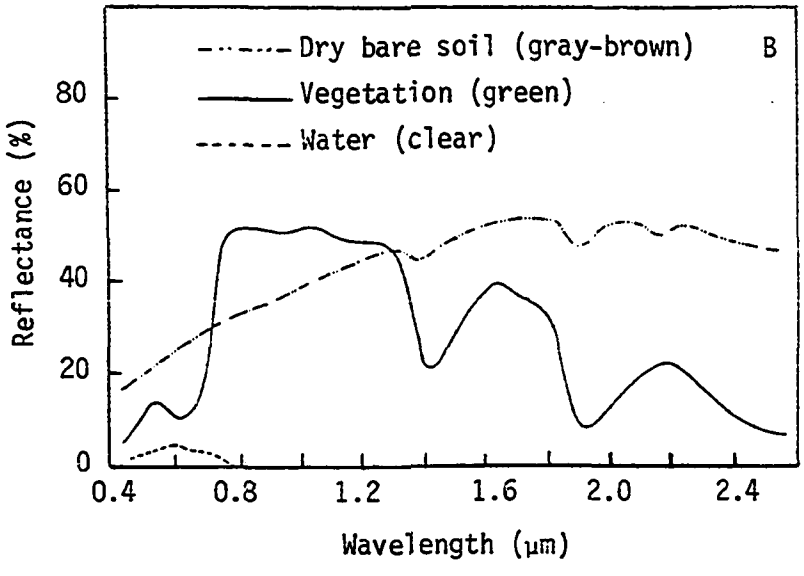
B
Dry bare soil (gray-brown)
Vegetation (green)
Water (clear)
Reflectance (%)
Wavelength (μm)
0
20
40
60
80
0.4
0.8
1.2
1.6
2.0
2.4

Figure 5. Infrared (top) and color (below) aerial photo of the same scene over Ames, Iowa

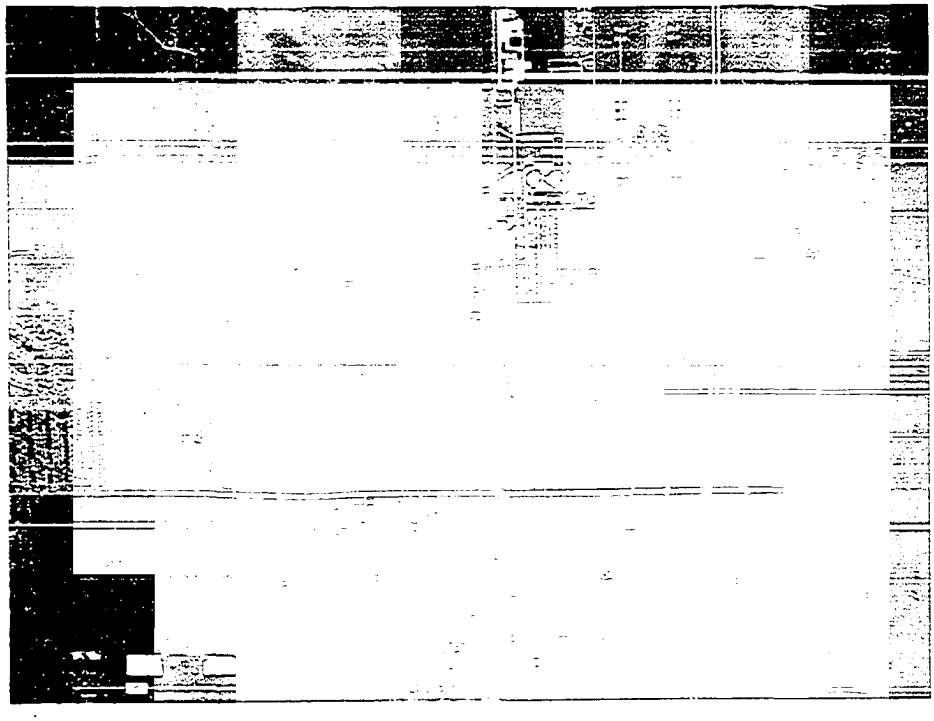

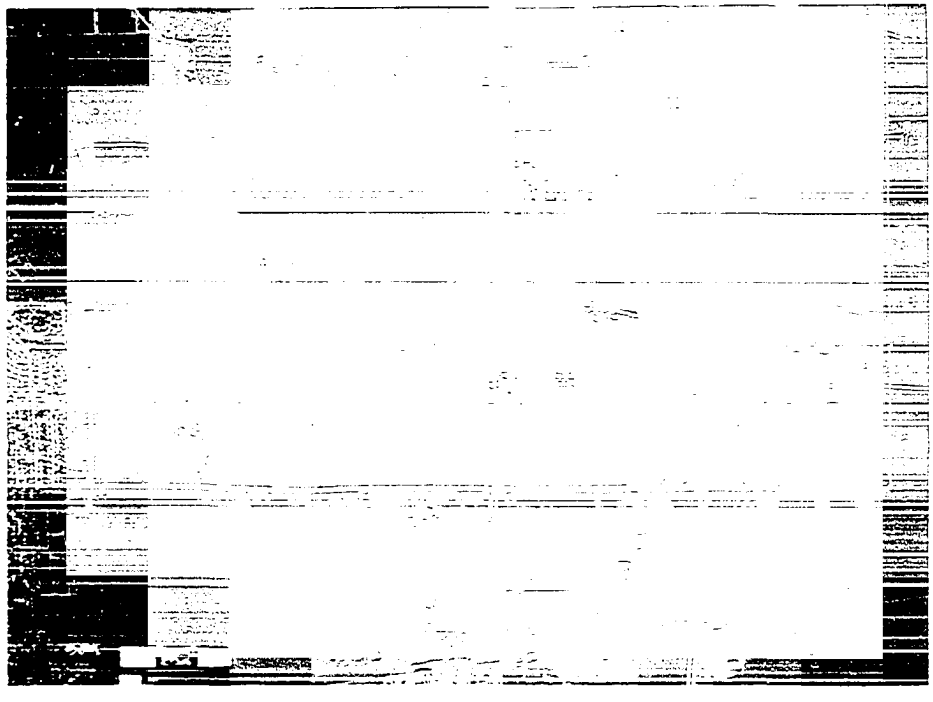

(August 25, 1980), the corn had tasseled, resulting in a decrease in the reflectivity from the corn compared to the higher reflectivity for soybeans. Also, soybeans show a more uniform texture in the picture than the nearby corn. These factors give an easy recognition between these two crops.

Another characteristic of color infrared film is the clarity with which these false colors are seen in aerial photography. This is a result of the haze effect reduction due to use of the filter (elimination of blue light). The blurring effect of haze is primarily due to the scattering of the blue light by particles composing the haze layer. This fuzziness is checked by eye and by color film as well. This is not the case with color infrared film images on which the blue light has been filtered out.

Basics of qualitative image interpretation

Energy radiated from objects can be recorded on images representing different ranges of the spectrum. Thus, an image can be a collection of many features and elements, which are viewed as an object or set of objects in a scene. Most important of these characteristics or features are color or tone, size and shape, resolution, pattern, texture, and context. Color has been discussed and is a representation or transformation of bands on the spectrum into the visible portion. It basically represents the thermal (spectral) properties of the objects. For example, power-plant effluents and suspended-sediment loads discharged into a lake display a color and tone recognizable from the remainder of the body of the lake.

Knowing the scale of a photo, the size of any object can be estimated or calculated. Scale is a ratio between one unit of size on a map or photo to one unit of size on the ground. The size gives the interpretator a limit of expectation in his search. Shape refers to the outline of an image. It is the particular triangle shape of airports' runways which make them easily distinguished. A circular shape among a mass of farmland is very likely to be a center pivot irrigation system.

Repetitive shapes of natural and manmade features make a pattern among those features. Physical and environmental geologists have used the pattern of objects on the ground to determine geological structure and function. Patterns on LANDSAT images help scientists to capture the geological features which are often overlooked on the ground. Drainage, formations that outcrop due to geological structure, and soil patterns can be readily observed in the images. Manmade features consist mostly of straight lines or smooth curves, while natural objects are distributed in their random patterns (a meandering river or a fault).

The smallest size object on the ground that can be seen or defined in the image is called the resolution. Resolution is the ability of an optical system to resolve and define objects. "Spatial resolution" is commonly used in remote sensing in conjunction with the size of objects on the ground that can be observed. On higher spatial-resolution imagery, smaller objects are more defined and sharpened. To avoid confusion, note that, for example, spatial resolution of 30 meters is higher than spatial resolution of 80 meters.

Texture of an image refers to its roughness or smoothness. Texture is the visual impression of a mixture of individual objects or portions of an object. Texture is usually associated with the size of the object and the scale of the photo. In a large scale image, for instance, a close-up of a tree shows leaves and branches distinctly, but at a smaller scale, no leaves and branches can be recognized separately, and they contribute to the texture of the tree crowns. From a considerable height, or on small scale images, the individual tree crowns vanish and contribute to the texture of the whole group of trees. For example, the texture of a soybean farm is "smooth" in contrast to the "coarse" texture of a corn field (Figure 5).

Context is the type of association which exists in the environment. Certain types of vegetation are associated with certain types of soil or certain levels of moisture. An eutrophic lake would be expected to contain one or more species of aquatic vegetation growing around its periphery. Conversely, the presence of such vegetation, which can be determined by remote sensing, would indicate that the eutrophication had happened.

To make a conclusive interpretation, all elements discussed above should be considered. Separate study of each one of these characteristics may create confusion and lead to diversity in decisions. The advantage of color infrared photography is that it combines the enhanced spectral region with these elements, providing an excellent remote sensing tool which has a broad use in environmental surveillance.

LANDSAT System

The first LANDSAT satellite, formerly called Earth Resources Technology Satellite (ERTS), was launched in July, 1972, and ceased its operation in January, 1978. The second satellite of this type, LANDSAT-2, was launched in January, 1975, and stopped functioning in November, 1979, only 10 months after LANDSAT-1 had ceased its operations. The only currently active satellite in this series is LANDSAT-3, which was launched in March, 1978. The next satellite, which is planned to be launched in late 1981, is LANDSAT-D. Once launched and in operation, LANDSAT-D will be designated as LANDSAT-4.

The LANDSAT satellite (Figure 6) is sun-synchronous, that is, the earth revolves beneath it as it moves in a fixed near-polar orbit at an altitude of approximately 900 km. The satellite circles the earth every 103 minutes, completing 14 orbits per day. It views the same area of the earth every 18 days at the same local time. Table 2 summarizes the characteristics of the LANDSAT orbit. Figures 7 and 8 provide information for visual inspection of these characteristics.

Table 2. Orbital parameters of the LANDSAT[a]

Period.	103 minutes (14 orbits/day)
Time of equatorial crossing .	9:42 am (11 am planned for LANDSAT-4)
Coverage cycle.	18 days
Distance between adjacent tracks at the equator. . .	159 km (185 km swath width - 26 km side lap)
Distance between successive tracks at the equator. . .	2760 km
Altitude.	880 -940 km

[a]Source: NASA (1979).

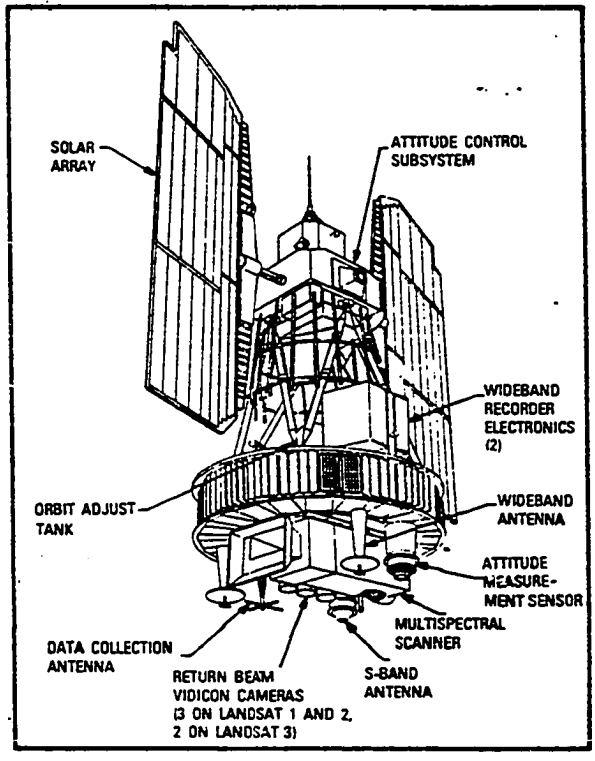

Figure 6. LANDSAT configuration (NASA, 1979)

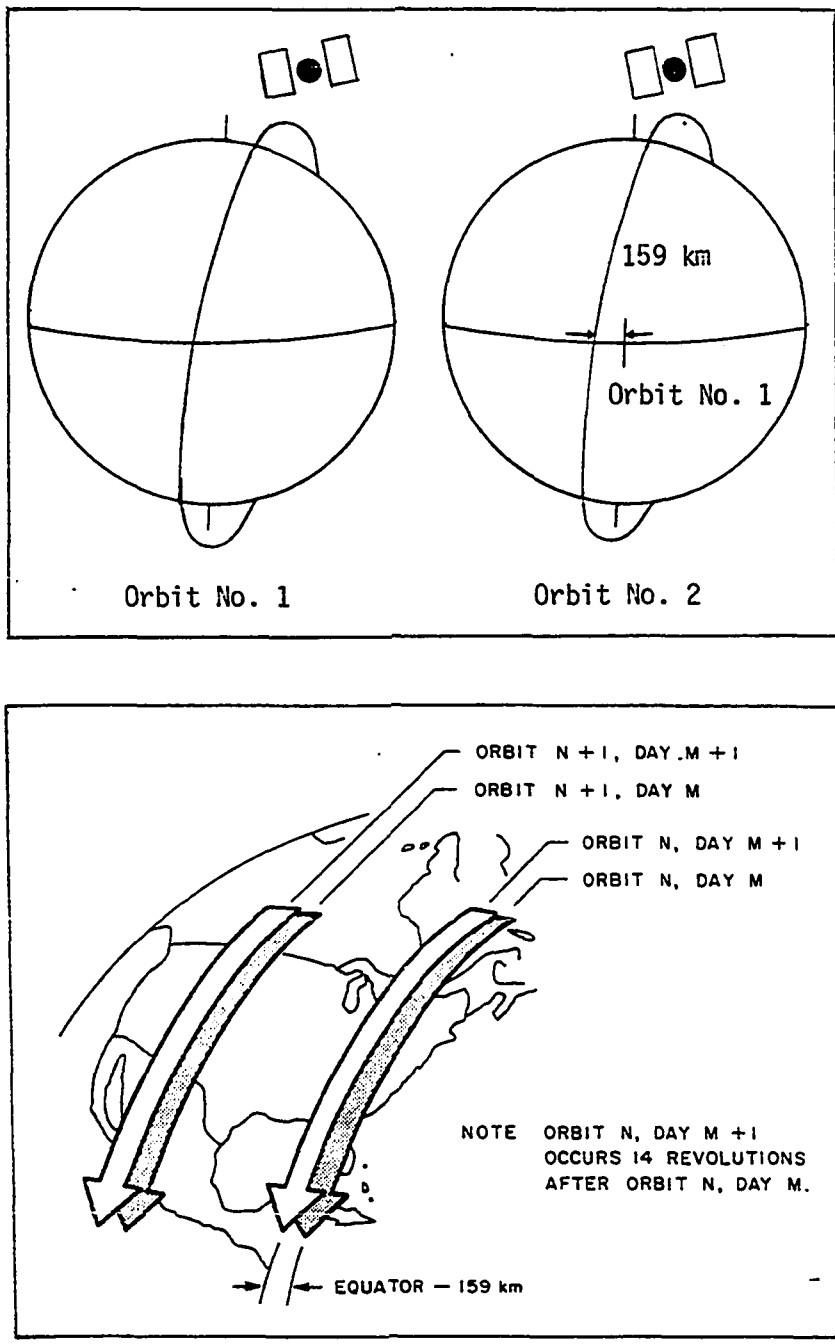

Figure 7. Characteristics of LANDSAT orbit (NASA, 1979)

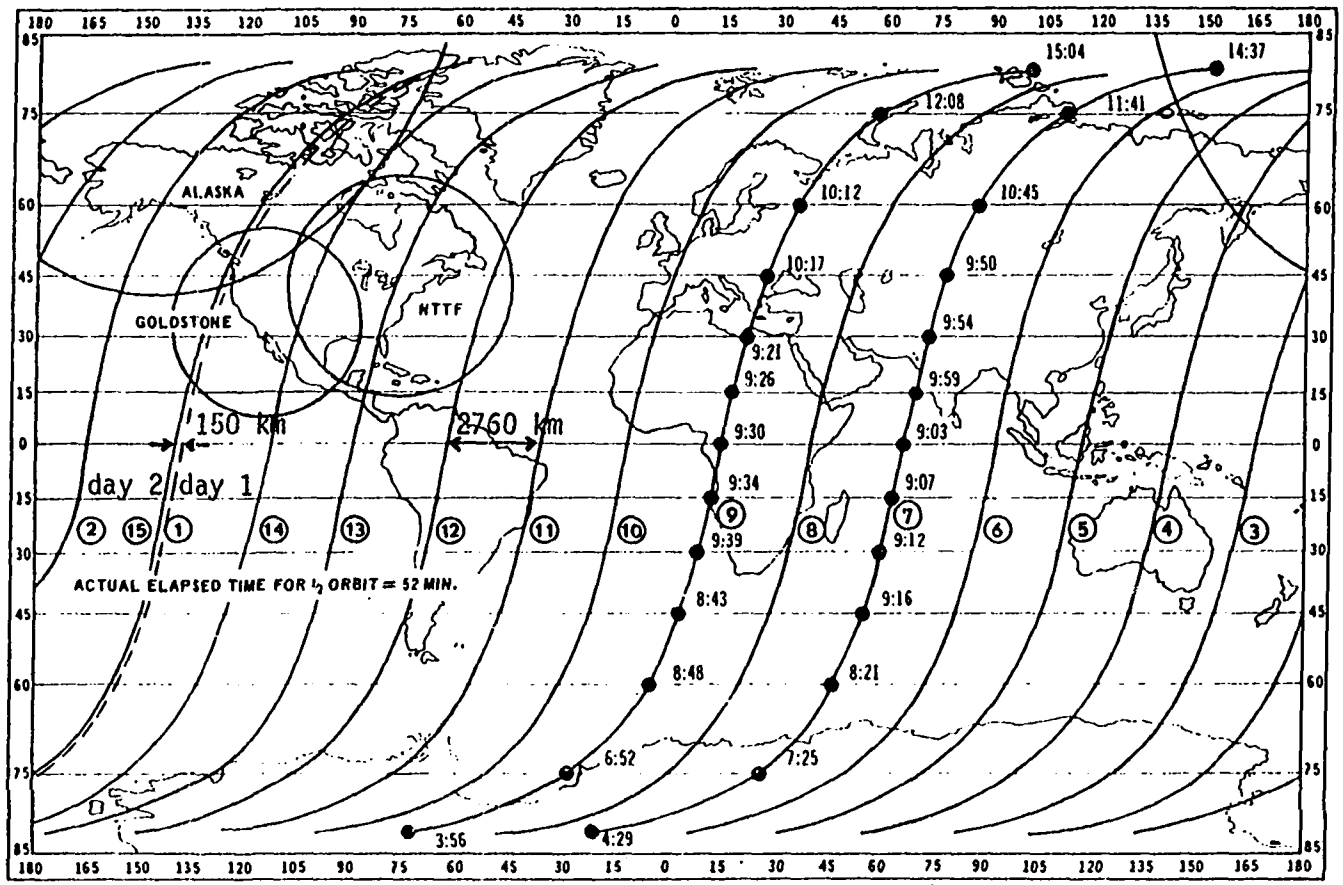

Figure 8. LANDSAT daily coverage (NASA, 1979)

Sensors onboard LANDSAT are designed to record those parts of the electromagnetic spectrum that relay information about earth resources. Distributions of land, water, snow, plants, cultural features, and earth material are the types of information that are being observed by LANDSAT. Dry soil, manmade structures, and vegetation have much higher spectral reflectances in the near-infrared region than the reflectance of water bodies and wet objects such as irrigated lands. This difference in reflectivity creates a high contrast between various types of backgrounds. Due to this contrast, most remote-sensing bands are selected around the near-infrared region.

LANDSAT-1, 2, and 3 were loaded with two imaging sensor systems, a return beam vidicon (RBV) and a multispectral scanner system (MSS). Both systems yield images of an area approximately 34,000 square-km (185 km by 185 km).

The RBV is a camera without a film. When the camera is shuttered, an image is stored on a photosensitive surface (vidicon tube), which is later scanned to produce a video output. There were three RBV cameras onboard LANDSAT-1 and LANDSAT-2, each producing an image of different bands along the spectrum: camera 1 for band 1 (0.475-0.575 micrometer or the blue to green), camera 2 for band 2 (0.580-0.680 micrometer or the orange to red), and camera 3 for band 3 (0.690-0.830 micrometer or the red to near-infrared). LANDSAT-3 has 2 identical RBVs on the range of 0.505-0.750 micrometer. Pictures produced by the RBV cameras of LANDSAT-1 and 2 were overlapping pictures of the same ground scene. The RBV system on LANDSAT-3 produces pictures of two side-by-side ground scenes, one scene per camera. Figure 9 shows the RBV arrangements on LANDSAT-1, 2, and 3.

Figure 9. The RBV systems on LANDSAT-1 and 2 (A) and on LANDSAT-3 (B) (NASA, 1979)

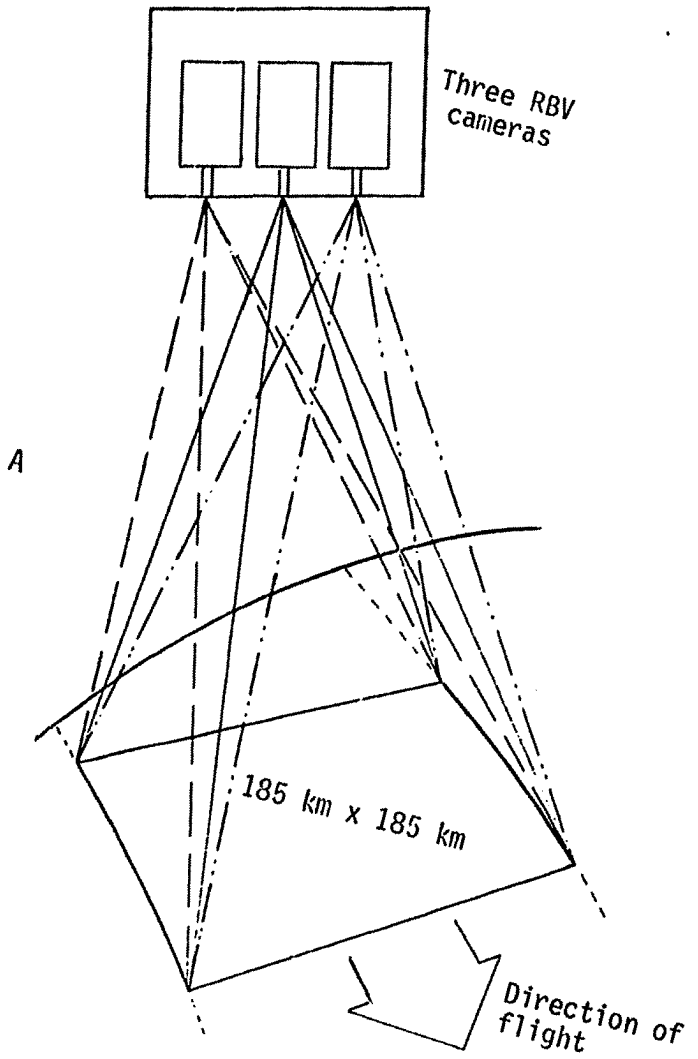
Three RBV cameras
A
185 km x 185 km
Direction of flight

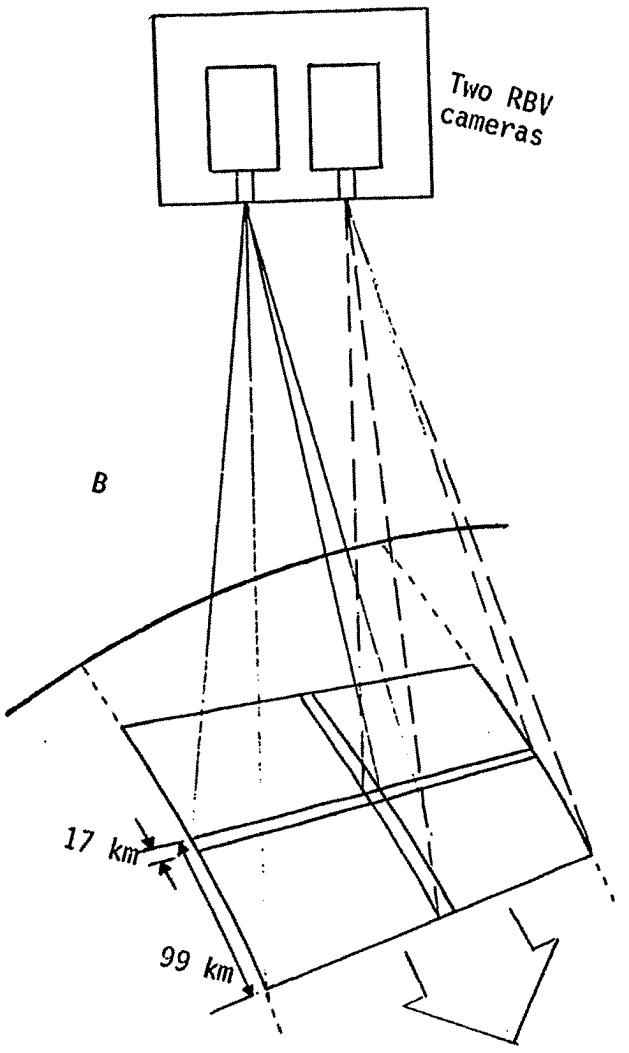
Two RBV cameras
B
17 km
99 km

The MSS is a multi-channel scanner with four channels or bands in LANDSAT-1 and 2, five channels in LANDSAT-3, and six or possibly seven channels in LANDSAT-D. The wavelength associated with each MSS channel of LANDSAT-1, 2 and 3 and the features best detected on each band are shown in Tables 3 and 4, respectively. The bands planned for LANDSAT-D are described in Table 5. LANDSAT-D will carry a new sensor called "Pointable Imager" or "PI" which has a high resolution of 10 m.

Table 3. Main characteristics of the multispectral scanning system (MSS) of the LANDSAT satellites[a]

Satellite	Band Number	Wavelength (μm)	Surface resolution (m)
LANDSAT-1, 2, 3	4	0.5- 0.6 (green)	80
	5	0.6- 0.7 (yellow-red)	
	6	0.7- 0.8 (red-near IR)	
	7	0.8- 1.1 (near-infrared)	
LANDSAT-3	8[b]	10.4-12.6 (thermal-infrared)	40

[a]Sources: NASA (1979) and Harnage and Landgrebe (1975).

[b]This part of scanner is called THIR or Temperature-Humidity Infrared Radiator.

Table 4. Suggested LANDSAT MSS bands for detection of natural features[a]

Feature identified	Band(s)
Water bodies	6,7
Depth of water	5,6
Suspended materials	4
Snow masses	5,6
Snow/water interface	5,6
Morphological features	6,7
Topographic lineaments	6,7

[a]Source: El Kassas (1977).

Table 5. Main features that will be detected by various LANDSAT-D MSS bands[a]

Band	Wavelength (μm)	Resolution (m)	Features detected
1	0.52-0.62 (green)	30	Green vegetation; coastal water; geologic and urban area
2	0.63-0.69 (yellow-red)		High contrast: soil boundary; geologic boundary; water bodies; within class (e.g., soil or water) discrimination
3	0.74-0.88 (near-infrared)		Green biomass; moisture in the vegetation
4	0.80-0.91 (near-infrared)		Growing crops; soil-crop contrast; water-land boundary
5	1.55-1.75 (mid-infrared)		Crop green matter; crop stress; moisture in the vegetation; surface soil moisture; land water delineation
6	2.08-2.35 (mid-infrared)		Research in rock spectral reflectance
7	10.4-12.4 (thermal-infrared)	120	Vegetation classification; crop stress; water estimation at some depth in the soil profile
*[b]	Pointable imager	10	

[a]Sources: Norwood (1974); Harnage and Landgrebe (1975), and Taranik and Lucas (1979).

[b]It is not known if it is going to be onloaded on the satellite. It is a MSS similar to that of LANDSAT-1, 2, and 3.

The MSS produces images by breaking a scene into many tiny segments, each 79 m in width and 185 km in length. The segments are obtained in rapid succession by means of an oscillating plane scan mirror of an optical system (Figure 10) that directs the image onto a detector.

Data obtained from each MSS channel, after having been modified to account for atmospheric effects, are either stored on magnetic tapes or form black and white renditions of every scene in each of the bands (NASA, 1979). It is the same process for data collected by the RBV system. Later, by combining different bands and using the additive color method (using color filters), a false color composite picture of the scene can be produced which has different combinations of colors on the image representing the different features on the ground. Figure 11 illustrates MSS product over the Mississippi River delta.

Geometry and resolution of the LANDSAT image

The main objective of the LANDSAT program is to use its multispectral imagery, which has a coarse-resolution synoptic view of large areas, in the analysis of earth features (Lintz and Simonett, 1976). Each LANDSAT image is formed by many picture elements, or "pixels." For the MSS bands, there are 3240 pixels in the across-track direction and 2340 in the along-track direction (about 7.6×10^6 pixels) in each image. Each pixel represents an area 79 meters square or 0.62 ha. Due to the overlapping of the instantaneous field of view of the scanner, the pixel is treated spatially as covering an area 56 m by 79 m, or 0.44 ha (General Electric, 1976). Figure 12 shows the formation of the MSS picture element (pixel).

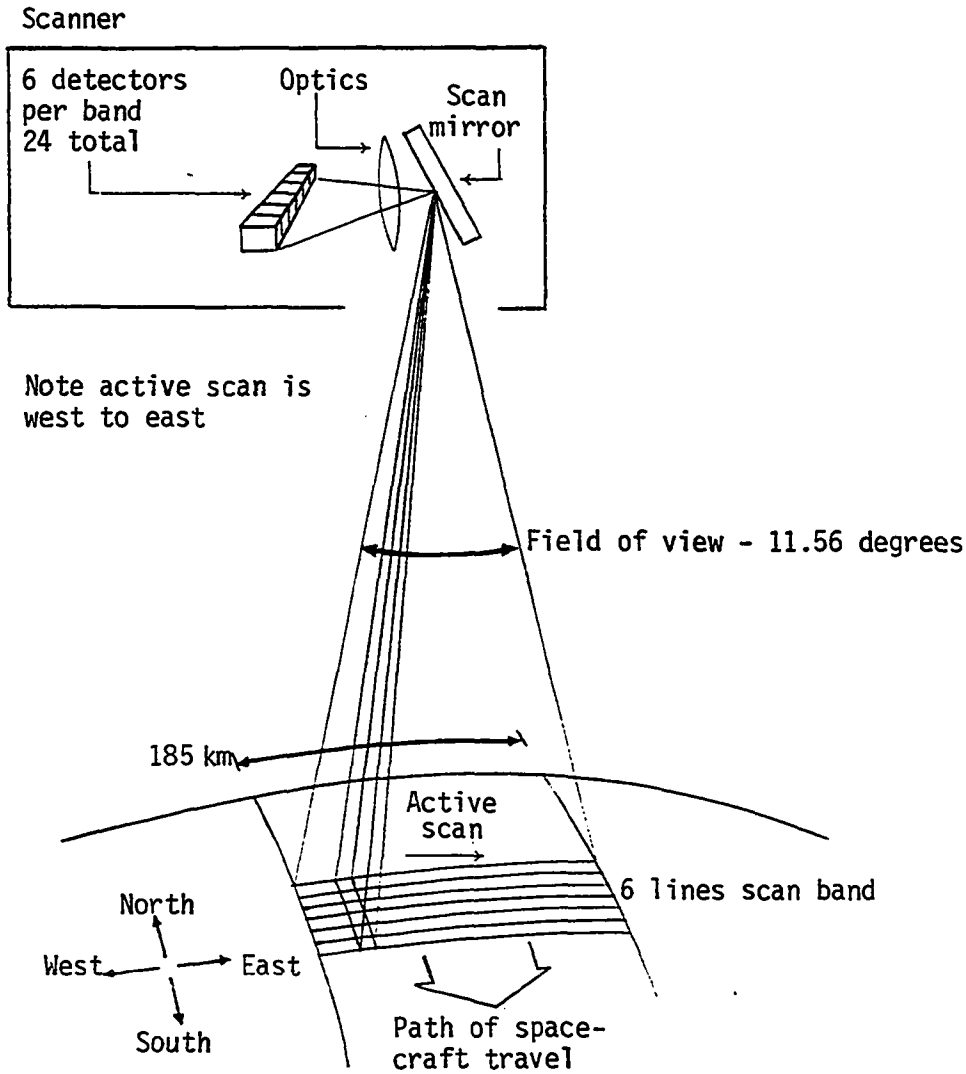

Figure 10. Schematic diagram of the MSS (NASA, 1979)

Figure 11. The MSS product over the Mississippi River delta

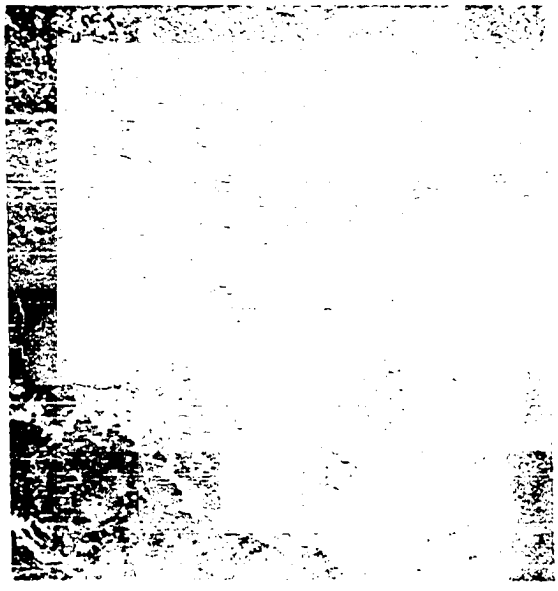

BAND 4

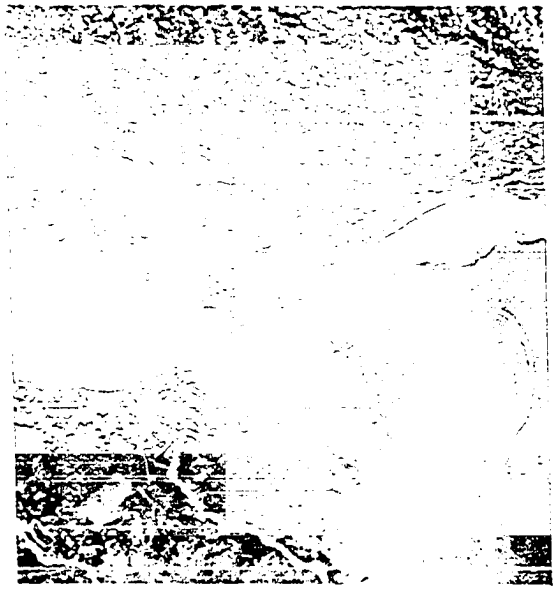

BAND 5

BAND 6

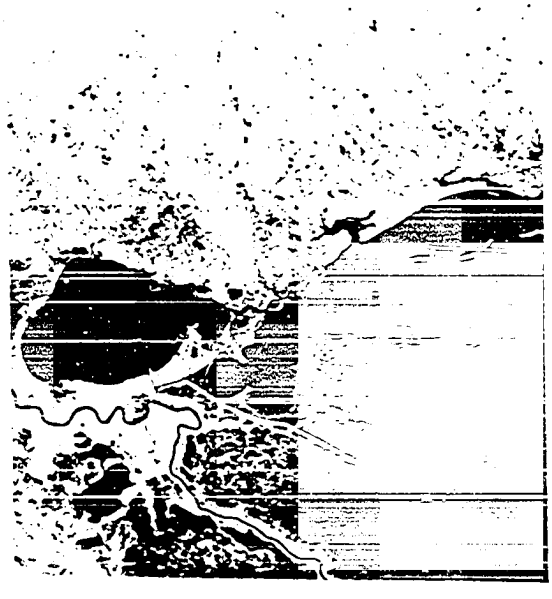

BAND 7

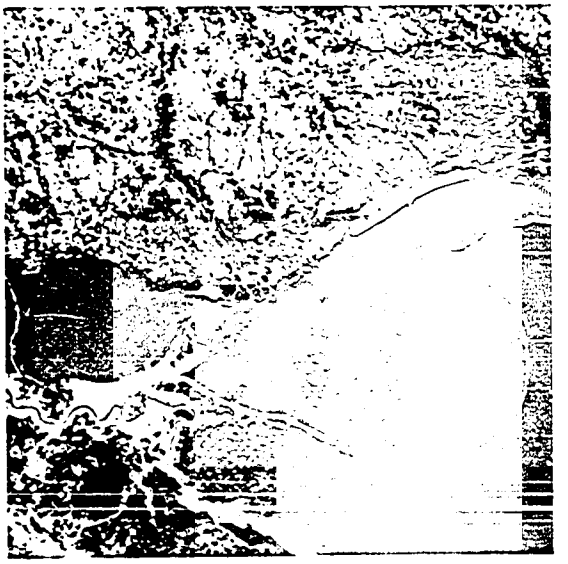

COLOR-COMPOSITE

Figure 11 (Continued)

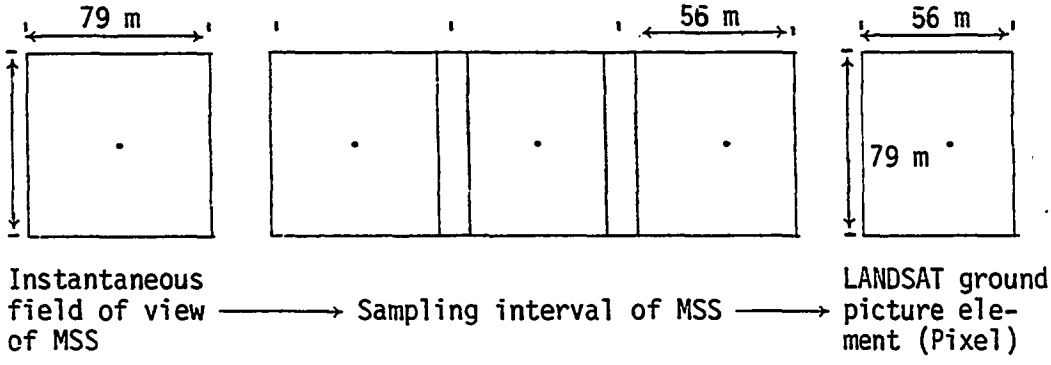

Figure 12. LANDSAT MSS picture element (Taranic and Lucas, 1979)

The reflectance for an individual data point is averaged over the 56 m by 79 m area. If half of the area of a scene within the pixel is black and another half is white, that area would appear gray in the picture (Hardy, 1977).

Although the effective resolution, determined by pixel size, is about 80 m, linear features like roads and faults as narrow as 10 m can be visible in sharp contrast to their surroundings (NASA, 1979).

LANDSAT functional network

In addition to the RBV and the MSS systems, LANDSAT-1 and 2 were equipped with a relay system, called the data collection system or DCS, that gathered data from remote widely distributed earth-based sensor platforms and transmitted them to a receiving station (Figure 13). The DCS system, although functioning well with LANDSAT-1 and 2, has now been

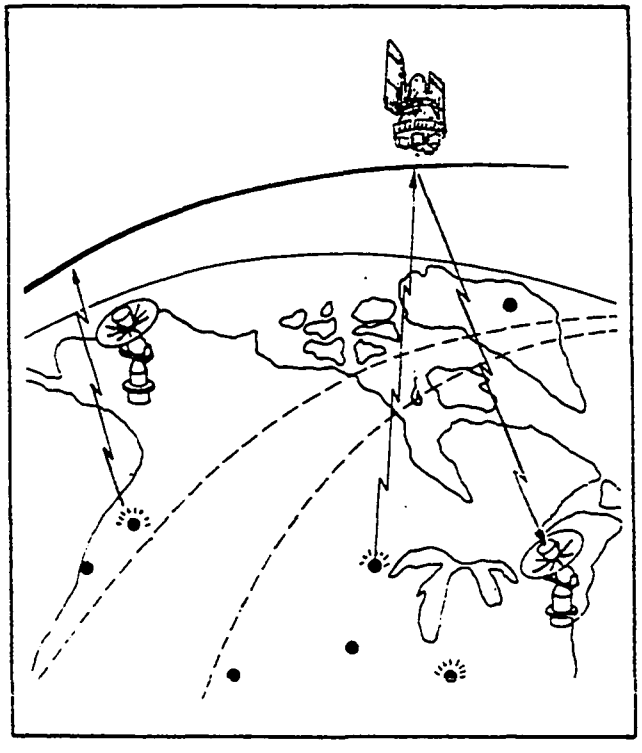

Figure 13. LANDSAT relay system (NASA, 1979)

transferred to other types of earth resources satellite such as GOES and NIMBUS (Carter and Paulson, 1978).

A Survey of Remote Sensing Application in Water Resources

Many areas in water resources and hydrology are beneficiaries of remote sensing techniques. These techniques have been applied in areas such as pollution control and water quality investigation, snow and ice measurements, flood damage assessment, surface water and drainage area mapping, groundwater hydrology and exploration, soil moisture and irrigation, and vegetation and land cover studies.

Water quality

Satellite surveillance of water color and turbidity can become a feasible practice. An optical or electronic scanner can be used to sense changes in the appearance of water and provide information about the water quality. Water color is less detectable in remote sensing where turbidity is high and it is difficult to separate water color and turbidity in remote sensing data (Goldberg and Weiner, 1972). High reflectivity of a turbid water can be detected at the visible and near-infrared part of the spectrum. Moore (1978) tabulated the qualitative estimate of different levels of water turbidity in different bands of LANDSAT data (Table 6).

The very turbid water discharge from the Mississippi River had light gray tones on bands 4 and 5 of the LANDSAT multispectral scanner. The tone is medium gray on band 6 and dark gray on band 7 (Figure 11).

Table 6. Tone of LANDSAT image for different level of turbidity (Moore, 1978)

Relative turbidity	Tone of Image				Hue of color composite
	Band 4	Band 5	Band 6	Band 7	
None	Dark	Dark	Black	Black	Black
Slight	Medium	Dark	Black	Black	Dark blud
Moderate	Light	Medium	Dark	Black	Medium blue
Heavy	Light	Light	Medium	Dark	Light blue
Very heavy	Light	Light	Light	Medium	White

Shih and Gervin (1980) used LANDSAT reflectance values in bands 4, 5, 6, and 7 to estimate chlorophyll a, turbidity, and suspended sediment in Lake Okeechobee, Florida. Their estimates proved to be accurate.

In a digital analysis of the LANDSAT image of the Potomac River basin in the Washington, D.C. area, Schubert and MacLeod (1973) employed multispectral processing with computer-compatible digital tapes (CCT) to reveal different classes of sedimentation (Figure 14). Areas of high sedimentation were identified as caused by sand-and-gravel operations and runoff from construction sites; organic pollutants were identified as coming from major sewage outfalls in the estuary (scene A in Figure 14). Analysis of a second scene (B) indicated that a high concentration of sediment in the water caused by heavy rainfall obscured effluent outfalls in the estuary. Results of this study indicated that sedimentation levels can be readily classified. Also, organic effluents may be detected and monitored.

Sinkholes or enlarged joints are considered a geologic hazard to many construction activities. They are also undesirable from a water supply standpoint, because they allow concentrations of surface contaminants, such

Figure 14. Digital analysis of the LANDSAT image of the Potamac River basin (Schubert and MacLeod, 1973)

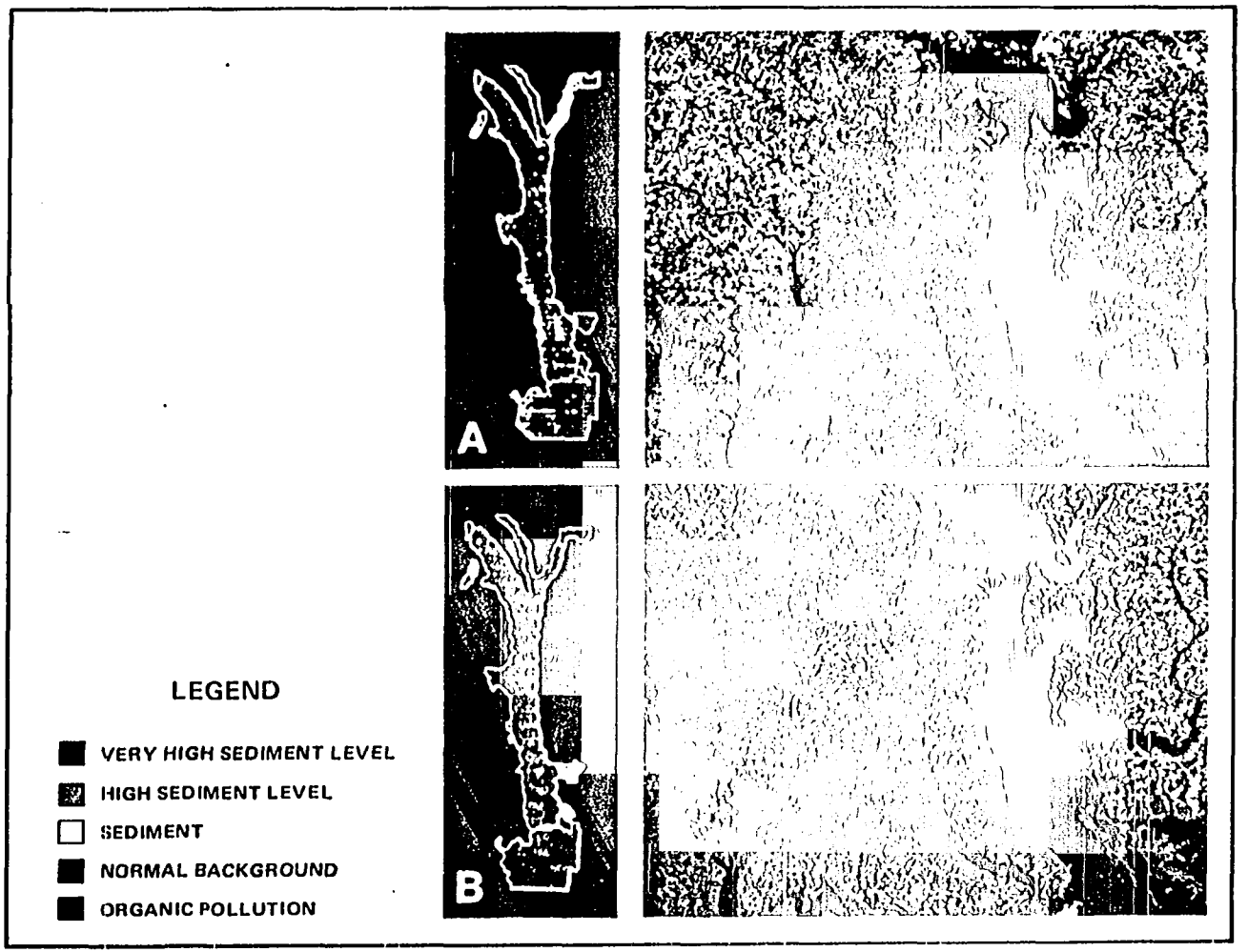
LEGEND
VERY HIGH SEDIMENT LEVEL
HIGH SEDIMENT LEVEL
SEDIMENT
NORMAL BACKGROUND
ORGANIC POLLUTION
A
B

as pesticides, organic material, and other chemical and physical waste material, to enter the ground water. In a site selection study, it is desirable to maximize the distance from known surface depressions or sinkhole activity. In such determination, remote sensing is an essential tool (Prosser, 1980).

Though nonpoint sources of pollution rarely are cited as significant pollution sources, they can have enormous impact on a water body. The expensive monitoring of all river basins can be lessened by monitoring land use changes using LANDSAT images. This was done by MacDonald and Waite (1977) as they reviewed the historical water quality information of Arkansas. They analyzed and evaluated LANDSAT-1 and 2 images for changes in land use. Their approach was based on the expectation that the land use changes affect the water quality of an area, and, therefore, variations of regional surface water quality data collected by state and federal agencies should correlate with grassland use changes detected by LANDSAT image analysis. They concluded that the updating of land use maps to include historical water quality data analysis should prove a valuable technique for defining, monitoring, and predicting regional water quality.

Soil erosion Land use changes affecting soil erosion can be monitored using remote-sensing techniques. These techniques have been used to make a qualitative assessment of sediment problems. Williams and Morgan (1976) used aerial photographs to show the type, intensity, and location of erosion. They also determined the nature of sediment movement and distinguished between natural and accelerated erosion. Ruff (1974) monitored sediment movement and located sediment discharge points in a river system using aerial photography. Morgan et al. (1978) used high-altitude color

and color infrared photos in conjunction with the universal soil loss equation to predict inter-rill and rill erosion on cropland areas of different soils, topography, and land use. Their soil loss prediction based on remote-sensing interpretations agreed closely with predictions based on field studies.

Snow

Many uses of water resources are dependent on snow melt. Monitoring snowcover on mountainous terrain using conventional methods is a difficult task. LANDSAT images have proven to be helpful in making such difficult measurements.

Many studies have confirmed that snowlines (the boundary of significant snowcover) could be observed to within 60 meters under good conditions, that snowcover could be empirically related to water runoff and that snowcover area could be calculated with a low percentage of error (Mercanti, 1974).

LANDSAT images of successive dates in spring can provide information about the rate of snow melting and the volume of water released. LANDSAT views of the entire Wind River Mountains area, which is the ungaged and inaccessible area shown in Figure 15, depict the 1973 spring snowmelt.

Floods

Effective flood plain management requires an updated geographical knowledge of the areas covered by most recent floods. The broad synoptic LANDSAT views have proven to be useful in this situation. Low-altitude remote sensing techniques, such as aerial photography, can provide detailed information supplementing the synoptic picture of the satellite. Of

21 MAY 1973

08 JUNE 1973

Figure 15. LANDSAT view of the Wind River Mountains area

course, the role of the satellite is to provide a background study of the whole site at once and pin-point the areas where aerial pohtography is needed. This practice will reduce the expense of the procedure.

In contrast to on-site farm damage inspection of flood and adjustment, which is a labor-intensive and costly task, Anderson (1978) illustrated the use of color-infrared aerial photography in the assessment of flood damage on agricultural lands. He also showed how computer-assisted techniques offer the potential to perform the damage assessment much faster and more efficiently when time is critical.

The capability of LANDSAT to assess flooding has been demonstrated in the literature. Kalensky et al. (1979) used LANDSAT multispectral data to delineate the flooded area around the Saint John River in New Brunswick, Canada. They were successful in their work and were able to compile flood hazard maps for that area. Similar work has been conducted by McAdams (1979), who used LANDSAT images for flood mapping of the areas near Ames, Iowa, where, in June, 1975, Squaw Creek and South Skunk River reached record flood levels.

An example of spring flood of the Mississippi River observed by LANDSAT is shown in Figure 16. The area flooded at the confluence of the Mississippi, Missouri, and Illinois rivers near St. Louis, Missouri, can readily be approximated from these pictures.

Surface water

A wide range of mathematical models is being used by water resources planners, many of them to compensate for lack of adequate data which are necessary for decision making. Input data to these models are mostly

Figure 16. LANDSAT-1 scenes showing the confluence of the Mississippi, Missouri, and Illinois rivers near St. Louis, Missouri, before and after 1973 massive flood (Perry et al., 1974)

related to geomorphic parameters of the watershed, its geology, soil types, and type of land use and cover within the basin. Collecting information about these parameters becomes a problem, both in economic terms and time, when the size of the drainage basin increases significantly. In situations of this nature, remote sensing techniques can help to define the input parameters of the hydrologic models. Among the hydrologic models those requiring input parameters that relate to land cover are the most appropriate for the use of remote sensing data. Once the model has been calibrated, any future changes in land use patterns and their consequent hydrologic effects can be observed and evaluated.

Ragan and Salomonson (1978) studied the use of LANDSAT data to define input parameters for an array of hydrologic models that are used to synthesize streamflow and water quality parameters in planning or management processes. The sizes of the areas which he was able to study were in excess of 6,000 square kilometers.

One model used by the United States Soil Conservation Service (SCS) (1972) is the precipitation-runoff relation.

$$Q = (P-0.2\,S)^2 / (P + 0.8\,S) \tag{8}$$

where

Q = actual runoff

P = potential maximum runoff

S = potential maximum storage (including initial abstraction)

$$CN = \frac{1000}{10 + S} \quad . \tag{9}$$

To solve the first equation, one has to find S from the second equation. This requires information about the soil-cover complex. In other words, CN is obtained by determining the distribution of land cover and soil groups. SCS has classified the soil types in four groups, A, B, C and D, ranging from low to high runoff potential. The type of a soil for a given area can be determined from a soil map. Land cover, which is a determining factor in the curve number (CN), can then be found from remote sensing data or by conventional land observation. Ragan and Salomonson (1978) developed a table of the runoff curve number (CN) for various land cover categories by using LANDSAT data, and compared the results with those obtained in conventional ground surveys (Table 7).

Table 7. Runoff curve number for different land use from LANDSAT and ground survey. Adpated from Ragan and Salomonson (1978) and U.S. Soil Conservation Service (1972)

Land use treatment	Hydrological soil group							
	LANDSAT				Ground survey			
	A	B	C	D	A	B	C	D
Forest land	25	55	70	77	45	66	77	63
Open space grass cover	36	60	73	78	39	61	74	80
Commercial and business areas (large parking lots)	90	93	94	95	81	88	91	93
Residential	60	74	83	87	61	75	83	87
Bare ground	72	82	88	90	72	81	88	91

Askari and Raust (1981) derived the curve number for the watersheds in Mill Creek, Ohio, from multispectral data obtained by remote sensing. They estimated curve numbers for the preselected sample sites by ground measurements of the land cover, surface condition, and soil type. They then developed regression models using the curve numbers of each sample site as the dependent variable, and the mean radiance measurements in the four LANDSAT bands as the independent variables. The mean curve number (CN) derived for the test watersheds compared favorably with those obtained from ground observations.

A potential method for obtaining the requisite information on land cover and soils over broad areas is through the utilization of LANDSAT data in computer compatible tape (CCT) formats. Slack and Welch (1980) have studied the possibilities of deriving SCS curve numbers for large watersheds from these data (CCT). They generated a classification map of the Little River watershed near Tifton, Georgia, with four hydrologically important land use classes (agricultural vegetation, forest, wetland, and bare ground) from LANDSAT data. Then, using these data, they computed the curve numbers for sites under study and compared them with SCS values for the same areas. They found agreement between these curve number units.

Another hydrologic parameter is the watershed area. Considering existing scale of the LANDSAT image and its resolution, it may not be possible to measure watershed area accurately. However, other parameters, such as stream length, can be accurately measured from LANDSAT data in many areas. Later, this stream length can be correlated with the area of the watershed. This stream length can be fed into the modified model in

place of the area. This method of watershed area determination has been demonstrated by Rango et al. (1975).

Although LANDSAT offers considerable potential for hydrologic investigations, its usefulness may be limited for use in small areas by low resolution (80 meters for existing satellite), but its use for large watersheds is significant. Applicability of LANDSAT data for mapping and monitoring water regimen as an aid in interpreting hydrologic conditions throughout the interior watersheds of Iran has been demonstrated by Akhavi (1980). He compared stream discharge rates and then estimated volumes of standing water in playa lakes through optical and digital analyses of the LANDSAT data. These analyses were used to quantify and evaluate the hydrologic regimen and to detect the significance of groundwater discharge.

Reservoir inventory In a dam inspection program, once the dams are identified, the next step is to classify them based on their destructive potential in the case of failure. There are many ways to carry out programs like this, but often economics and time are critical constraints. McKim et al. (1972) reported that the dam inventory program can be fast and inexpensive when LANDSAT-1 images are used. Dams on streams can be identified on the LANDSAT imagery by abrupt changes in stream width. A linear termination on a water body is a reliable indication of a dam, particularly when it is inconsistent with the normal drainge pattern. General information derived from this study indicated that size and shape of water bodies, their location, and their relative depths can be recognized. Note that, as of now, LANDSAT imagery generaly does not supply information suitable for determining depth of water bodies, or information about dam's height or type of dam construction.

High contrast between water and land in the near infrared region makes the LANDSAT images a good source for monitoring land/water interfaces. River courses as narrow as 80 meters and water bodies as small as 1 hectare can easily be delineated from the land, making a surface water inventory possible. This method of surface water survey was conducted by Reeves (1973) to map the playa lakes in the southern high plains.

Groundwater

Drainage density and fault and fracture density are two major factors in determining and exploring groundwater resources. These factors can be readily measured from remote sensing imagery. Drainage density is one of the items of watershed physiographic information which have been measured from LANDSAT data. One such study was conducted by Rango and Salomonson (1975). They conducted research over Southern Wisconsin, Eastern Colorado, and a portion of the Middle Atlantic States. Drainage density can be correlated with groundwater because usually where drainage density is lower the permeability is higher. Karst topography above limestone formations, which have a high permeability, may have little or no surface drainage. It is also the same in many unconsolidated sand and gravel areas.

Many drainage channels develop along fractures. Flow of runoff in these channels increases the possibility of recharging the groundwater. The fractures are cracks in the rock that are clustered in zones 2 to 20 meters wide and up to 2 kilometers in length. There is usually more water in the fracture zone than its surroundings, for the reasons mentioned above. Greater chance of finding adequate water exists if drilling is done at the intersections of these fractures. The presence of fractures,

though they may be buried under overlying surfaces, can be detected through the surface expression they create. Such surface expressions, which can be detected by remote sensing procedures, have different soil tone colors due to differences in moisture content, alinement of valleys or sinkholes, and the presence of different types of vegetation in a form of line.

The fracture-trace techniques are becoming a progressive tool in groundwater exploration and more drillers are using this method to locate water sources. This results in more successful location of wells with higher yields of water, up to 50 times or more than the wells located randomly in a given area (OWRT, 1978).

Akers (1964) found that water well production in northern Arizona sandstone aquifers depends on deep fracturing. Where these fractures are expressed on the surface, their pattern then can be identified with a synoptic view. Short (1973) reported that, in the regions with sparse vegetation where distinctive outcrop patterns occur, geologic reconnaissance maps can be prepared from satellite pictures. Foster et al. (1980) have reported the result of a study to determine the ease and feasibility of using satellite images as a tool in exploring for new sources of groundwater in Arizona. They detected linements on LANDSAT images and developed correlations between the linement density and water well data in the two study sites. The result of their research supports the existence of relationships between regional geologic structure and the presence of groundwater.

Soil moisture and cover

Infrared photography and infrared scanners have been used in soil moisture studies. The results of these studies indicate that differences in soil moisture can be recognized easily, but it is difficult to measure the amount of moisture in soil. Data from infrared scanners do not indicate subsurface soil moisture. Whereas difficulties are encountered in using infrared images for subsurface soil moisture, they are a very practical tool to locate seepage areas (Whiting, 1979).

From the fact that wet soil has lower spectral reflectivity than dry soil, delineation of soils having different levels of soil moisture is possible in the near infrared region. MacDowall (1972) has shown that the reflectance of a sandy-texture soil drastically increased when the moisture content dropped below 10 percent. In a study of the effects of moisture content on soil reflectance by LARS (1971), it was found that the total percent reflectance largely decreased as moisture content increased. In another study, Beck (1975) showed that variation in soil moisture content was a primary contributor to differences in the spectral response.

Where soil types are different, it is usually more difficult to differentiate between dry and wet soil (Hoffer, 1972), because many factors other than moisture content affect the reflectance of soil materials, such as texture and mineral and chemical compositions (Gates, 1970). However, Kirschner et al. (1977) identified soil boundaries and easily quantified soil map units through correlations between soil mositure characteristics and spectral soil classes derived from LANDSAT data. LANDSAT multispectral

scanner data portray only surface reflectance properties. Soils that vary widely with respect to horizontation and parent material may exhibit the same spectral properties. Ancillary data, in the form of physiographic boundaries, provided additional information and allowed for correlation of soil series and spectral soil classes (Weismiller et al., 1977).

The first map based on remotely sensed data in Jennings County, Indiana, was made by Bushness in 1929, from black and white aerial photographs. Since 1960, color photography has been preferred over black and white, but, because of the high cost of color photography, black and white panchromatic photography has remained the major soil mapping aid. Dominiques (1960) reported that boundaries between soil types could be differentiated more accurately from color photography than from black and white. The usefulness of color and color infrared photography was proven by Parry et al. (1969), who identified soil drainage characteristics, slopes, and organic matter content.

Gross variation in soil features can be identified through the synoptic view of LANDSAT. Westin (1973) observed and delineated repeating soil patterns, land use, slope effects, and drainage patterns from LANDSAT-1 images. A soil association map was produced in about one and one-half months from LANDSAT pictures for the entire state of South Dakota (Westin and Frazee, 1976).

Soil cover Along with soil moisture studies, many researchers have also researched the capabilities and potential for satellite crop surveys. Among them are Thamann (1974), Erb (1974), Draeger et al. (1974), Morain and Williams (1975), and, most recently, Lee Williams and Poracsky (1979). All of these people have used different approaches to locate,

identify, and measure the area of crop fields. Despite the varieties in approaches, they have followed the basic of light theory and used differences in reflectivity among different crops, considering other elements of image interpretation, such as tone, texture, and field patterns on the photo.

Satellite crop survey techniques have been successfully tested and used in a project conducted by scientists from the U.S. Department of Agriculture (USDA), the National Aeronautics and Space Administration (NASA), and the National Oceanic and Atmospheric Administration (NOAA) to estimate crop production over the whole world. The project, called the Large Crop Inventory Experiment (LACIE), was designed to demonstrate the applicability of remote sensing technology for globally monitoring world food production.

APPLICATION OF THE LANDSAT IMAGERY OVER WESTERN IOWA

Site of Study

The Monona County area in western Iowa was selected because this county had the largest number of irrigated permits to this date, according to information from the Iowa Natural Resources Council. The Missouri River (Figure 17) forms the western boundary of this county. Monona County contains about 180,530 hectares, of which about 172,730 hectares, or almost 96 percent, is farmland. There are two distinct areas of the county, the bottomlands or very flat Missouri River flood plain, and the uplands in the eastern part of the county. Elevations of the uplands are between 30 to 100 meters higher than the flood plains, and, unlike the bottom lands, the uplands are rolling to steep slopes. Monona County has a humid continental climate with warm summers and moderately cold winters. The normal monthly and annual temperature and precipitation at Onawa, the county seat, is given in Table 8.

Soil associations of Monona County

Soil associations are important in remote sensing studies of the earth's surface because they constitute the background of the imagery. The most important factor which should be considered is the effect of soil type on the reflected energy measured on the image. Differences in soil types may cause significant differences in reflectivity of the scene within the image.

The map of soil associations (Figure 18) shows the general patterns of the soils in Monona County. This map is helpful in studying the soils

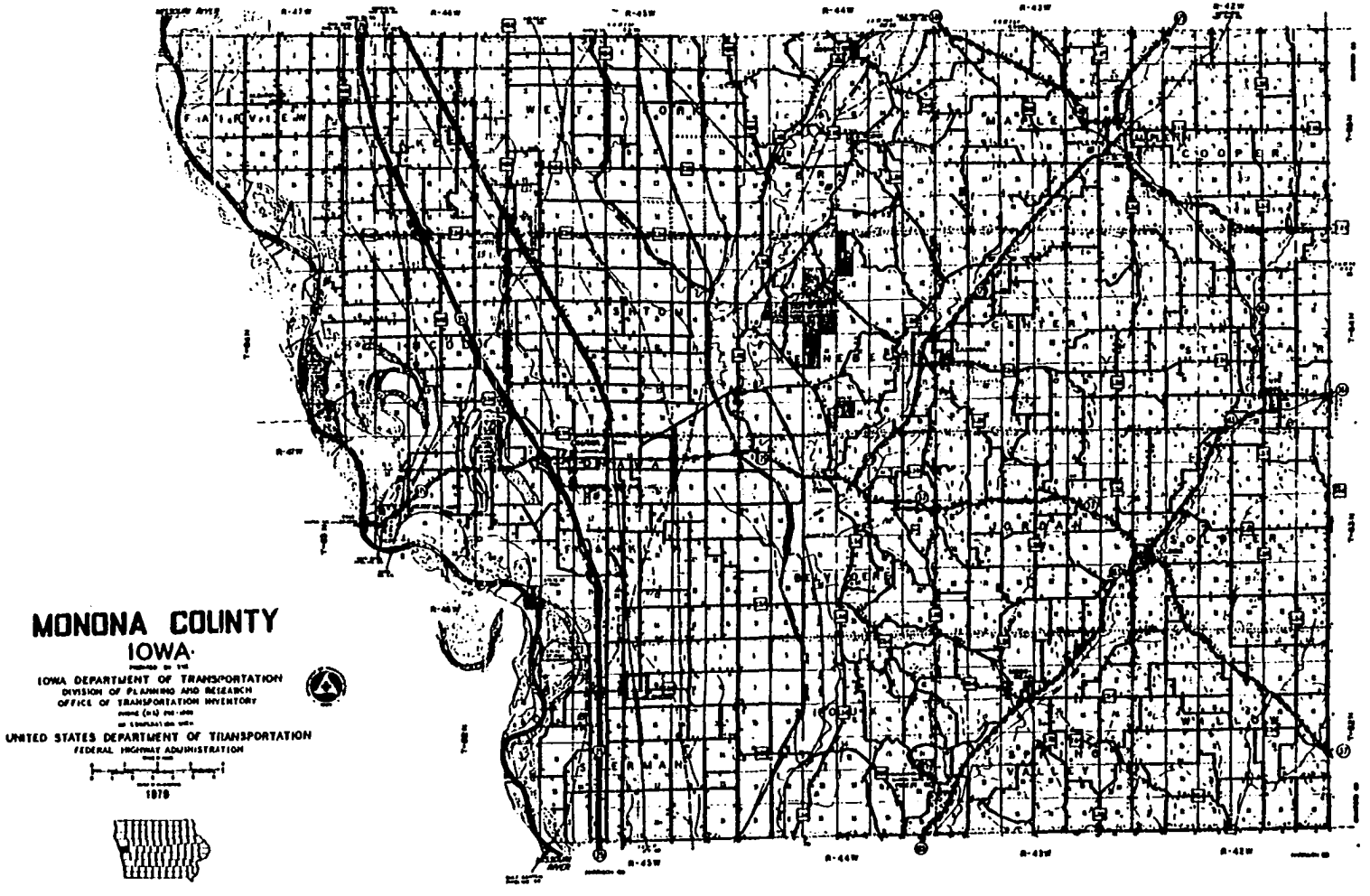

Figure 17. Monona County, site of the study (Iowa Department of Transportation, Ames, Iowa)

of the county in general. Each association contains several different soil types, arranged in a characteristic pattern. In most places, the pattern is related to the nature of the soil materials and the shape of the land surface.

Table 8. Average temperature and precipitation at Onawa station, Monona County, Iowa

Month	Temperature, °C	Precipitation, cm	Snowfall, cm[a]
December	- 3.7	2.25	15.50
January	- 6.1	1.88	18.75
February	- 4.4	2.58	20.25
March	2.9	3.38	18.25
April	10.3	6.25	4.25
May	16.6	9.43	0.50
June	21.6	11.13	---
July	24.6	9.28	---
August	23.2	9.35	---
September	18.6	9.03	---
October	12.0	4.48	1.00
November	3.4	3.55	7.25
Year	9.9	72.85	85.75

[a]Not water equivalent.

Figure 18. Soil associations of Monona County, Iowa (United States Department of Agriculture, 1959)

1. Recent alluvial light-colored soils of the Missouri River flood plain
2. Principally dark colored soils of the Missouri River flood plain
3. Soils of the flood plains of tributary streams
4. Mostly steep soils formed from loess and local alluvium
5. Gently sloping to steep soils formed from loess and local alluvium

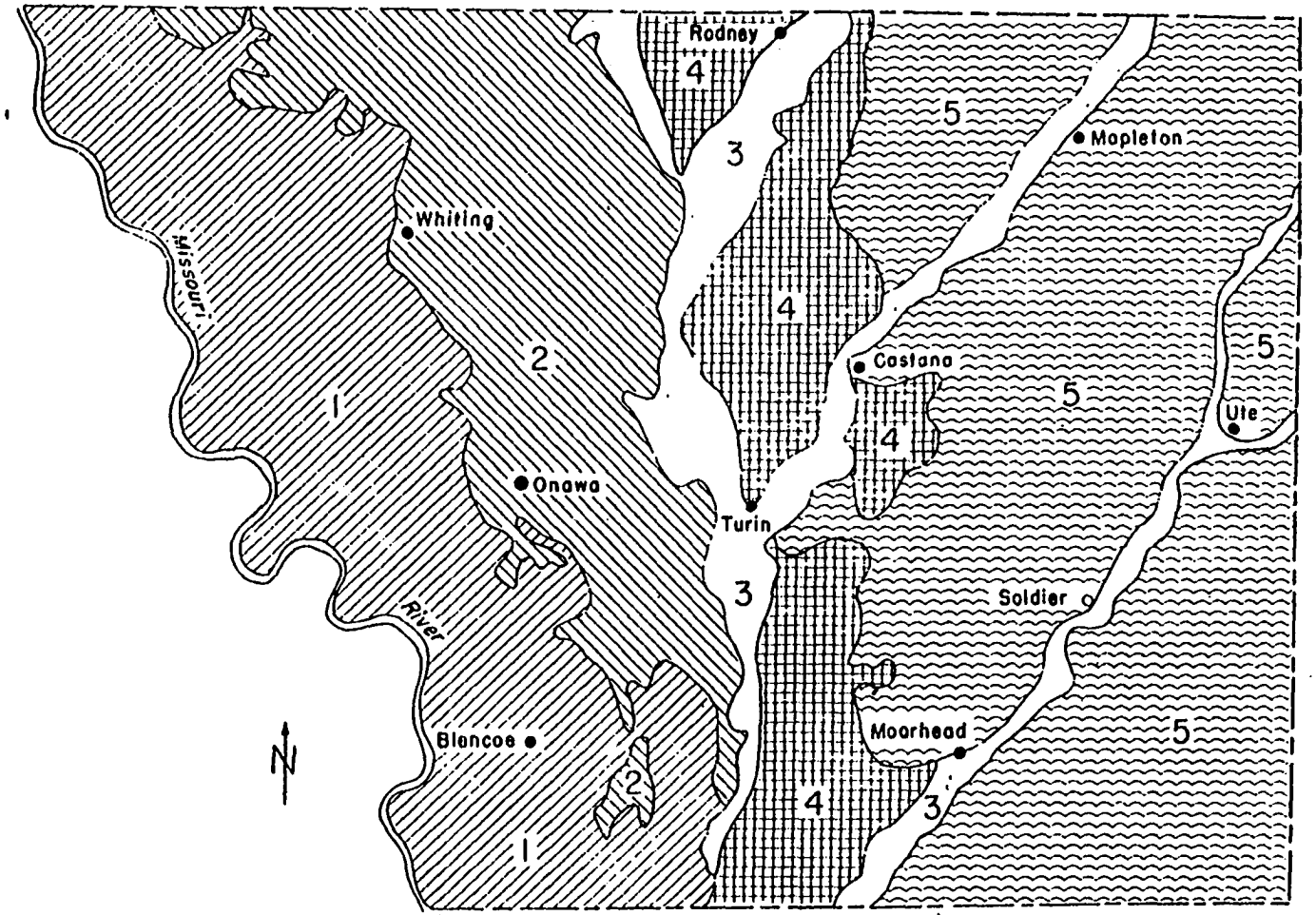
Rodney
Mapleton
Whiting
Missouri
River
Castana
Ute
Onawa
Turin
Soldier
Blencoe
Moorhead
N
1
2
3
4
5

Imagery Selection

Four different types of images were used for interpretations in this study. The types of images are basically determined by the photo finishing material, color, and scale. The materials of selected images were paper, film negative, black and white film positive, and false color film positive. Except for the false color film positives, which are a composition of bands 4, 5, and 7, the images reflect only single bands of the multispectral scanning system (MSS).

The paper print images have dimensions of 370 by 370 centimeters with the nominal scale of 1:500,000. Both black and white film positive and color film positive pictures have dimensions of 185 by 185 centimeters and the nominal scale of 1:1,000,000. The scale of the 5.6 by 5.6 centimeter film negatives is 1:3,369,000, but paper print of any larger scale can be produced from these negatives. Also, by projecting the black and white and color positive transparencies on a screen, images of very large scale can be observed.

Each LANDSAT image covered an area of about 185 by 185 kilometers. The imagery for a given area has a nominal scene center point which represents the actual scene center of repetitive coverage of the same region. The actual scene centers are kept close to the nominal center point by orbit stabilization of the satellite.

Orbit stabilization

LANDSAT satellite is stabilized for pitch, yaw, and roll by a system of flywheels and rate gyros (NASA, 1979). This type of stabilization maintains the attitude of the satellite with respect to the Earth's

surface. Satellite orbits are configured to offset the gravitational forces of the Earth-Moon-Sun systems. Some orbital precessions do occur, however, and the orbit must be adjusted so there will be nominal repetitive coverage within each ground swath. These adjustments are accomplished with a gas reaction jet system. Orbital precession and variation in the satellite attitude cause variations in the area covered by repetitive overpasses (Figure 19). Scene centers shown in Figure 20 are the nominal center points of many actual scene centers over Iowa (one actual scene center for every 18 days). These scene centers are part of a Worldwide Reference System (WRS) which is a global notation system for LANDSAT data. This system enables a user to inquire about satellite images over any portion of the world by specifying a nominal scene center. Note that the center points of repetitive scenes covering a given area are not at the same exact geographic point, but form a cluster around a nominal center point, as illustrated in Figure 19.

The United States Geological Survey (U.S.G.S.) has provided index maps of nominal center points for the United States and for the entire world. These index maps are available from EROS Data Center at Sioux Falls, South Dakota. The WRS notation assigns sequential numbers from east to west to the 251 nominal satellite tracks, called "paths," starting with number 1 for the first track that includes mainland North America. The "row" refers to the latitudinal center line of a frame of images. The state of Iowa by WRS notation lies between paths 26 to 31 and rows 30 to 32. Fifteen images are needed to cover the whole state of Iowa.

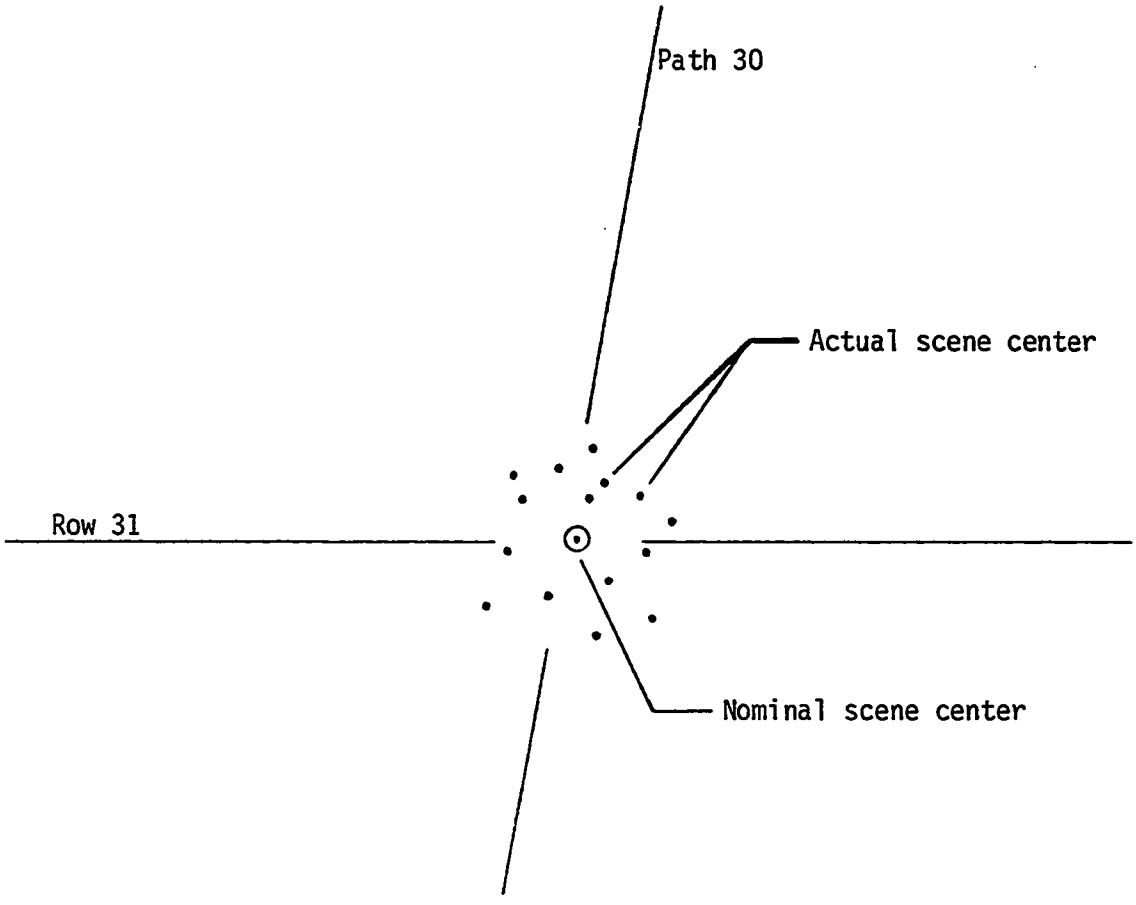

Figure 19. Actual scene centers of repetitive overpasses and their nominal center point

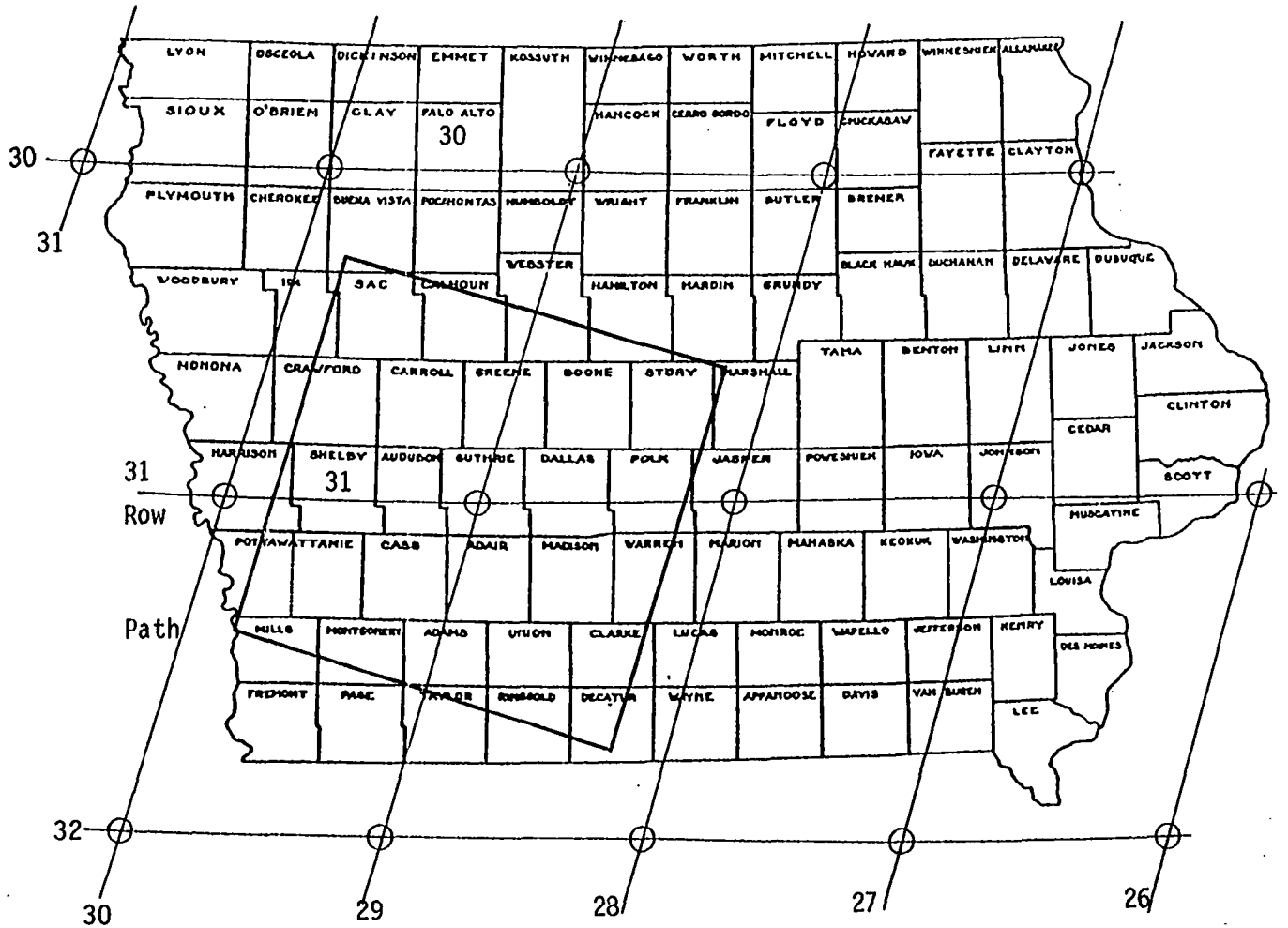

Figure 20. LANDSAT nominal scene center points for Iowa; square template reflects actual coverage for each center point

For the study site, which is located in western Iowa, the nominal center point on path 30 - row 31 was selected. The images over this point cover Monona, Crawford, Harrison, Mills, Pottawattamie, and Shelby Counties in western Iowa, as well as about the same size area in eastern Nebraska (Figures 21 and 22).

Prior to image selection, a computer listing of available data and images of LANDSAT was obtained from EROS Data Center. This list provided information about the LANDSAT data, such as: location, image type, scene identification, film source (e.g., black and white), quality, percentage of cloud cover, and exposure date (Figure 23). Table 9 is a preliminary list of images selected for this study. Additional images were later obtained and some others were produced as required through the course of the research.

Since the images had to be selected prior to interpretation, selection was based only on the image quality, the cloud coverage and recommendations from other studies. After the study was completed and experience had been gained, many new criteria for image selection were developed, some of them different from those on the initial list. These new criteria will be discussed in the appropriate chapters later in this thesis.

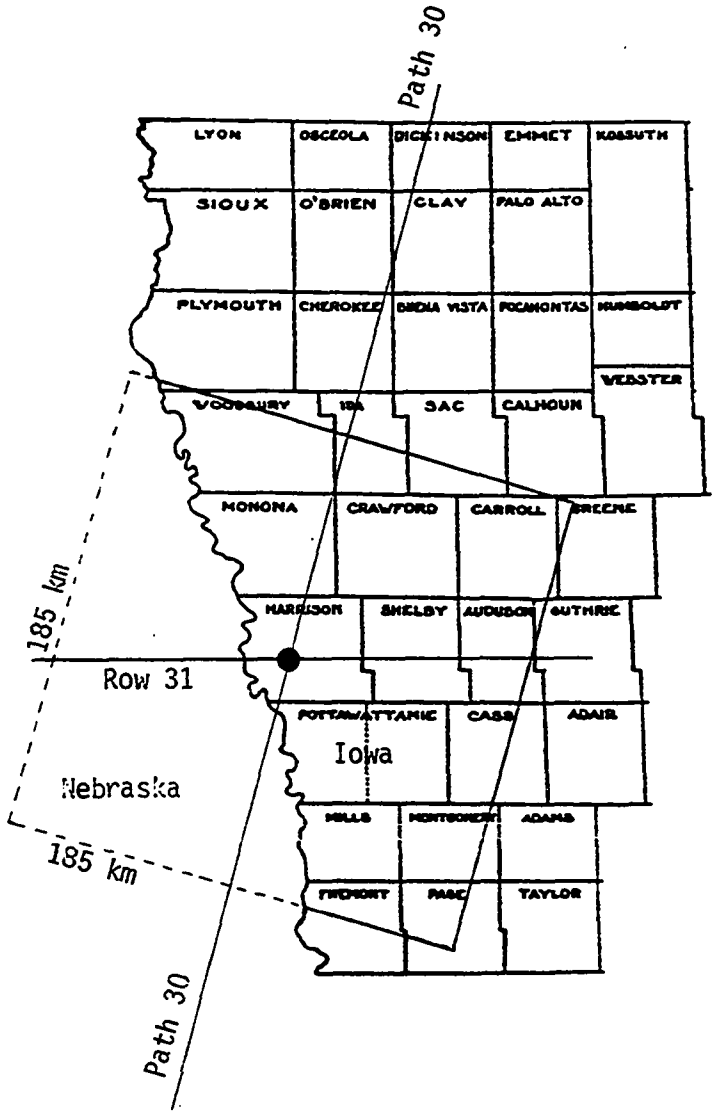

Figure 21. Nominal areas covered by LANDSAT image in western Iowa

Figure 22. Actual LANDSAT coverage over area under study with the nominal center point on path 30 and row 31 in the Worldwide Reference system of LANDSAT data

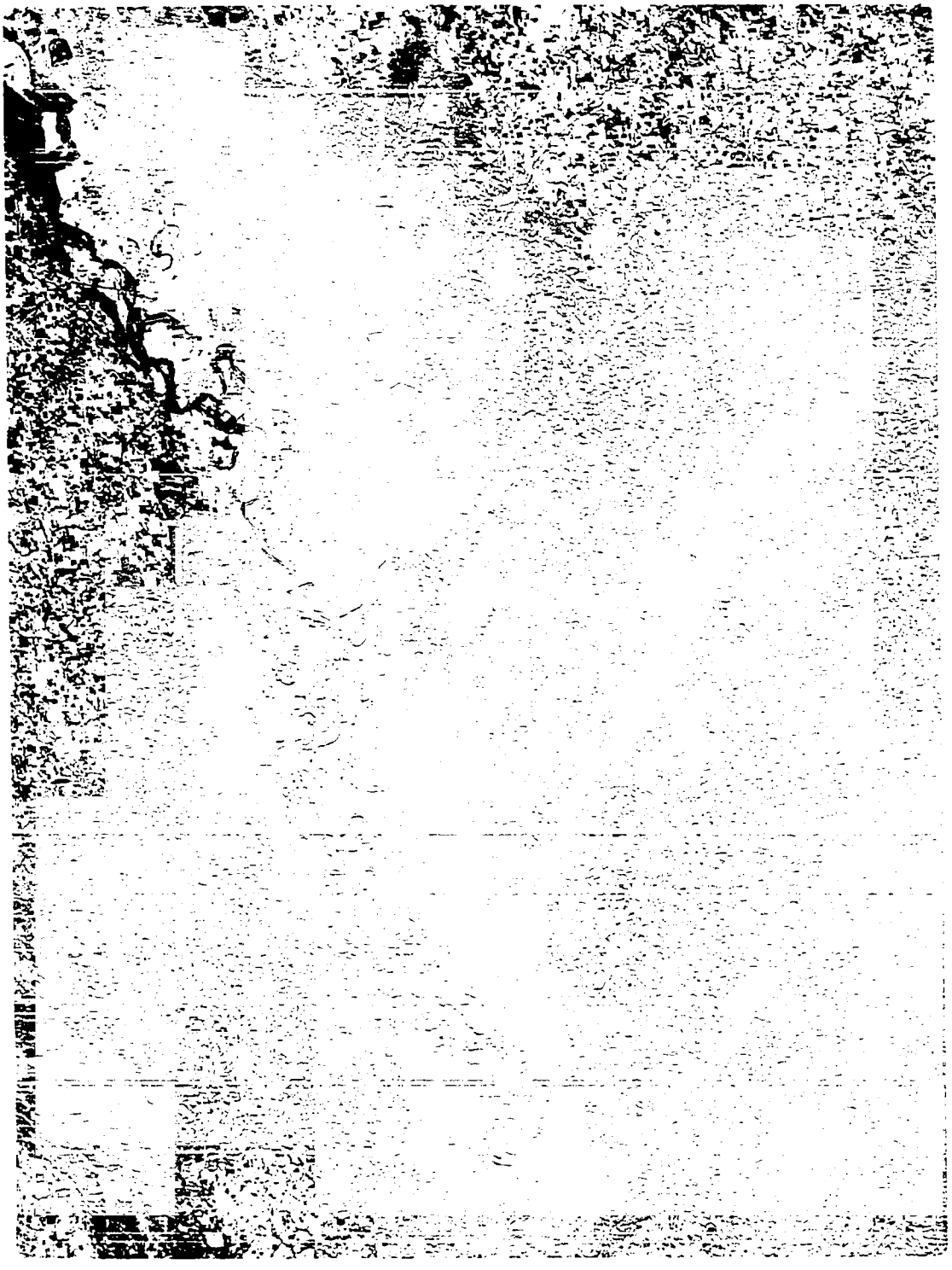

```
                                   E R O S  D A T A  C E N T E R                                  REPORT NO.-OL001-1
                                 SIOUX FALLS, SOUTH DAKOTA  57198                                 DATE        06/12/79
                          CONTACT-NUMBER-0004309121          TERMINAL-T83A61                      TIME        08:43
                                 SV IRAN                                                          PAGE          16

                                            DATA TYPE  LANDSAT

                                                                                                         CA MO BP2
     IMAGERY-TYPE         SCENE  ID    FILM-SOURCE-QUALITY-CLOUD-EXPO-DATE--SCENE-CENTER-POINT---SCENE-SCALE--MICROFORM-COL-IN-DE-COT--

   PATH=179  ROW= 38  LANDSAT
   LANDSAT-2 (MSS)          8204206452500 B&W-02.1"   8888=   00%  03/05/75 N31D45M00S E047D13M00S 1:3,369,000 B2200021115 P  X  X   N
      CORNER POINT COORDINATES=#1:N32D21M04S E040D24M19S #2:N32D38M46S E046D51M49S #3:N31D09M19E E046D02M33S #4:N30D51M00S E047D53M19S

   LANDSAT-2 (MSS)          8207406453500 B&W-02.1"   8868=   00%  02/15/75 N31D40M00S E047D11M00S 1:3,369,000 B2200020196 B  X  X   N
      CORNER POINT COORDINATES=#1:N32D16M26S E040D22M53S #2:N32D34M10S E046D29M28S #3:N31D02M56E E046D00M00S #4:N30D45M36S E047D51M39S

   LANDSAT-1 (MSS)          8137006562500 B&W-02.1"   2888=   00%  07/28/73 N31D45M35S E046D54M33S 1:3,369,000 B1200261175 P  X  X   N
      CORNER POINT COORDINATES=#1:N32D23M02S E040D06M11S #2:N32D39M39S E046D11M40S #3:N31D07M51E E045D43M50S #4:N30D51M16S E047D36M31S

   LANDSAT-1 (MSS)          8135206544500 B&W-02.1"   8288=   00%  07/10/73 N31D44M30S E046D53M37S 1:3,369,000 B1200250620 P  X  X   N
      CORNER POINT COORDINATES=#1:N32D21M55S E040D05M00S #2:N32D38M31E E046D10M56S #3:N31D06M43F E045D43M08S #4:N30D50M29S E047D35M24S

   LANDSAT-1 (MSS)          8122606572500 B&W-02.1"   8888=   10%  03/06/73 N31D47M12S E046D58M07S 1:3,369,000 B1200161276 P  X  X   N
      CORNER POINT COORDINATES=#1:N32D24M16S E040D09M52S #2:N32D41M22S E046D15M39S #3:N31D09M30S E045D47M17S #4:N30D52M47S E047D39M42E

   LANDSAT-1 (MSS)          8120806571500 B&W-02.1"   8888=   00%  02/16/73 N31D45M35S E047D04M10S 1:3,369,000 B1200150897 P  X  X   Y
      CORNER POINT COORDINATES=#1:N32D22M05S E040D15M45S #2:N32D39M40S E046D22M22S #3:N31D00M26S E045D53M29S #4:N30D51M16S E047D45M06

   LANDSAT-1 (MSS)          8117206564500 B&W-02.1"   5888=   00%  01/11/73 N31D39M33S E047D11M27S 1:3,369,000 B1200120671 P  X  X   Y
      CORNER POINT COORDINATES=#1:N32D17M07S E040D25M01S #2:N32D35M12S E046D20M24S #3:N31D01M20E E045D50M50S #4:N30D43M30S E047D53M25S

   LANDSAT-1 (MSS)          8101006561500 B&W-02.1"   8555=   00%  08/02/72 N31D36M10S E047D07M02S 1:3,369,000 B1200011026 P  X  X   N
      CORNER POINT COORDINATES=#1:N32D12M36S E040D10M39S #2:N32D30M31S E046D25M30S #3:N30D59M27S E045D56M17S #4:N30D41M51S E047D47M41S

   ********************************************************  DONE  ********************************************************
```

Figure 23. Information about LANDSAT data

Table 9. Characteristics of selected LANDSAT images over western Iowa

Satellite	Scene identification Number	MSS bands				Image material[a]	% Cloud cover	Exposure date
		4	5	6	7			
LANDSAT-2	82198016255X0		X		X	Paper	10	6/24/80
LANDSAT-2	82171016223X0		X			Film negative	00	9/28/79
LANDSAT-2	82171016223X0			X	X	Film positive	00	9/28/79
LANDSAT-3	83016716280X0					Film positive	00	8/19/78
LANDSAT-3	83009516270X0		X			Film negative	00	6/08/78
LANDSAT-3	83009516270X0				X	Film positive	00	6/10/78
LANDSAT-1	8585515144500		X			Paper	10	8/21/77
LANDSAT-1	8549815473500					Film positive	00	8/29/76
LANDSAT-2	8257616191500		X			Film negative	00	8/20/76
LANDSAT-2	8219816264500		X			Paper	10	8/08/75
LANDSAT-1	8510216141500		X			Paper	10	7/30/75
LANDSAT-1	8515616110500		X			Film negative	00	7/22/75
LANDSAT-1	8170616311500		X			Film negative	00	6/29/74
LANDSAT-1	8170616311500		X			Film positive	00	6/29/74
LANDSAT-1	8140016381500					Film Positive	00	8/27/73
LANDSAT-1	8102216382500		X			Paper	00	8/14/72
LANDSAT-1	8102216382500	X		X		Film positive	00	8/14/72

[a]Where MSS bands are marked, it means one black and white print of each band. No mark under MSS bands means false color composite print.

Instrumentation

The main instrument used in this study was a Zoom Transfer Scope. The Zoom Transfer Scope (ZTS^{TM}) used for the research is a Bausch and Lomb ZTS model ZT4 (Figure 24), which has the capability of enlarging, rotating and translating the image of a photo or other input material such that it may be viewed in superimposition with the image of a base map or other output material. This enables significant data to be transferred from the photo to a base map. In other words, this instrument enables the user to view two separate images simultaneously (Baush and Lomb, 1975).

Zoom magnification with the model ZT4 is up to 14X. The output material (base map) is viewed at 1X. With the photo scale smaller than the map scale, as is the case with the high altitude coverage (e.g., satellite), the operator turns the zoom dial (magnification dial) until the image is magnified to the same scale as the base map. This process provides more detail information about the image. The ZTS also has the capability of stretching the input image to obtain a better match with the base map.

In order to increase the familiarity with the area under study, the location of geographical features, such as lakes and streams, was reviewed by imposing the LANDSAT image over the county map. Later, the county map was replaced by a base map of the same scale. The base map was made by overlying a tracing paper on the county map and copying the boundary and the main features, such as the major roads and streams.

A microdensitometer was used in monitoring the soil moisture (Figure 25). This instrument is made by the National Spectrographic Laboratories, and its operational features are as follow:

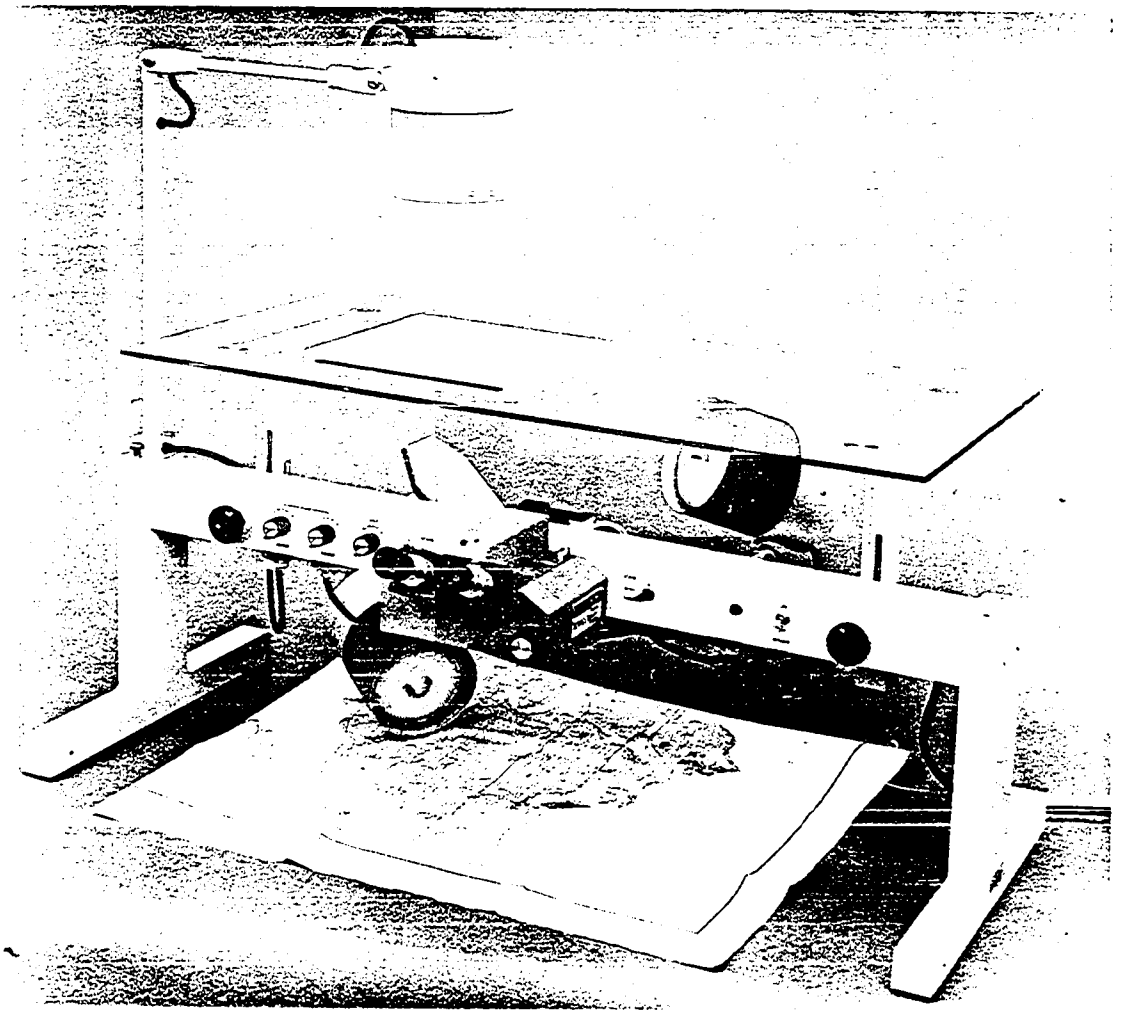

Figure 24. Zoom Transfer Scope (ZTS)

Figure 25. Microdensitometer

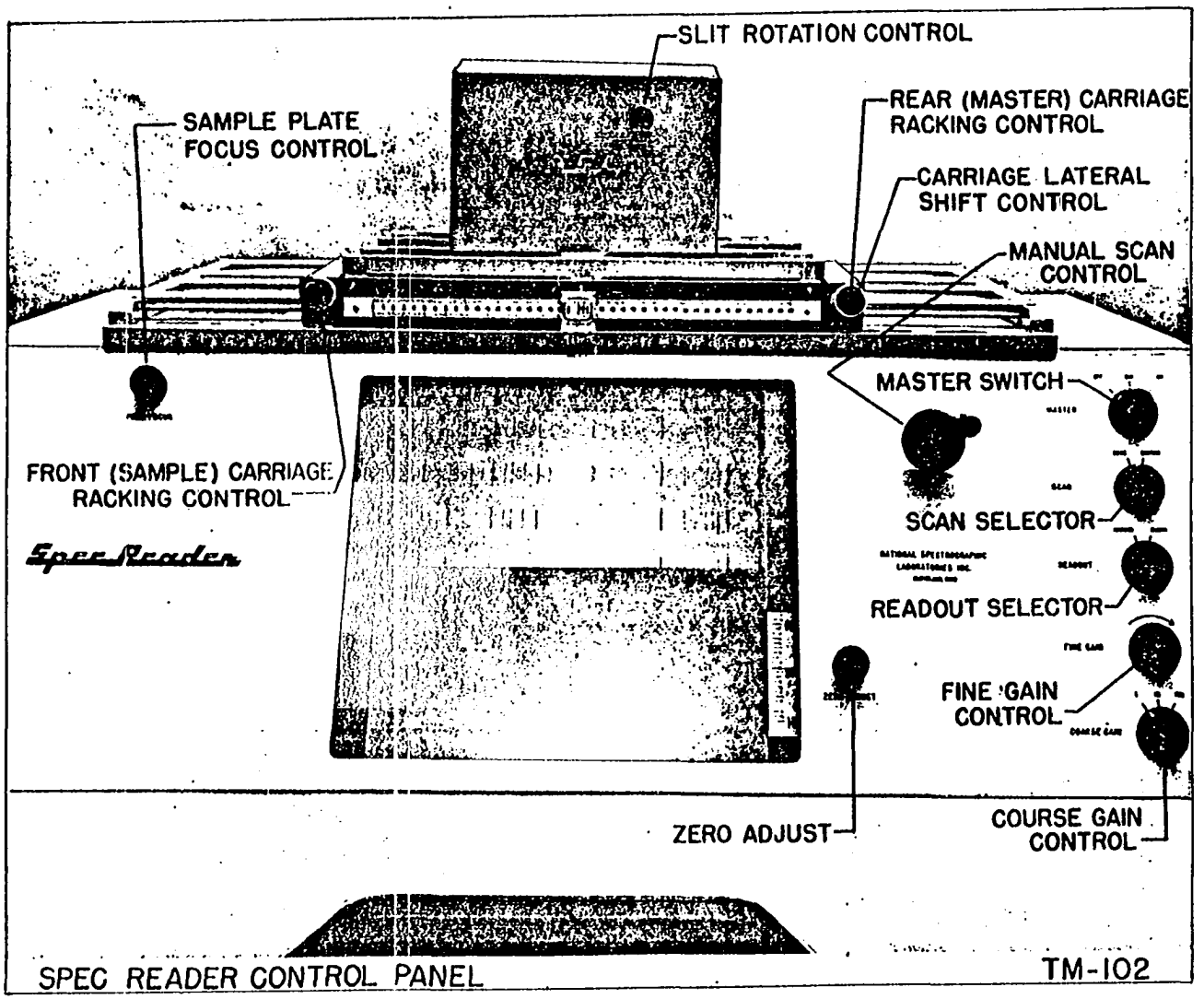

SPEC READER CONTROL PANEL TM-102

- Large viewing screen: the image is projected onto a 35 cm by 30 cm anti-reflection, high contrast screen;
- Magnification: 15X at screen;
- Scanning control: duration of scanning spectra is at operator's discretion with foot-switch control;
- Scanning method: a bright line of light line (slit) at the emulsion--can be rotated for parallel alignment with spectrum;
- Scanning speed: 4.5 microns at the emulsion;
- Slit width: 3, 5, 7, 8, 10, 17 microns at the emulsion.

Additional detailed description of the microdensitometer is found later in this thesis.

Monitoring Soil Moisture

Soil moisture data for the Castana research station in Monona County were obtained for the years 1972 to 1980 (Table 10). These data have been collected for the crop growing season, which is from early May to late August and early September. Only the surface soil moisture is of interest for the purpose of monitoring the soil moisture using LANDSAT images.

Before any correlation between the surface soil moisture data and the surface reflectivities on the satellite images could be verified, the surface reflectivities on these images had to be quantified. Two methods of quantification were designed and tried. The first method was to observe visually the values of different shades of gray on the black and white images of different dates. The second method was to use a microdensitometer to measure the reflectivity of the image along a scan line.

Table 10. Soil moisture data for Castana, Iowa in centimeters

Year	Depth (cm)	May 1	June 1	July 1	Aug. 1	Sept. 1	Oct. 1
1972	0-30	5.00	2.28	0.15	5.00	3.85	5.00
	0-150	22.38	21.03	15.98	18.93	19.93	20.24
1973	0-30	4.60	4.03	1.95	3.75	1.85	5.00
	0-150	24.60	24.03	19.00	16.98	9.70	18.29
1974	0-30	2.53	4.40	0.25	1.88	3.68	1.85
	0-150	17.23	22.40	8.75	2.53	8.13	4.39
1975	0-30	4.38	4.55	3.15	0.00	0.00	1.75
	0-150	21.75	23.43	21.75	6.30	0.83	1.75
1976	0-30	3.25	2.90	0.00 July 26: 0.00	0.00	0.00	1.27
	0-150	15.40	18.25	10.30 July 26: 3.25	2.93	1.25	1.27
1977	0-30	2.50	4.28	3.40	2.60	5.00	5.08
	0-150	9.48	11.55	6.43	5.78	10.00	9.91
1978	0-30	2.88	5.00	0.63	0.28	1.78	3.05
	0-150	19.13	24.58	15.50	8.05	8.18	8.13
1979	0-30	2.50	2.70	2.68	0.73	5.00	2.54
	0-150	19.50	19.95	17.95	9.08	10.65	8.92
1980	0-30	3.38	4.35	2.68	0.00	3.45	1.17
	0-150	14.63	16.35	14.95	2.38	5.13	2.95

Visual quantification of surface reflectivity

The primary step in this part of the study was to decide which band would be most suitable for visual observation. After reviewing different images of different bands, it was determined that the positive print of band 5 was the most suitable type of image to work with in this study. The image scale was selected as 1:500,000. This size was a compromise between the high cost of larger scale photos and the difficulty of working with smaller scale photos. A grid overlay transparency was made (Figure 26) in order to measure the tone of the area within each grid on the image and to assign a relative brightness value to that area. The grid overlay transparencies were designed such that they would represent equal size areas by adjusting their scale to the scale of positive print imagery.

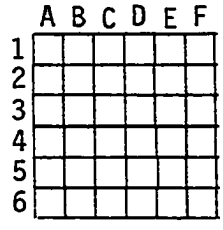

Figure 26. Grid overlay used in visual measurement of image density (actual size 7/8"x7/8")

To do the scale adjustment and location determination, it was first necessary to check and reexamine the scale of each image. The LANDSAT image was imposed on the general highway and transportation map of Monona County using the Zoom Transfer Scope and a distance between two known locations on the image was checked against the distance between the same points on the map. The scale of the image then was examined using the formula:

$$\frac{\text{Scale of the image}}{\text{Scale of the map}} = \frac{\text{Distance on the image}}{\text{Distance on the map}} .$$

Note that, due to the very small scale of the LANDSAT image (nominal 1:500,000), the measurements had to be repeated several times in order to improve the accuracy.

The quantification of reflectivity was begun after preparing the images. The amount of light an image reflects -- in other words, its lightness or darkness -- determined its relative value. Obviously, white reflects the most light. By gradually increasing the amount of black in the reflecting body, less and less light is reflected, until at the extreme, a black object will absorb almost all the light. Value gradations apply equally to the hues between white and black. Hue is what is visualized as a color. Colors are commonly named by their standard hues, as affected by values, such as dark gray or light blue. The hue of a black and white print is gray. To measure different values of gray, a gray scale is needed. The gray scale is a device that helps the interpretator to compare tone values of reflection. The Kodak Gray Scale is a scale that has twenty increments between a nominal "white" of 0.0 density and a practical "black" of 1.9 density. By this scale, perfect (nominal) "black" would have a density of 2.0. For convenience in calculations, the density values on the Kodak Gray Scale were multiplied by 10, so most of the density values from nominal white to nominal black ranged from 0.0 to 20.0.

Before any further discussion about this method is presented, it is necessary to mention an important limitation. Every LANDSAT orbit is unique, and the relative reflectance values for a land cover type are not the same for every scene as they might have been for a previous, or even a

subsequent, scene of the same area. These reflectance values differ because of atmospheric and temporal conditions. For example, reflectance value of a field just after a rain storm might be different than the reflectance value from the same field after a long, dry period. Also, seasonal changes, clouds, fog, and haze cause enough variation in the picture that the analyst must have ground truth for each scene individually. Differences between reflectance values of a field during different moisture conditions are helpful in delineating dry and wet conditions on the image. To cope with all the problems stated above, the gray scale was adapted to each print individually by assigning a value to the "gray" scale printed at the bottom of each image. Table 11 represents the values assigned to the different shades of gray in all images. In general, one can presume that the darker values are related to higher soil moisture and lighter values to lower soil moisture, provided the same soil type exists.

Table 11. Gray scale used to measure reflectivity on LANDSAT image

Value (tone)	Density (darkness)	Possible wetness	Initial
Black	20	High	B20
Dark gray	16	↑	DG16
Medium gray	10	|	MG10
Gray	8	|	G8
Light gray	6	|	LG6
Very light gray	4	|	VLG4
White	0	Low	WO

To calculate the average density within each grid, the percentage of the area of a given tone in that grid was multiplied by the density value assigned to that tone. The average density, thus, is the sum of the results of multiplications for all tones within the grid. The same procedure had to be repeated 36 times (number of grids) in order to cover the area under observation. The average densities within the grids were added and then divided by 36. The result represented the overall density of the area at the time of photography. The results of the measurements are listed in Tables I to VI in Appendix A.

Evaluation of the results Statistical analyses of the data were conducted to find out if there was any relationship between the reflectivity -- visually measured on the images -- and the surface soil moisture. Table 12 is a summary of measured relative darkness values (density) for different dates and their corresponding surface soil moisture.

Table 12. Observed image densities and their corresponding surface soil moisture data

n	Date	Surface soil moisture (cm)	Relative density (darkness)
1	August 8, 1975	0.0	7.4
2	July 30, 1975	0.0	7.6
3	August 14, 1972	4.5	8.0
4	July 16, 1977	3.0	8.3
5	August 21, 1977	4.3	9.8
6	June 24, 1980	3.0	11.5

The sample correlation coefficient, r, as an estimator for population correlation coefficient, ρ, was calculated using the formula:

$$r = \frac{xy}{\sqrt{\Sigma x^2 \cdot \Sigma y^2}} \quad .$$

The calculated r was about +0.52 and to test the hypothesis that the variables are not linearly related, that ρ is zero, the relation

$$t = r\sqrt{\frac{n-2}{1-r^2}} \quad ,$$

which has the t-distribution with n-2 degrees of freedom, was used. To test the null hypothesis (H_0) $\rho = 0$, t was merely evaluated by the above equation, and, compared with the tabular t-values for different significance levels (calculated t for n=6 and r = +0.52), was 1.233. The conclusion about the hypothesis, $\rho = 0$, is summarized below:

Significance level	t-table (df=u)	H_0, ρ=0
20%	1.533	Not rejected
40%	0.941	Rejected

Therefore, it may be stated that, at the 40 percent level, there is no evidence that surface soil moisture and measured density are not linearly related. Figure 27 illustrates surface soil moisture versus measured density values. As it appears in this graph, the data points do not seem to be linearly related. This, plus not rejecting the null hypothesis, $\rho = 0$, at a smaller level of significance, contributes to a poor confidence in the method of analysis.

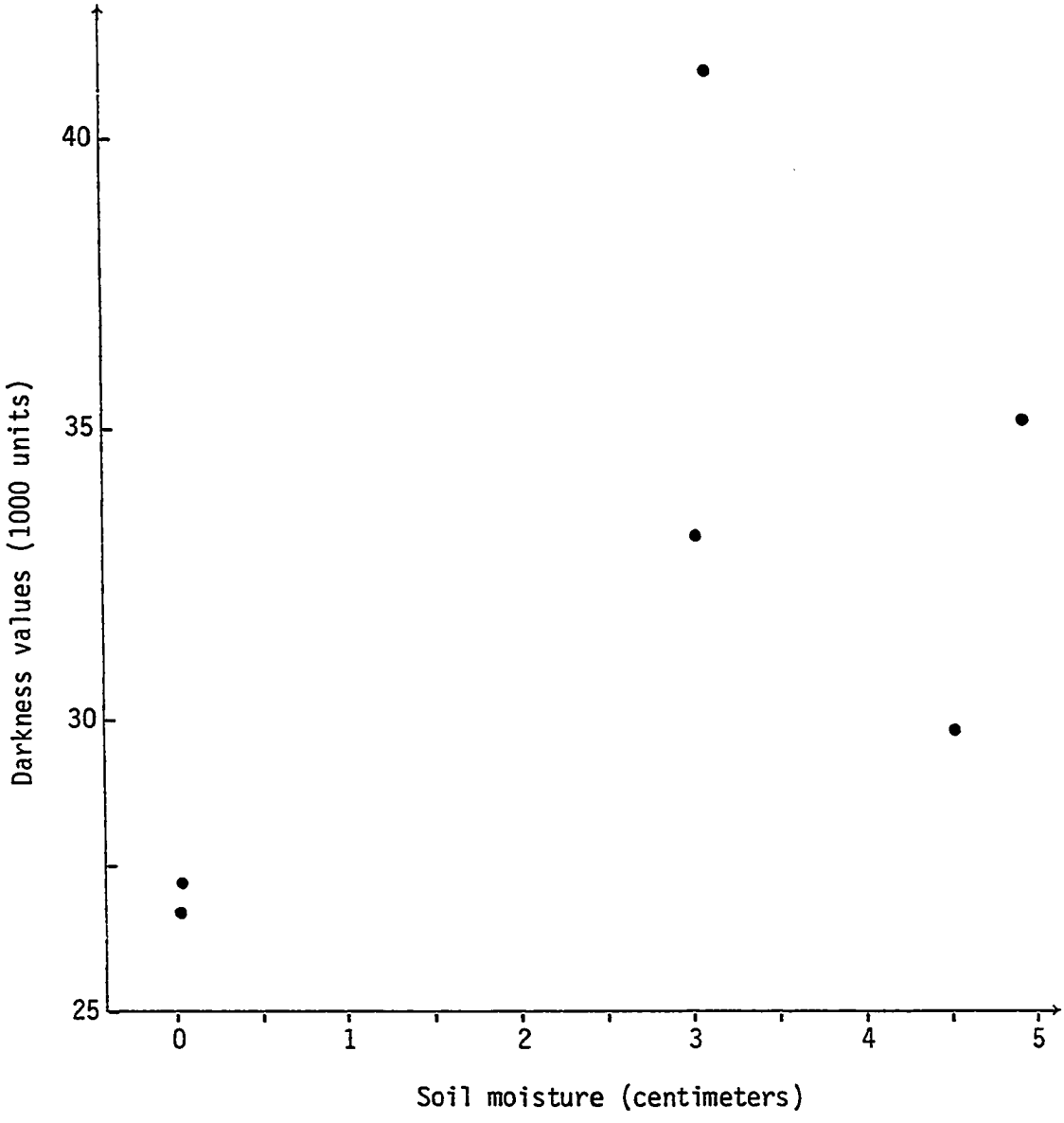

Figure 27. Relation between the visually measured darkness values and soil moisture

Note that these results are applicable only for a given location, in this case, the area under observation. For other areas and under different conditions, the same result may not necessarily be achieved.

Density measurement

A microphotometer (microdensitometer) called a Spec Recorder, a trade name made by National Spectrographic Laboratories (NSL), was used to scan and measure the reflectivity of LANDSAT images. This instrument is very convenient to use and has a remarkably high level of sensitivity in measuring changes in density on an image. This microphotometer measures reflectivity on an area less than 100 square microns or a pixel size of 10 by 10 microns on the image. For an image with the scale of 1:1,000,000, a sensitivity of 10 microns is equal to 10 meters of ground resolution. LANDSAT resolution of 80 meters ensures that every point will be well-covered by the slit width of 10 meters which scans over the image. The instrument has a screen for visual inspection of the image while it is being scanned. The screen magnification is 15X for length or 225 X for area. The scanning speed of the instrument is 4.5 microns (on the image) per second and the distance of scanning is controlled by the operator. A picture of the Spec Recorder is shown in Figure 25.

Methodology LANDSAT's film negatives for 5 different years were used for scanning by the microdensitometer. Two scan lines across these negatives were made, one from east to west and one from north to south (Figure 28). The reflectances of the images were recorded on a strip chart recorder (Figure 29). The noise in the data is caused by the very narrow width of the scanning slit (8 microns), which was one third of the

Figure 28. Scan line directions

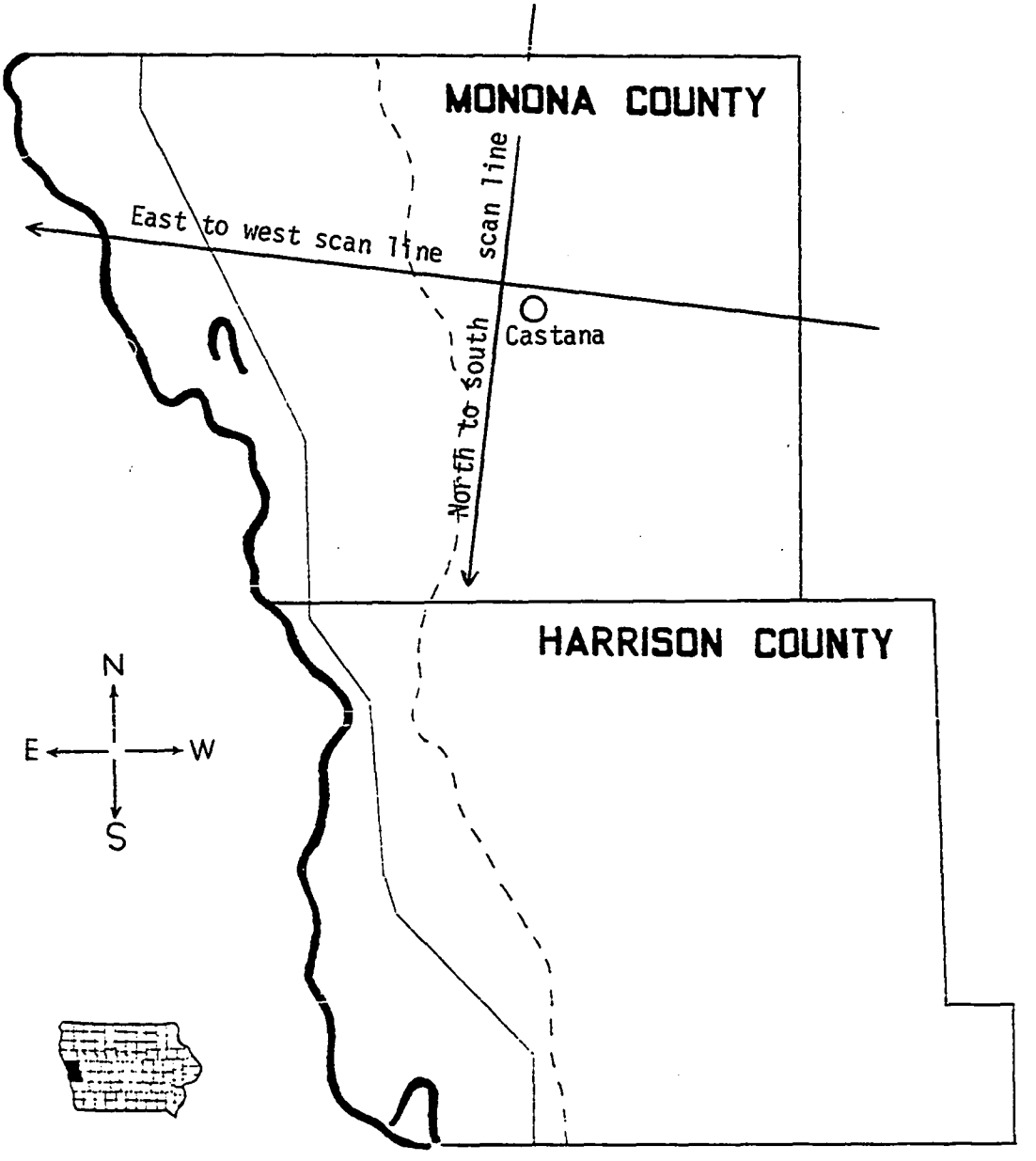
MONONA COUNTY
East to west scan line
North to south scan line
Castana
HARRISON COUNTY
N
E
W
S

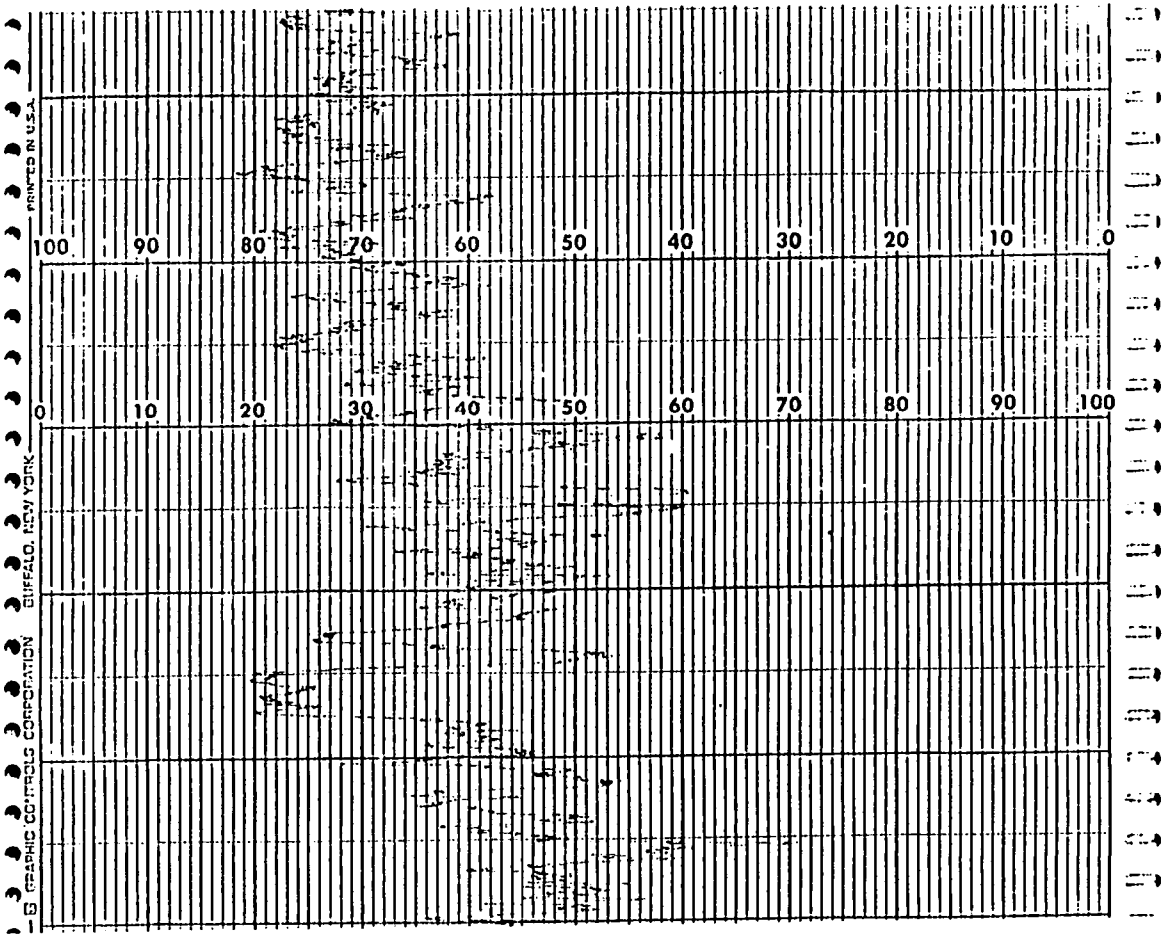

Figure 29. Original chart produced by densitometer

pixel size of the LANDSAT image (the nominal scale of film negative was 1:3,369,000). To reduce these variations in the graphs, the data were manually digitized every other 2 millimeters and a moving average of 4 consecutive readings were plotted (Figures 30 to 34). These graphs are the result of east to west scanning. Since the readings were corrected relative to the "black" scale (zero reflectivity), they were termed "relative reflectivity." Note that, since negative transparencies were used, the redrawn graphs are the inverse of what the original (uncorrected) graphs were on the chart records, i.e., the 100 percent line on the chart was considered as a base line (zero percent). For example, if the "relative reflectivity" of a point on the original chart record was 60 percent, it was converted to 40 percent on the corrected graph. When these graphs are being superimposed, they can represent general soil moisture conditions for the time when the images were taken. A greater reflectance is expected when surface soil moisture is lower.

Repetitive measurements were made to observe the effect of magnification changes on the results of scanning. It was learned that the result of the microdensitometer readings did not change significantly when the scale or magnification of images were changed.

Evaluation of the results Statistical inferences were used to analyze the results obtained from microspectrometer scanning. The analysis was based on the relative reflectance values obtained for different dates. These values and the surface soil moisture data corresponding to the date of images are listed in Table 13. The sample correlation coefficient r was calculated to be -0.9985 from data in Table 13. This can be assumed

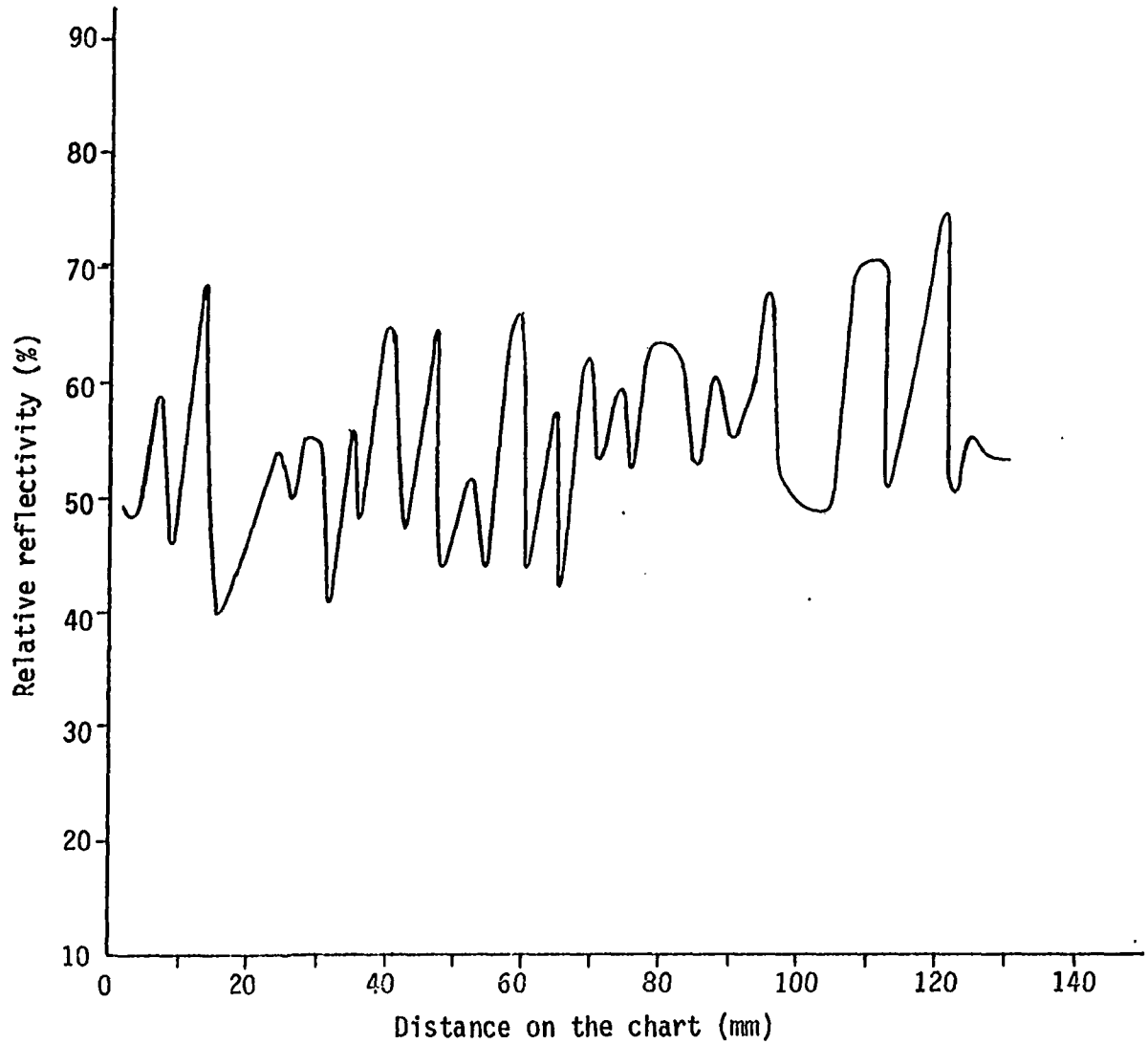

Figure 30. Recorded relative reflectivity of east to west scanning of 20 August 1976 image

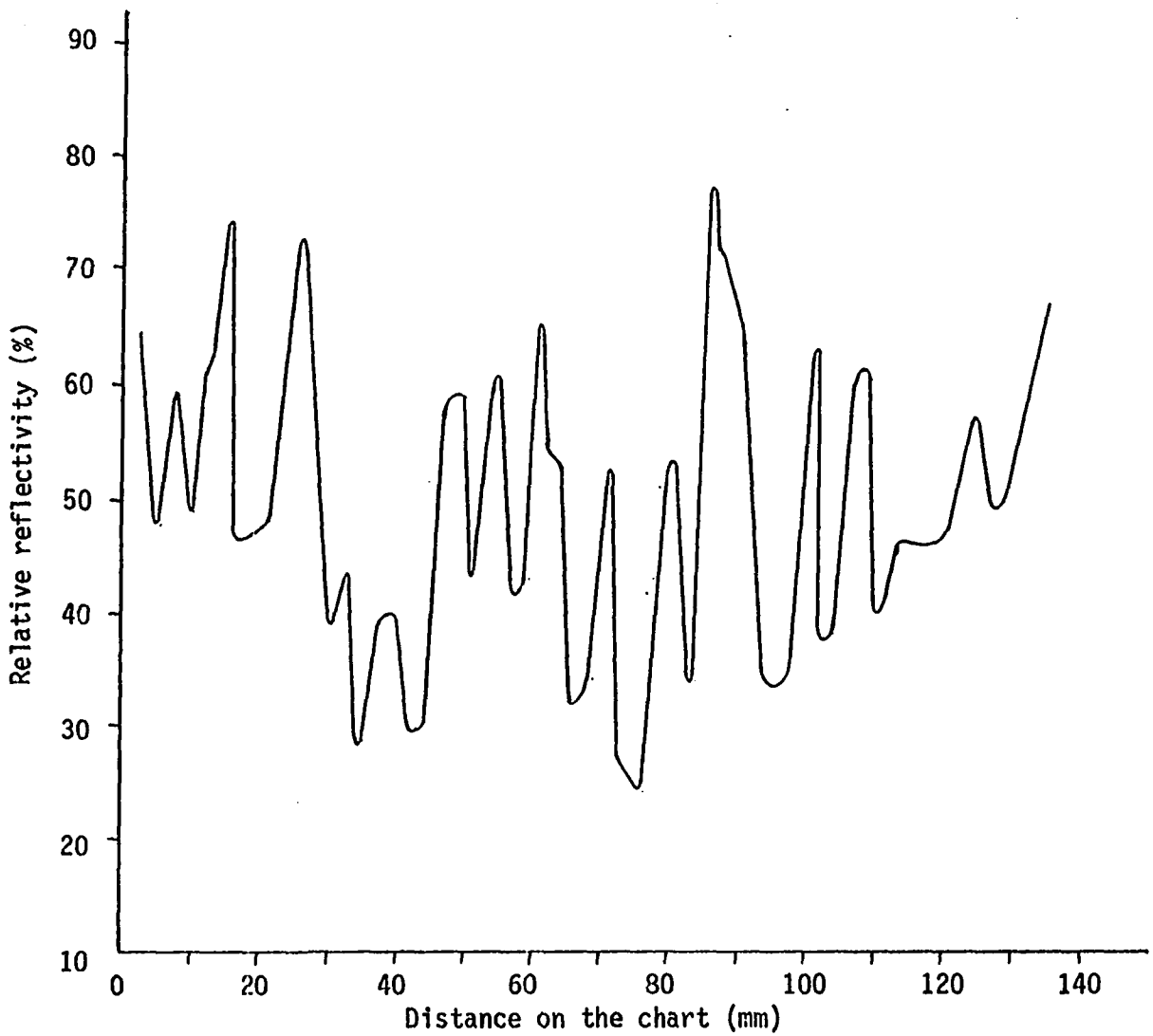

Figure 31. Recorded relative reflectivity of east to west scanning of 29 June 1974 image

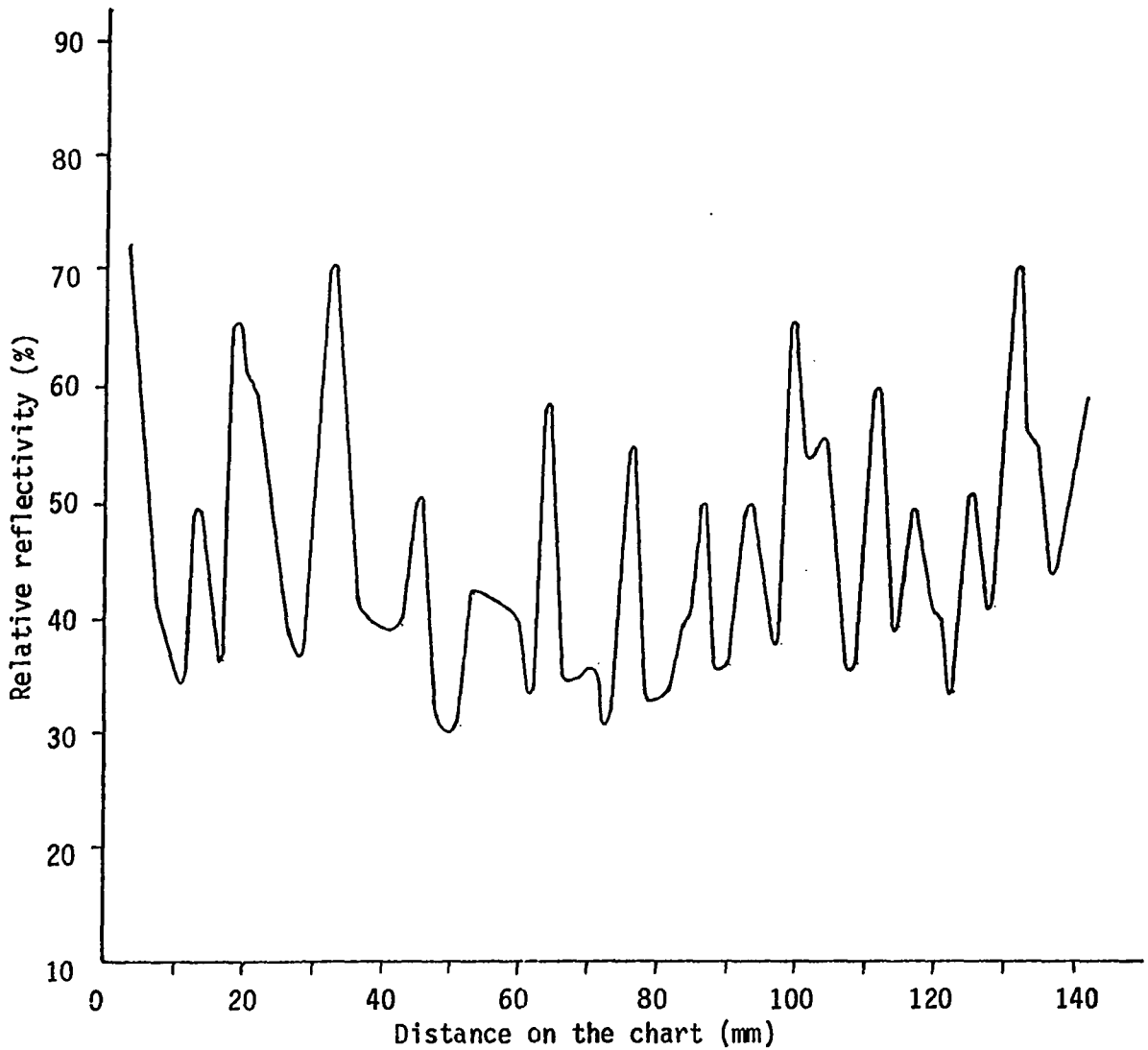

Figure 32. Recorded relative reflectivity of east to west scanning of 22 September 1975 image

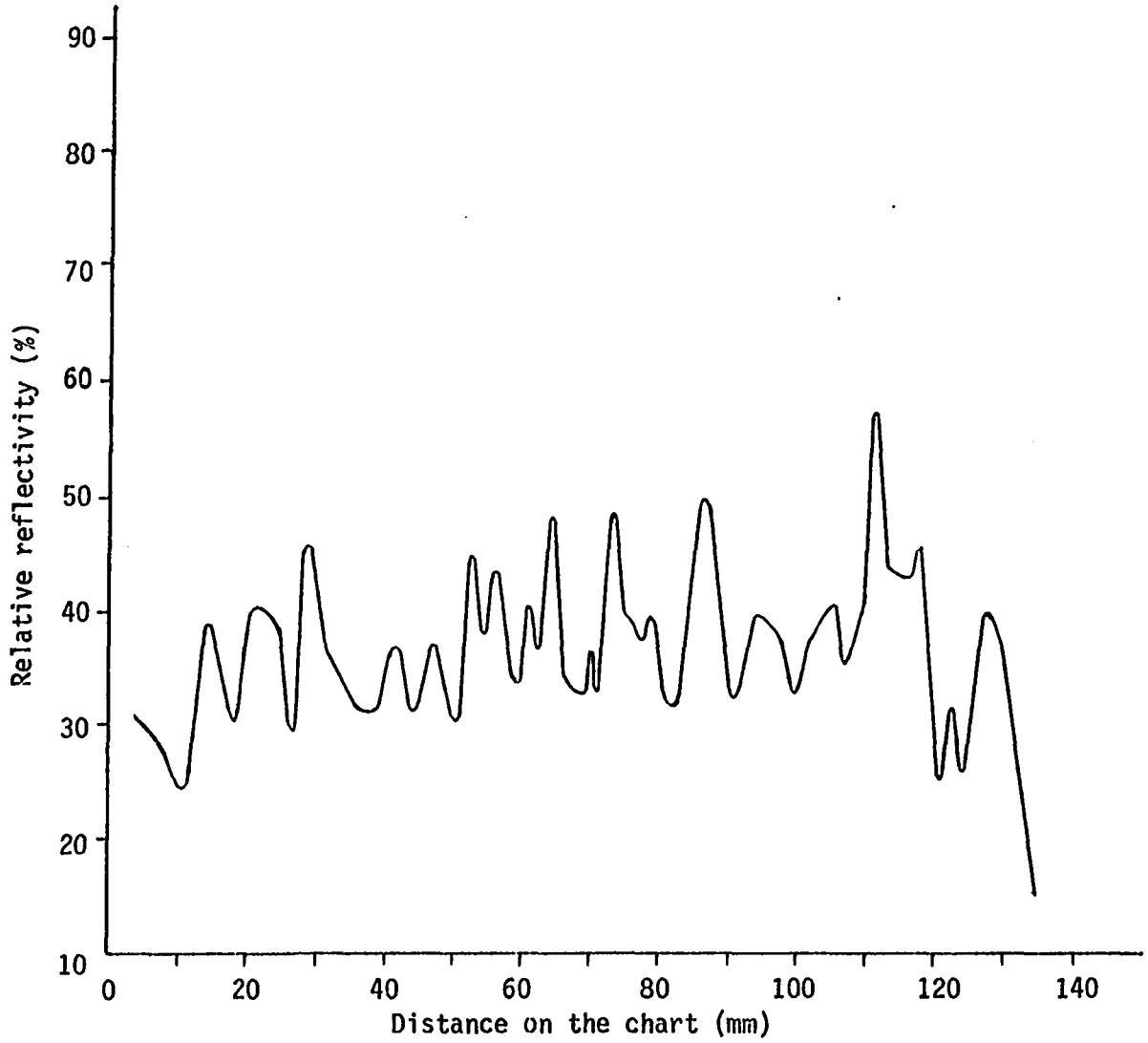

Figure 33. Recorded relative reflectivities of east to west scanning of 28 September 1979 image

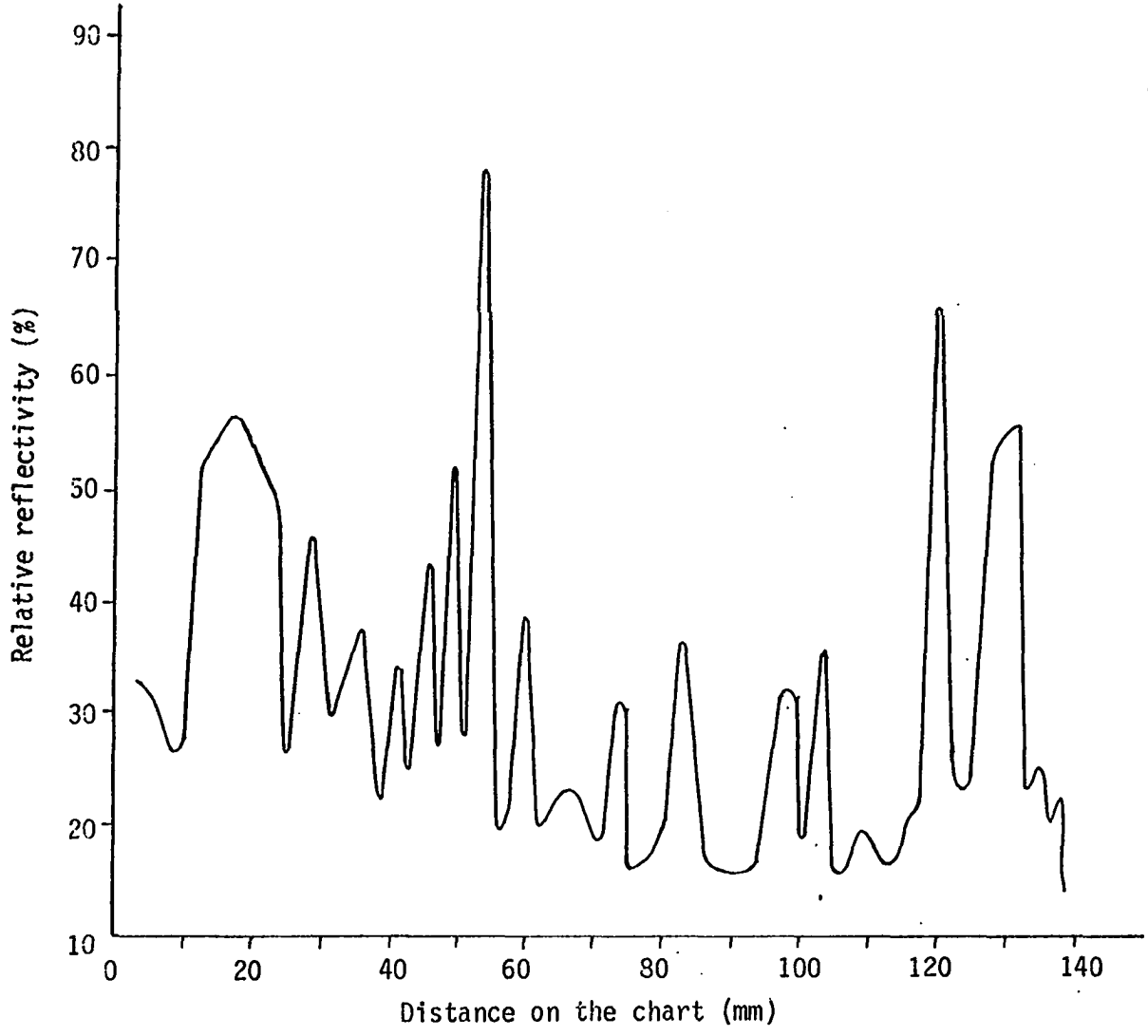

Figure 34. Recorded relative reflectivity of east to west scanning of 8 June 1978 image

Table 13. Measured image reflectances and their corresponding surface soil moisture

n	Date	Surface soil moisture (cm)	Average relative reflectance (%)
1	20 August 1976	0.00	52
2	29 June 1974	0.4	50
3	22 September 1975	1.30	45
4	28 September 1979	2.80	39
5	8 June 1978	4.0	33

as a strong indication of a linear relation between the surface soil moisture expected since the higher soil moisture is associated with lower reflectivity. The test of null hypothesis was used here again to evaluate the results. The calculated t for $r = -0.9985$ and $n=5$ is 31.5526. The tabulated t statistic at a 1 percent level of significance for 3 degrees of freedom is 5.841. Therefore, the null hypothesis, $\rho=0$, is rejected. Thus, it can be stated at this level (1%) that there is no evidence that there is no linear relation between the measured relative reflectivity and the surface soil moisture. The arrangement of the data is shown in Figure 35. The frequency distribution of measured relative reflectivities for images of different dates have been plotted in Figures 36 to 40. In these graphs, the higher relative reflectivities are more frequent for dryer soil and the lower reflectivities are more frequent for higher soil moistures. A comparison of all five samples (Figure 41) shows that the peak frequency of such sample falls in the reflectivity region that represents the soil moisture level for that sample, i.e., for the higher surface soil moisture, the peak is in the lower reflectivity region and vice versa.

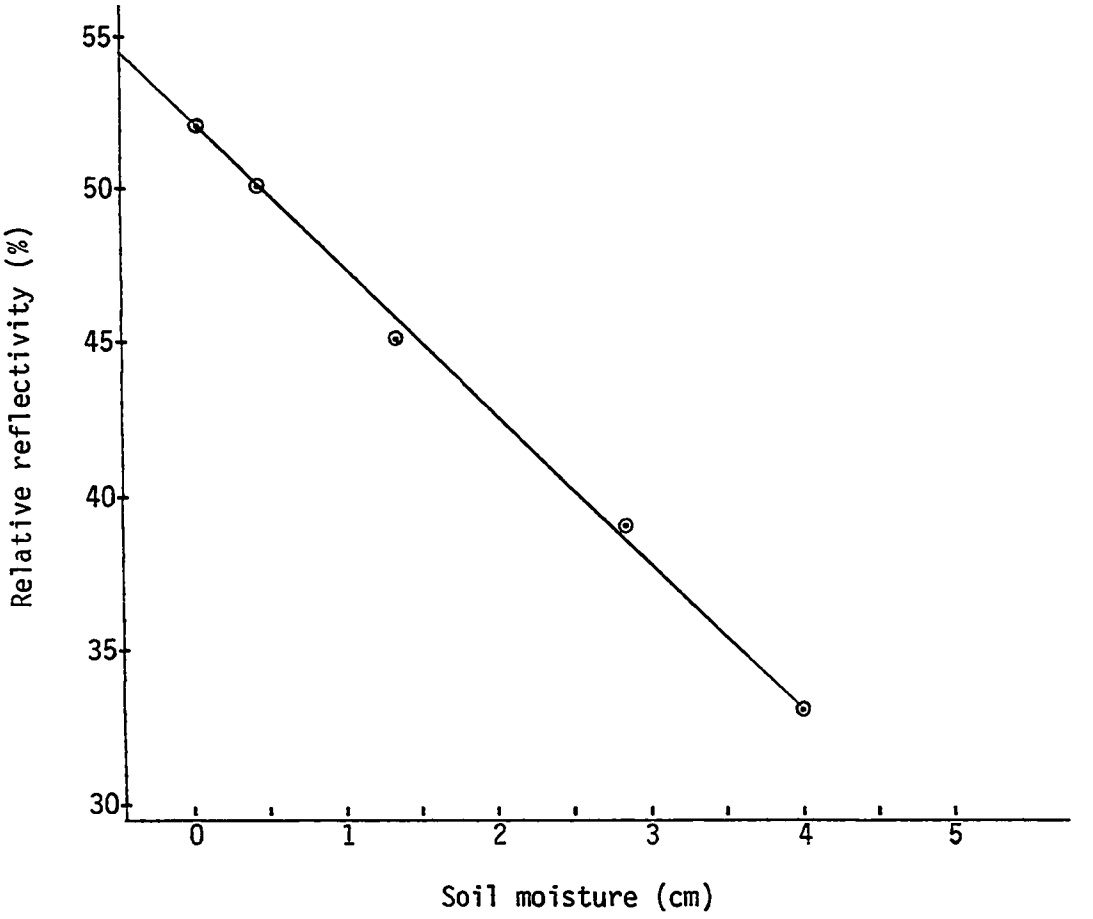

Figure 35. Relation between the soil moisture and the measured relative reflectivity

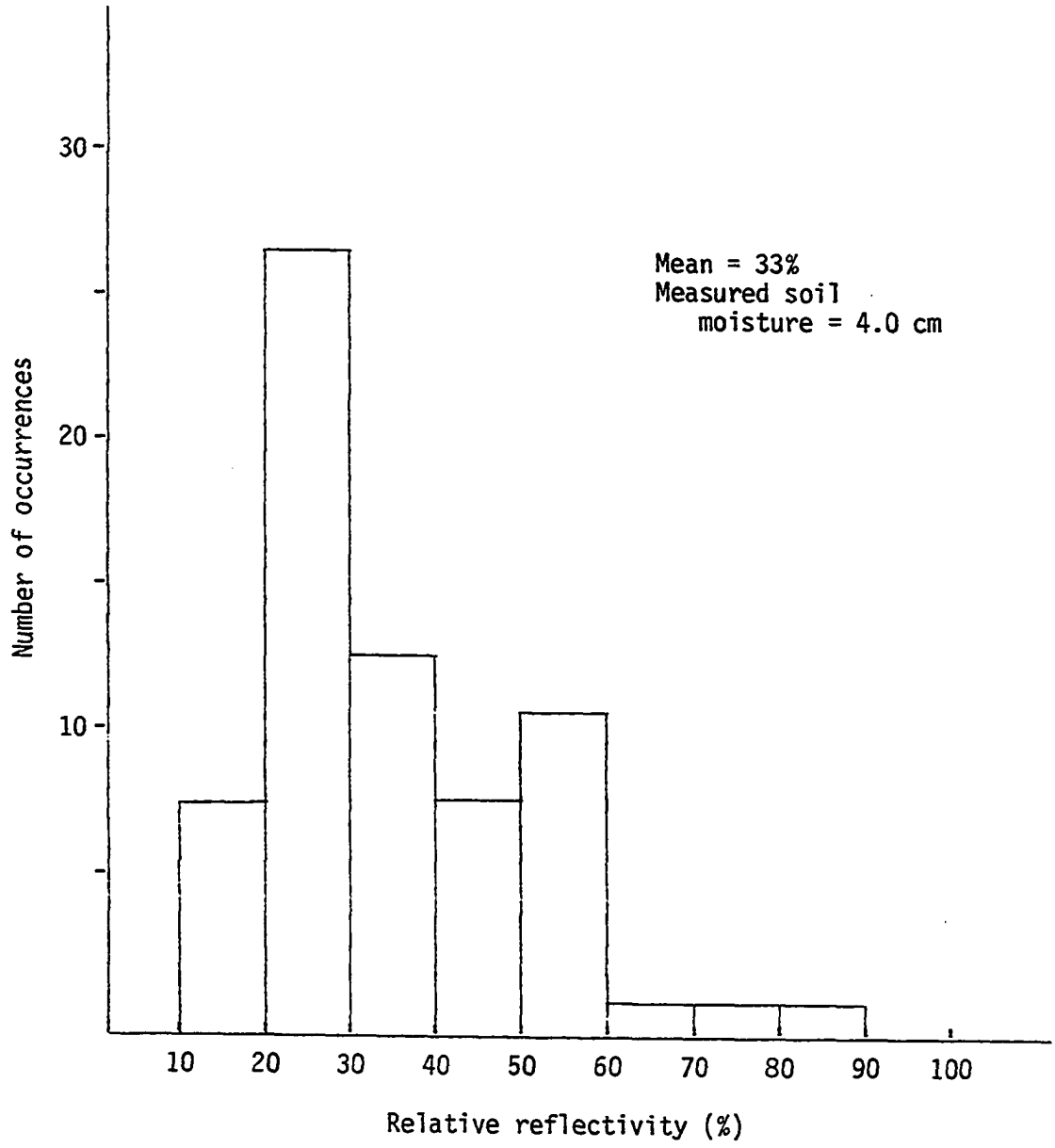

Figure 36. Distribution of relative reflectivities measured from north to south scanning of July 8, 1978, image

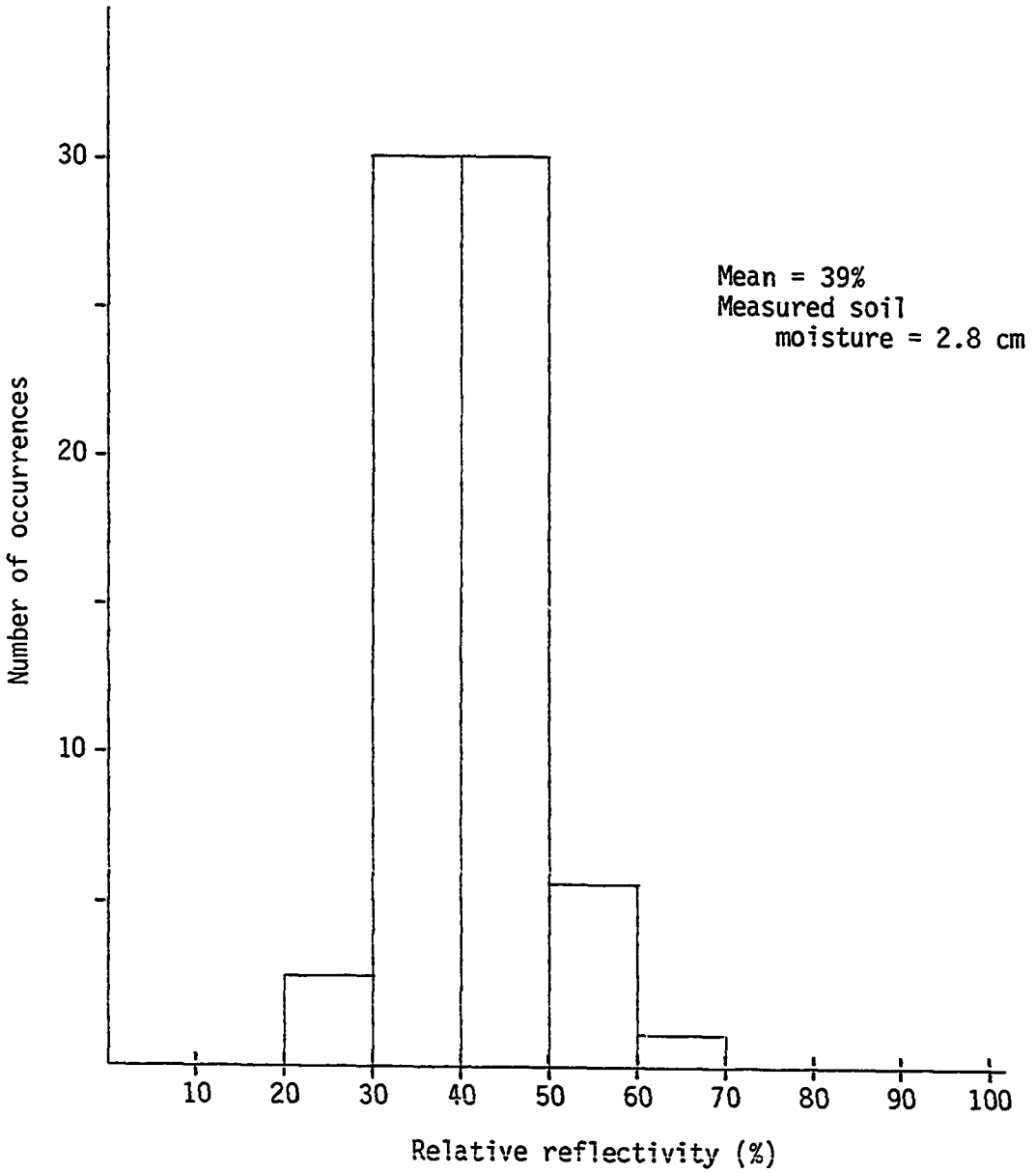

Figure 37. Distribution of relative reflectivities measured from north to south scanning of 28 September 1979 image

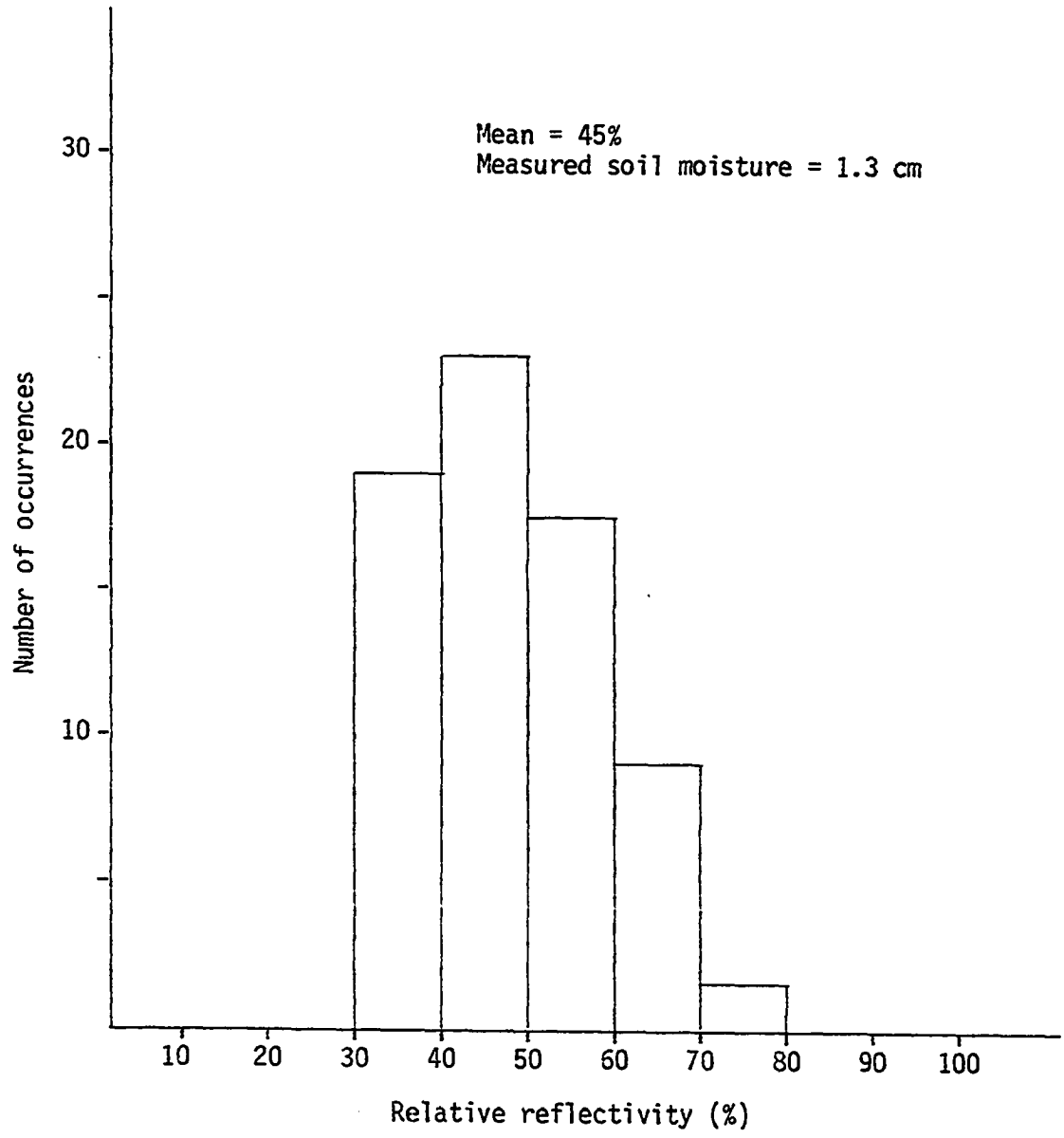

Figure 38. Distribution of relative reflectivities measured from north to south scanning of 22 September 1975 image

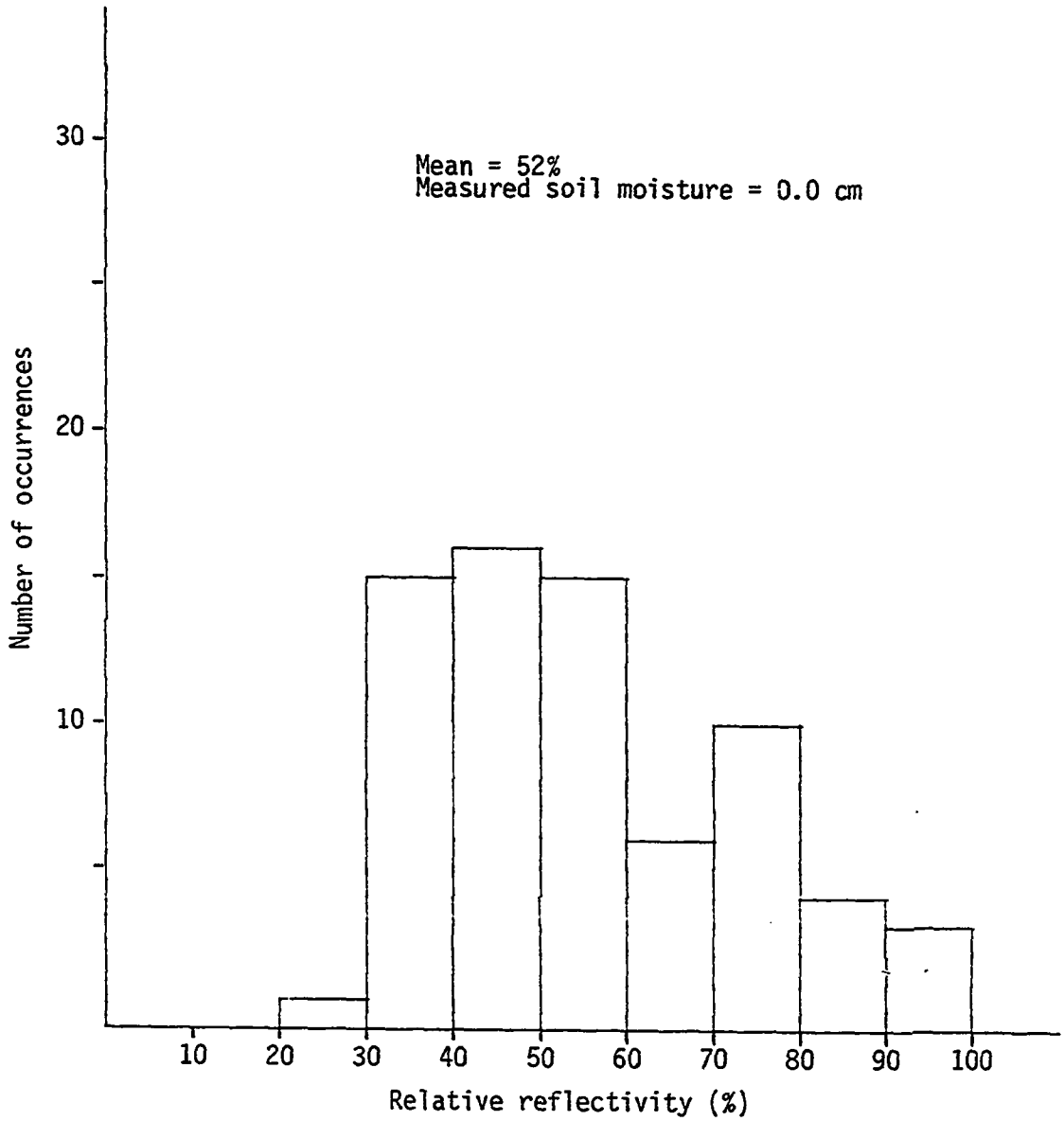

Figure 39. Distribution of relative reflectivities measured from north to south scanning of 20 August 1976 image

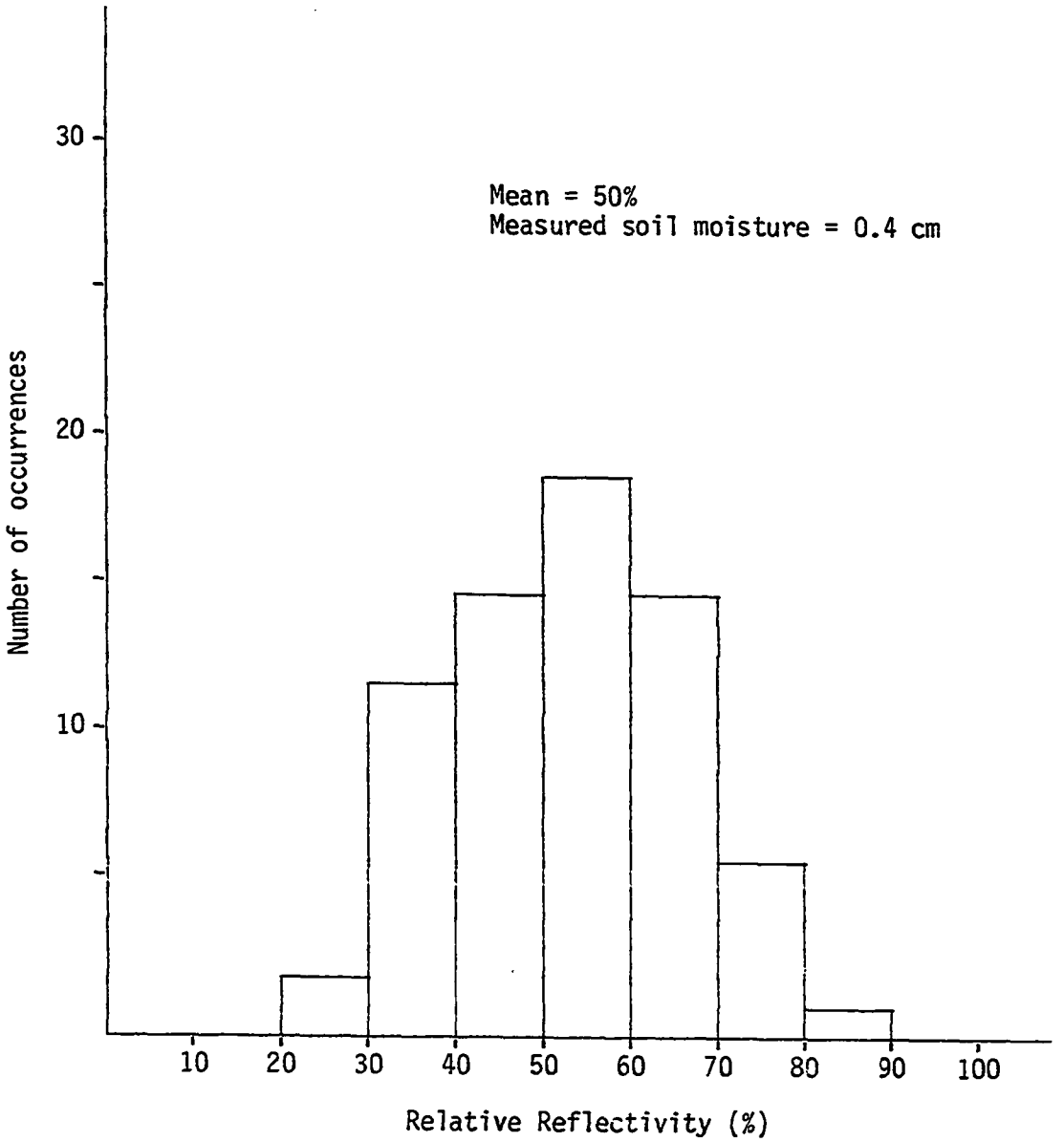

Figure 40. Distribution of relative reflectivities measured from north to south scanning of 29 June 1974

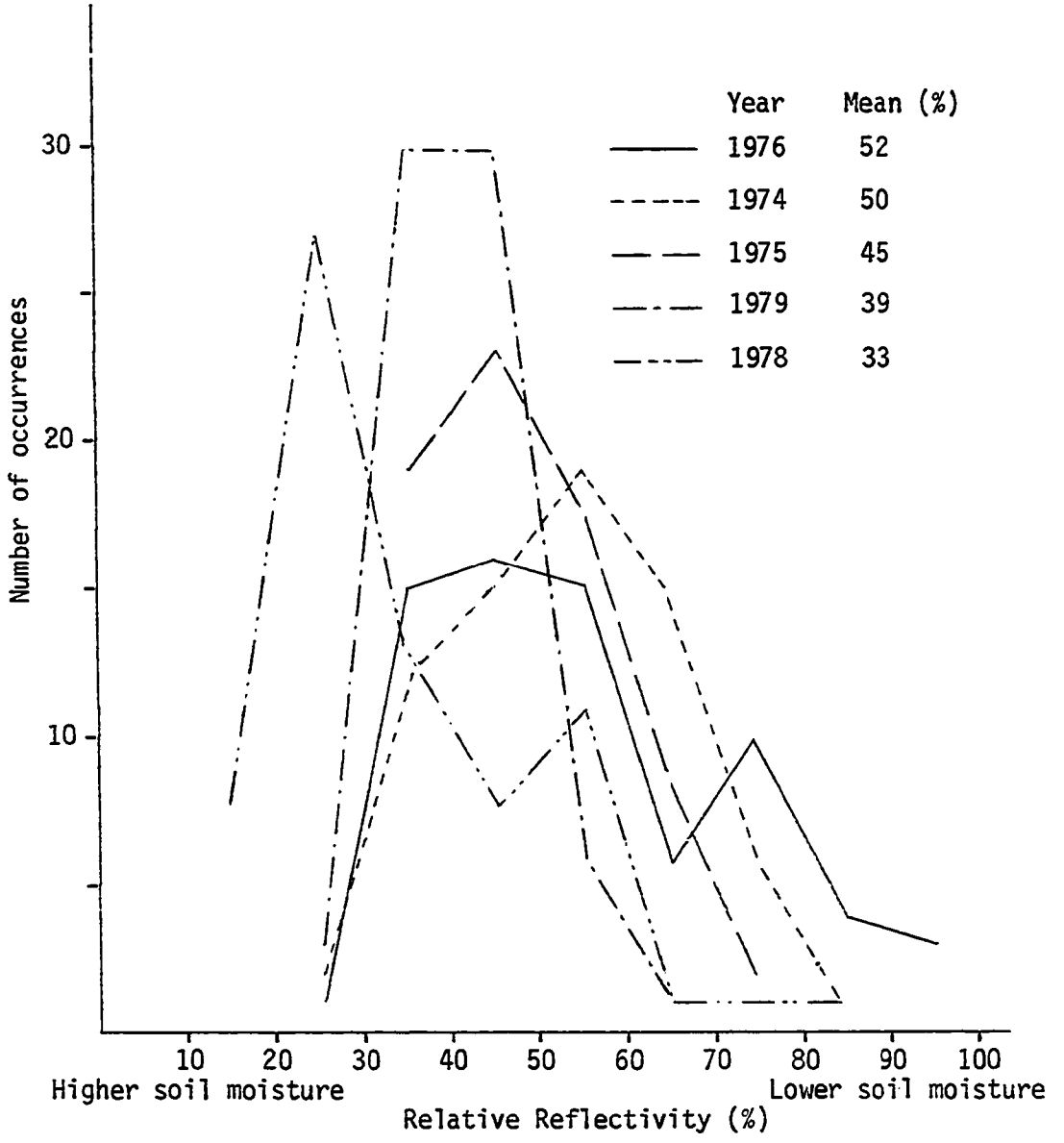

Figure 41. Comparison of distribution of relative reflectivities measured from north to south scanning at different images of different dates

Most of the curves show a positive skew in that their mode is less than their mean. The relative reflectivities for the various years show that, though there are times when soils were drier, light absorption and scattering by the surface cover provides a darker background than that expected for a perfectly dry-bare soil, resulting in the distribution of relative reflectivities shown on Figure 41. The soil color itself also contributes to a darker image. In planes where the soils are rich in organic materials, the soils tend to be dark in color, and this must not be mistaken for a high moisture level.

The highest surface soil moistures among the data were found in 1978 and the lowest soil moistures were for 1976. To check if the scanning method using the microphotometer can separate the relative reflectivities on the images for these two dates distinctly, the inverse relative reflectivities (relative reflectivity of a negative film) measured on each image were plotted in Figure 42. The values used to draw this figure were derived from data obtained by the east-west scanning (Figure 28). As it is apparent on the graph, the 1976 data are very distinct from those of 1978. The measured reflectivities by densitometer are listed in Appendix B.

Irrigated Lands Measurement

Factors affecting the interpretation of irrigated areas

Plant physiology Chlorophyll is highly absorbent of the red light from the spectrum. Photosynthesis is more active in nonstressed growing plants than in plants suffering moisture stress. Thus, irrigated crops such as corn and soybeans, which may be growing more actively than those that are nonirrigated, absorb more red light. Thus, the nonirrigated

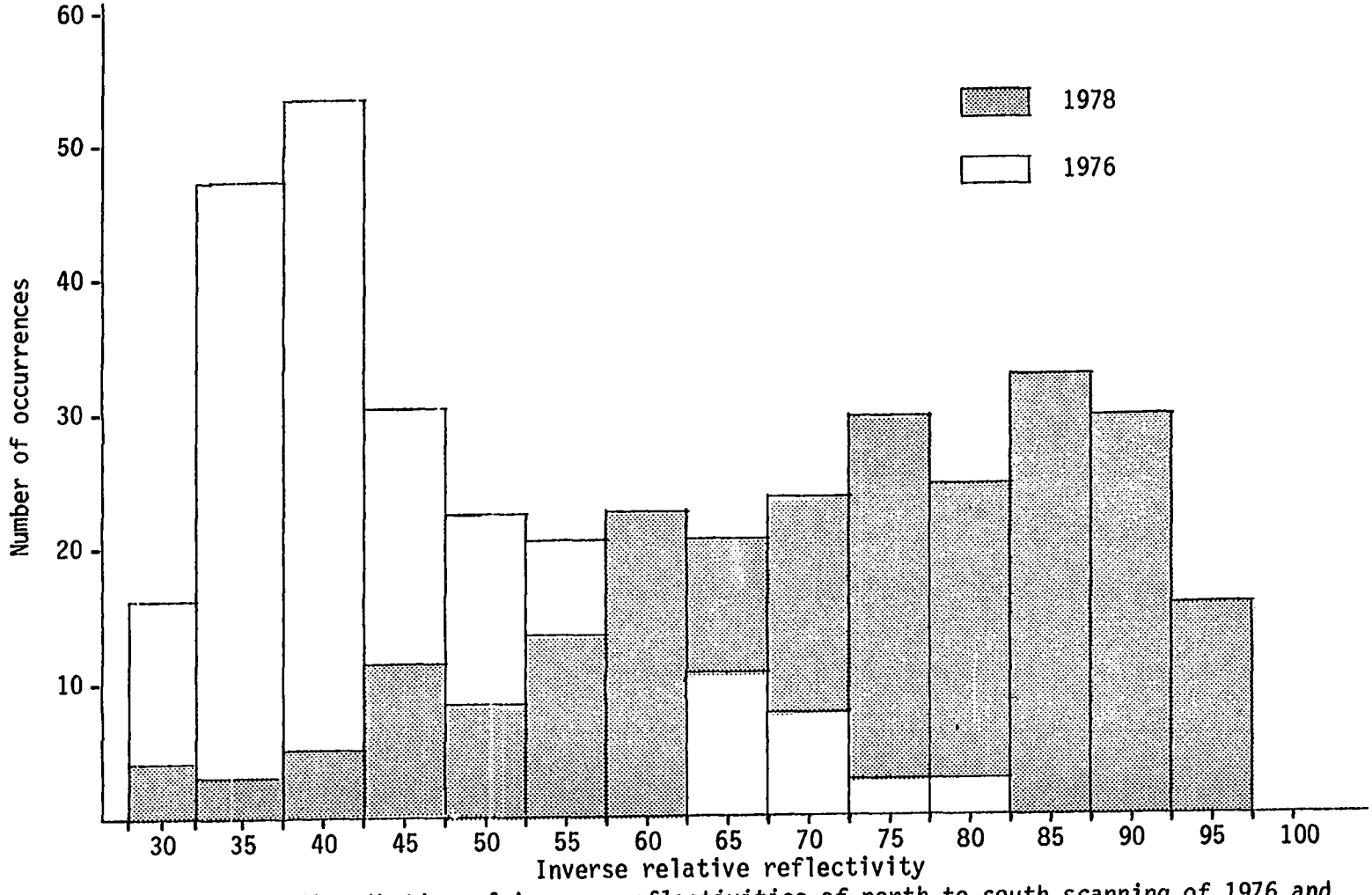

Figure 42. Frequency distribution of inverse reflectivities of north to south scanning of 1976 and 1978 images

crops tend to reflect more red light than irrigated crops, provided moisture is limited. This provides a contrast between irrigated and nonirrigated lands in the red range of light spectrum. Reflectivity of light is monitored by band 5 in the LANDSAT image. Band 5 was used to try to measure irrigated lands in western Iowa.

Water budget An average water budget for Des Moines is shown in Figure 43. Between October and May, the actual and potential evapotranspiration are equal because adequate moisture is available and the potential evapotranspiration is low. From June through September, potential evapotranspiration exceeds the available moisture and the actual evpotranspiration may be less than potential. Moisture demands by the crops and other vegetation exceed precipitation during this period, requiring soil moisture reserves to make up the difference. If the soil moisture reserves are not adequate, supplementary irrigation is required to maintain high crop yield. Irrigation is normally practiced during this time of water deficiency. For the Des Moines area, one would expect the highest intensity of irrigation to occur during July if the irrigation could be exercised there. The expected time of irrigation application is a major factor in selecting the images for analysis. In western Iowa, the irrigation season usually starts in early July and continues to the end of August. Thus, images for this study were selected between these months.

Precipitation Precipitation during the growing season is another factor to be considered when studying irrigated lands. It is important to be able to differentiate an active crop due to irrigation from an active crop due to natural precipitation and soil moisture.

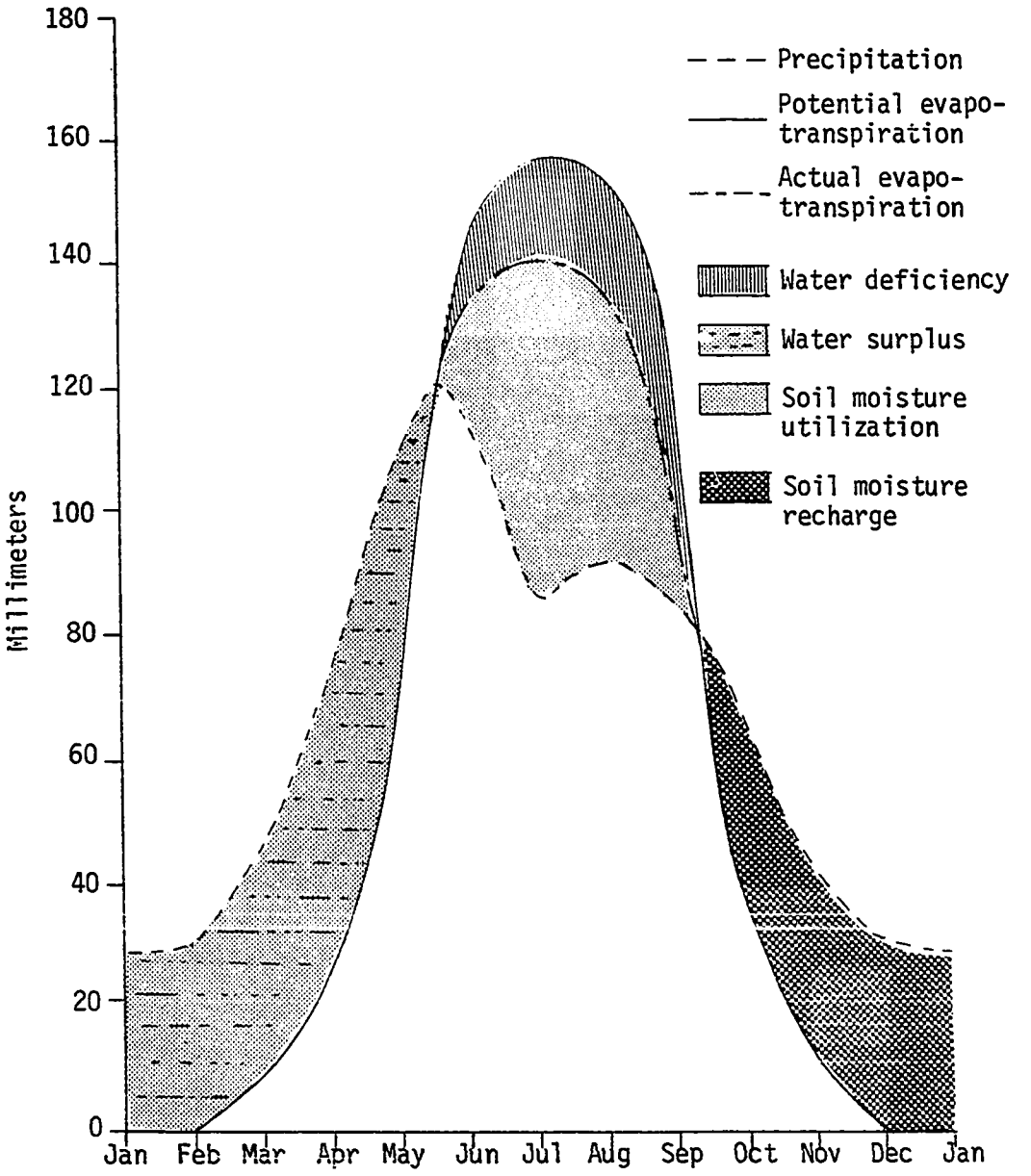

Figure 43. Water budget for Des Moines (Iowa Natural Resources Council, 1978)

There is no point in looking for a differentiation between irrigated and nonirrigated lands immediately after precipitation events. The date of the image should be as long after the last precipitation as possible when unirrigated fields are dry and will contrast with irrigated fields on the images. Thus, those images should be selected at a time when no rain has occurred.

Table 14 lists the precipitation during the growing season for the Castana research station in Monona County. These data were used in the selection of LANDSAT images for use in this study.

Soil temperature The soil temperature is a parameter that should be considered for a better interpretation work. Table 15 shows the near-surface soil temperatures for the Castana station during the months of June, July and August, 1979. Higher soil temperature tends to give a lighter background on the image, due to a higher brightness temperature caused by the higher surface temperature. Thus, the higher surface temperature provides a better contrast between the irrigated and nonirrigated lands.

In summary, it can be said that any factor which affects the soil moisture influences the tone of the image on which differentiation between irrigated and nonirrigated crop lands is based. For this reason, it is advised that the soil mositure data be checked in addition to the factors explained earlier.

Table 14. Precipitation data of growing season for Castana, Iowa, in centimeters

Day	1972					1973				
	May	June	July	August	September	May	June	July	August	September
1	4.98	--	--	1.85	0.48	--	--	--	--	--
2	0.80	--	2.33	--	--	1.00	0.25	1.95	--	--
3	--	--	--	--	--	--	--	0.63	--	0.18
4	--	0.65	--	--	0.80	--	0.78	--	--	--
5	0.15	--	--	--	--	--	0.20	--	--	--
6	4.68	--	1.63	--	0.05	0.15	--	--	0.03	
7	--	--	--	--	--	3.03	--	--	--	--
8	--	--	--	2.15	--	--	--	--	3.55	--
9	--	--	--	--	--	0.25	--	2.30	--	--
10	--	0.30	--	--	2.38	0.45	--	--	--	--
11	0.53	--	1.45	0.18	3.73	--	--	--	0.23	--
12	0.88	--	1.80	--	3.63	--	1.18	--	--	--
13	0.20	0.18	--	--	--	--	--	--	0.85	--
14	0.23	1.80	0.38	--	--	--	--	--	--	--
15	--	--	0.13	--	--	--	1.00	--	--	2.45
16	--	0.30	--	--	--	--	--	--	--	--
17	--	--	5.30	--	--	--	--	--	--	0.93
18	--	--	--	--	--	--	2.83	0.05	--	--
19	--	0.65	--	--	--	--	--	--	0.13	--
20	--	--	--	--	1.15	--	--	0.98	--	--
21	--	--	--	0.33	--	--	--	1.93	--	--
22	--	--	--	0.05	--	--	--	--	--	--
23	0.40	--	--	0.63	--	--	--	--	--	--
24	0.13	0.20	0.20	--	--	0.30	--	1.93	--	--
25	--	0.25	--	2.23	0.60	--	--	--	--	0.43
26	0.30	--	2.80	--	--	3.10	--	--	--	6.55
27	0.20	--	--	--	--	4.13	--	--	--	--
28	--	--	--	--	--	--	--	--	--	3.18
29	--	--	--	--	0.55	0.23	--	0.20	--	--
30	--	--	--	0.88	--	--	0.28	2.25	--	--
31	--	--	0.18	--	--	--	--	--	1.58	--

Table 14. *Continued*

Day	1974					1975				
	May	June	July	August	September	May	June	July	August	September
1	--	--	--	1.88	--	0.13	0.05	--	--	--
2	--	0.13	--	--	0.73	1.33	--	--	1.08	--
3	--	--	0.85	--	--	--	--	--	--	0.50
4	--	--	--	--	--	--	0.98	--	--	0.95
5	--	--	--	--	--	--	--	0.08	--	0.13
6	--	1.28	--	--	--	--	--	--	--	--
7	0.45	0.85	--	--	0.08	0.35	--	--	--	--
8	0.55	--	--	1.50	--	--	0.20	--	--	--
9	0.13	1.40	--	5.43	--	--	0.85	--	--	--
10	--	0.10	0.13	2.30	--	--	--	--	0.50	--
11	--	0.05	0.43	--	--	0.45	0.80	0.18	0.20	1.30
12	--	--	--	--	1.40	--	0.20	--	0.18	--
13	0.78	0.15	--	5.35	--	--	--	--	--	--
14	--	0.08	--	1.13	--	--	0.50	--	--	--
15	--	--	--	0.30	--	--	--	--	--	--
16	0.98	--	--	0.08	--	--	0.95	--	0.53	--
17	--	--	--	1.03	--	--	--	--	--	--
18	5.38	--	--	--	--	--	0.50	--	2.83	0.40
19	1.98	--	--	--	--	--	--	0.90	--	--
20	--	--	--	--	--	--	1.65	--	--	--
21	1.83	--	--	0.68	--	--	--	--	--	--
22	--	0.80	--	--	--	--	0.55	--	--	--
23	--	--	--	--	--	0.65	0.20	1.83	--	--
24	--	--	--	--	--	--	0.08	0.15	0.90	--
25	0.40	--	0.15	--	--	--	--	--	--	--
26	--	--	--	--	--	0.63	0.08	--	--	--
27	0.13	--	--	1.50	--	--	--	--	--	--
28	--	--	--	--	--	3.78	--	--	0.20	0.33
29	2.60	--	--	--	--	--	--	--	0.18	--
30	0.15	--	--	--	--	--	--	--	--	--
31	--	--	--	--	--	--	--	--	--	--

Table 14. *Continued*

Day	1976					1977				
	May	June	July	August	September	May	June	July	August	September
1	--	--	--	--	--	--	--	1.08	0.45	--
2	--	--	--	--	--	0.40	--	0.23	--	--
3	--	--	--	--	--	0.08	0.20	--	0.03	1.20
4	--	--	--	--	--	1.15	--	--	--	--
5	--	--	--	0.08	--	--	--	--	0.40	--
6	--	--	--	--	--	1.03	--	--	--	--
7	--	--	--	--	--	--	--	--	--	0.78
8	--	--	--	--	0.53	--	--	--	0.70	--
9	--	--	--	--	--	--	--	--	3.10	1.30
10	--	--	--	--	--	--	--	--	0.08	--
11	--	--	--	--	--	--	0.25	2.83	--	--
12	1.45	--	--	--	--	--	--	--	--	1.20
13	--	--	--	--	1.85	--	1.53	--	--	--
14	--	--	--	1.13	--	--	--	--	--	--
15	--	--	--	--	--	0.33	--	0.35	4.00	--
16	0.73	--	--	--	--	--	2.00	--	--	--
17	--	0.10	--	0.55	--	--	0.50	3.13	--	0.25
18	--	--	--	--	--	0.08	--	--	--	--
19	--	--	--	--	1.05	0.80	--	--	--	--
20	--	--	--	--	--	--	--	0.03	--	--
21	--	--	--	--	--	0.88	--	3.33	--	--
22	6.58	--	--	--	--	1.03	0.13	--	--	--
23	2.50	--	--	--	--	--	--	--	--	1.75
24	--	0.30	--	--	--	--	1.53	2.68	--	--
25	--	--	--	--	0.38	--	--	--	0.08	--
26	--	0.45	0.13	--	0.15	--	--	--	--	--
27	--	--	0.10	--	0.10	2.65	--	--	--	--
28	--	--	0.35	--	--	--	0.15	--	--	0.08
29	--	--	0.50	--	--	--	--	--	--	0.83
30	--	--	--	--	--	0.08	--	--	--	0.18
31	--	--	--	--	--	--	--	--	7.35	--

Table 14. *Continued*

Day	1978					1979				
	May	June	July	August	September	May	June	July	August	September
1	--	0.23	0.25	--	--	--	--	--	--	5.43
2	--	--	--	2.16	0.10	3.10	--	--	--	--
3	--	--	--	--	--	--	--	--	--	--
4	--	0.08	--	--	--	--	0.69	--	--	--
5	--	--	--	--	--	--	--	--	--	--
6	--	--	0.58	--	--	--	--	--	--	1.76
7	2.46	--	4.42	--	--	--	--	--	--	--
8	0.05	--	--	--	--	--	0.43	--	--	0.79
9	--	--	--	--	--	0.76	1.83	--	--	--
10	--	--	--	--	--	--	0.41	--	--	--
11	--	--	--	--	--	--	--	--	--	--
12	--	--	0.92	--	2.82	--	--	--	--	2.21
13	0.43	--	--	--	13.74	--	--	--	0.23	--
14	--	--	--	--	1.30	--	--	0.38	--	--
15	--	--	--	4.60	--	--	--	0.18	0.05	--
16	--	0.05	--	--	--	--	--	--	--	--
17	--	0.18	--	--	0.79	--	0.38	--	--	--
18	--	--	0.53	0.08	0.74	1.04	0.30	--	--	--
19	0.13	--	--	--	--	--	--	--	--	--
20	--	0.66	0.43	--	1.63	--	1.91	--	--	--
21	--	0.43	0.91	--	0.23	--	--	--	2.24	--
22	--	0.18	2.26	--	--	--	--	1.30	1.88	--
23	0.13	--	--	--	--	--	--	--	0.13	--
24	--	--	--	0.15	--	--	--	--	--	--
25	0.20	1.04	--	0.48	--	--	--	--	0.41	--
26	0.64	--	--	0.28	--	0.76	--	--	3.68	--
27	0.33	0.43	--	1.19	--	--	0.13	--	0.05	--
28	5.00	--	--	--	--	--	--	--	--	--
29	1.32	--	--	--	--	--	--	0.20	--	--
30	--	--	--	--	--	--	--	1.24	--	--
31	1.07	--	--	--	--	0.46	--	--	--	--

Table 14. *Continued*

Day	1980 May	June	July	August	September
1	--	0.18	--	--	--
2	--	0.41	--	0.05	--
3	--	--	--	--	--
4	--	--	0.23	1.02	2.26
5	--	--	--	--	--
6	--	0.89	0.25	--	--
7	--	--	--	--	--
8	--	--	--	--	--
9	--	--	--	0.99	--
10	--	--	0.28	0.76	--
11	--	--	0.13	1.42	--
12	0.18	3.53	--	--	--
13	0.64	--	--	0.81	--
14	0.05	--	--	--	--
15	0.25	2.72	0.58	--	--
16	1.22	--	--	4.22	--
17	0.43	--	--	0.23	--
18	0.13	0.18	--	--	--
19	--	--	--	2.03	--
20	--	--	--	0.86	--
21	--	--	--	--	0.08
22	--	1.70	--	--	0.13
23	--	0.43	--	--	--
24	--	--	--	--	--
25	--	--	--	--	--
26	--	0.13	0.56	0.36	--
27	2.03	--	--	0.13	--
28	--	--	0.10	--	--
29	--	--	0.08	--	--
30	0.63	--	--	0.33	--
31	0.13	--	--	1.47	--

Table 15. Soil temperature at the depth of 50 centimeters for different dates in 1979, Castana station, Iowa

Date	Temperature (°C)
June 12	16.1
June 20	18.8
June 26	18.8
July 3	21.1
July 11	20.4
July 18	20.5
July 25	20.8
August 2	20.1
August 16	18.6
August 28	19.0

Field size The size of the object under study is an important factor which affects the accuracy of any type of interpretation. The resolution of current LANDSAT images is an area 80 meters by 80 meters, or 6400 square meters. Thus, any parcel of land with an area of 6400 square meters or larger is recognizable on the image. The visual identification becomes more practical and more accurate as the size of the land parcels become larger. Most of the farms in the midwest are many times larger than the minimum recognizable size of 6400 square meters. In Iowa, the current average farm size (1981) is about 116 hectares, as shown in Table 16. As it appears in these data, the number of farms has declined steadily since 1915, and the average farm size increased. Also, there has been a decrease of 0.45 million hectares in the total cropland during the last 30 years. Fewer, but larger, farms provide a more recognizable scene and, thus, make the interpretation easier and more accurate.

Table 16. Number, average size, and land in farms in Iowa, 1935-81[a]

Year	Number of farms (Thousands)	Avg. size (ha)	Land in farms (million ha)	Year	Number of farms (Thousands)	Avg. size (ha)	Land in farms (million ha)
1935	222	63	13.92	1964	162	87	14.00
1940	213	65	13.80	1965	158	89	14.00
1945	209	67	13.96	1966	155	90	13.96
				1967	152	92	13.96
1950	206	68	14.08	1968	149	93	13.92
1951	205	69	14.12	1969	147	95	13.92
1952	203	70	14.12	1970	145	96	13.92
1953	200	70	14.12	1971	143	98	13.92
1954	197	72	14.12	1972	141	98	13.88
1955	195	72	14.12	1973	139	100	13.88
1956	193	73	14.12	1974	138	101	13.88
1957	191	74	14.08	1975	130	106	13.80
1958	189	74	14.08	1976	127	108	13.72
1959	187	75	14.04	1977	125	109	13.72
1960	183	77	14.04	1978	123	111	13.68
1961	178	79	14.04	1979	121	113	13.68
1962	172	82	14.04	1980	119	115	13.68
1963	167	84	14.00	1981	118	116	13.68

[a]Source: Iowa Department of Agriculture (1981).

The average farm size is useful in determining the total crop area in image analysis where the number of parcels of land under a certain agricultural practice has been counted. The estimated total area is found by multiplying the average size by the number of land parcels. If more accuracy is desired, the land parcels can be delineated on the base map using Zoom Transfer Scope (ZTS) and the area measured from the base map using a

planimeter. This second method is very tedious and requires a lot of time. However, from experience, it is expected that, for a relatively large region, the error introduced due to the use of the average farm size method is small, and the gross estimate of the area using this method is as useful for planning as the exact measurement by the second method. The average farm size can also be used to estimate the number of farms when only the total area is given in the data.

Monitoring irrigated areas in west-central Iowa

Irrigation, because of both the large volume of water withdrawn and consumed, is a water category of key interest to water resources planners and agencies. The Iowa Natural Resources Council (INRC), charged with the responsibility of allocating Iowa's surface and ground waters, issues water withdrawal permits to each irrigator. These permits show the owner, location of the land and the maximum amount of water that can be withdrawn annually. However, during any given growing season, there are some irrigators that do not irrigate, some that irrigate, some that have a permit but have not acquired their equipment. Due to these problems, it is not possible to determine how much land is actually irrigated in any year.

Remote sensing is a tool that may be able to provide these data. Table 17 shows trends in irrigation permits for Harrison and Monona Counties in western Iowa. Data for this table were taken from INRC permit system document described above. Table 18 is a summary of INRC permits issued for the eight townships in the floodplain area of Monona County. The drop in the number of permits in 1980 is due to the fact that the INRC has

Table 17. Number and the area of lands that have received irrigation permits from INRC for the years 1972 to 1980 (Iowa Natural Resources Council permit records)

Year	Harrison (number/ha)	Monona (number/ha)
1972	77/5475	115/9686
1973	83/5918	111/9714
1974	81/5993	108/9350
1975	102/7613	127/11455
1976	125/9348	166/14863
1977	215/16854	312/30056
1978	218/17304	321/31096
1979	222/17700	324/31222
1980	211/17204	306/30149

Table 18. Summary of INRC irrigation permits issued for the eight townships in the floodplain area of Monona County

Township	Township Code	Year								
		1972	1973	1974	1975	1976	1977	1978	1979	1980
Ashton	1	20	18	17	20	29	48	50	50	44
Fairview		2	3	3	3	4	10	11	11	10
Franklin	6	7	7	7	8	16	30	29	33	30
Lake	10	21	21	20	23	22	35	36	36	34
Lincoln	11	18	18	18	21	25	49	48	49	46
Sherman	14	3	3	2	6	10	25	25	25	24
West Fork	18	33	29	28	30	37	59	62	63	65
Onawa	22	1	1	1	1	2	3	3	3	2
TOTAL[a]		105	100	96	112	145	261	264	270	255
Monona[b]	133	115	111	108	127	166	312	321	324	306

[a]Total for townships listed in this table.

[b]Total for whole Monona County.

changed the permit validation period from 10 years to 1 year, and some farms have declined to renew their permits since the last drought period has ended.

In addition to water permit data, several other sources of information were reviewed in order to establish ground truth for the image interpretation. The sources of this information are briefly described below:

A. Census of Agriculture - Preliminary Report. This contains selected county-wide summaries of farmland by use of category and crop harvested. An "irrigated land" category is included;

B. USDA-ESCS Estimates 1969-1978. This report gives estimates of irrigated area by crop throughout the period when LANDSAT satellites have been in orbit;

C. Soil Conservation District - Area 4 Estimates. A 1978 irrigated cropland estimate, by county, is given in these data prepared by the USDA-SCS;

D. Irrigated Area by System Type. The total areas were provided by the State of Iowa, with the breakdown by system estimated by USDA-SCS.

A comparison of the above information for 1978 is given in Table 19. The INRC water withdrawal permit data for 1978 have been included in this table. Examination of these data reveals wide differences in irrigated area estimates. These are due, in part, to differences in sampling procedures and irrigation definitions. Whether or not these data represent land actually irrigated, land suitable for irrigation, or land for which a water withdrawal permit has been obtained is most important. This is not

Table 19. 1978 irrigation data for Harrison and Monona Counties

	A		B		C		D		INRC	
	Harrison	Monona	Harrison	Monona	Harrison	Monona	Harrison	Monona	Harrison	Monona
Farms	83	124	--	--	--	--	--	--	218	321
Area (ha)	6777	11718	2961	4457	9959	29138	17343	30098	17304	31096
Farrow/border (ha)							4333	0		
Center pivot							11280	26050		
Other sprinkler							1730	4048		

always readily apparent from the records. To clear this problem, the agricultural extension agents and Soil Conservation Service representatives and some of the farmers in the area were interviewed.

To find out how many of those who had irrigation permits actually irrigated their fields, a simple "check out" was applied. First, the locations of lands for which a permit had been issued were marked on the township map of the area under study (Figure 44). Sherman Township was the selected site for the experiment. Information about the permitted lands in this township is summarized in Table 20 for years 1972 through 1980. Many of those who have permits and intend to use them usually obtain them a year ahead of time, so that they can provide the necessary equipment. For this reason, the permit data for the previous year was used in analyzing the results.

The second step was to superimpose the irrigated areas interpreted from the LANDSAT images over the same township map to determine if they corresponded with areas with a current INRC permit. The primary conclusion would be that the areas that overlap (one for permit and one for irrigation) are those lands that had permits and had also been irrigated. Of course, it should be realized that not all farmers will irrigate at the same time except during extremely dry periods. Thus, using only a single data image will not give an accurate estimate of those who have actually irrigated during the growing season. To minimize this problem, several images of different times during the same growing season should be used and their results compiled.

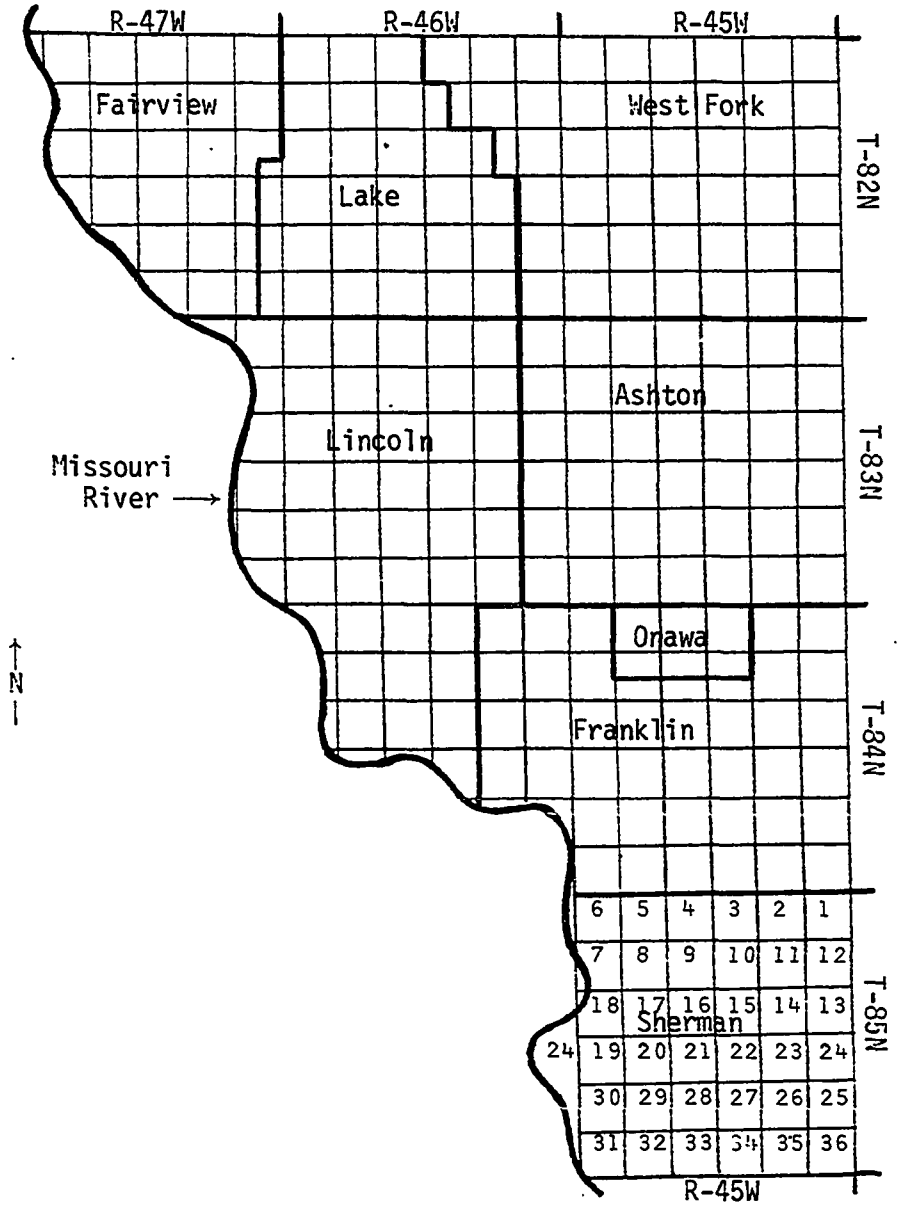

Figure 44. Township map of the area under study in Monona County

Table 20. Trend in Iowa Natural Resources Council's irrigation permits for Sherman Township[a] in Monona County, Iowa, 1972-1980

Year	Section	Area irrigated (ha)	Amt. of water (m m^3/y)[b]
1972	7	130	0.59
	13	65	0.30
	14	97	0.30
1973	7	130	0.59
	13	65	0.30
	14	97	0.30
1974	13	65	0.30
	14	97	0.30
1975	3	142	0.71
	3	30	0.09
	4	38	0.12
	13	65	0.30
	14	97	0.30
R-46:	24	243	1.18
1976	1	36	0.11
	3	142	0.71
	3	30	0.09
	4	38	0.12
	5	29	0.09
	13	65	0.30
	14	97	0.30
	20	70	0.21
	36	260	0.79
R-46:	24	243	1.18
1977	1	36	0.11
	2	57	0.20
	2	65	0.25
	3	142	0.71
	3	30	0.09
	4	38	0.12
	5	29	0.09
	6	76	0.29
	7	81	0.25
1977	7	76	0.29
	7	65	0.20
	8	36	0.14
	13	65	0.30
	14	97	0.30
	16	32	0.10
	19	97	0.37
	20	70	0.21
	22	65	0.25
	23	130	0.49
	28	63	0.20
	29	49	0.15
	34	97	0.30
	34	101	0.38
	36	260	0.79
R-46:	24	243	1.18
1978	1	36	0.11
	2	57	0.20
	2	65	0.25
	3	142	0.71
	4	38	0.12
	5	29	0.09
	6	76	0.29
	7	81	0.25
	7	76	0.29
	7	65	0.20
	8	36	0.14
	13	65	0.30
	14	97	0.30
	16	32	0.10
	19	97	0.37
	20	70	0.21
	22	65	0.25
	23	130	0.49
	28	63	0.20
	29	49	0.15
	34	97	0.30

[a]Sherman Township: T-85N, R-45W and R-46W.

[b]Million cubic meters per year.

Table 20. *Continued*

Year	Section	Area irrigated (ha)	Amt. of water (m m^3/y)[b]
1978	34	101	0.38
	36	260	0.79
R-46:	24	243	1.18
1979	1	36	0.11
	2	57	0.20
	2	65	0.25
	3	142	0.71
	3	30	0.09
	4	38	0.12
	5	29	0.09
	6	76	0.29
	7	81	0.25
	7	76	0.29
	7	65	0.20
	8	36	0.14
	13	65	0.30
	14	97	0.30
	16	32	0.10
	19	97	0.37
	20	70	0.21
	22	65	0.25
	23	130	0.49
	28	63	0.20
	29	49	0.15
	34	97	0.30
	34	101	0.38
	36	260	0.79
R-46:	24	243	1.18
1980	1	36	0.11
	2	57	0.20
	2	65	0.25
	3	142	0.71
	3	30	0.09
	4	38	0.12
	5	29	0.09
	6	76	0.29
	7	81	0.25
	7	76	0.29
	7	65	0.20
	13	65	0.30
	14	97	0.30
	16	32	0.10
	19	97	0.37
	20	70	0.21
	22	65	0.25
	23	130	0.49
	29	63	0.20
	29	49	0.15
	34	97	0.30
	34	101	0.38
	36	260	0.79
R-46:	24	243	1.18

To separate the irrigated from the unirrigated areas, the procedures previously described in this section were followed. Images used were positive prints of band 5, LANDSAT, with the scale of 1:500,000. The images were taken on the following dates:

June 24, 1980
August 21, 1977
July 16, 1977
August 8, 1975
July 30, 1975
August 14, 1972

These dates had to be evaluated against the precipitation and soil moisture data in order to screen out those images whose dates fall into the periods of high precipitation and high levels of soil moisture. Images that passed this test then were used in interpretation. Table 21 shows the results of interpretation versus the number of permits issued for the same years. Table 21 shows a good correspondence between the LANDSAT and INRC permit data.

Table 21. Number of irrigated land parcels derived from LANDSAT images for the years 1977 and 1980

Year	Land parcels	
	LANDSAT images	INRC permits[a]
1977	7	10
1980	22	25

[a]Based on previous year's INRC permits.

Center pivot irrigation systems An attempt to identify the number of center pivot irrigation systems in Monona and Harrison Counties was made. Images used for this part were the same positive prints of band 5 that were used previously.

Center pivot systems are seen as small circles on the image which are darker than the surrounding lands. In some places where neighboring areas are also irrigated, but not by center pivot systems, the circular shape of center pivot is not readily recognizable and they are hard to identify. Table 22 gives the results of the center pivot identification for years 1977 and 1980. These results were compared with the INRC permit data.

Table 22. Number of center pivot systems in Harrison and Monona Counties from LANDSAT images for 1977 and 1980

Year	County	Number of center pivot systems on LANDSAT image	INRC permits for all forms of irrigation	
			Previous year	Same year
1977	Harrison	46	125	215
	Monona	81	166	312
1980[a]	Harrison	58	222	211
	Monona	90	324	306

[a]Note: interpretation was based on a single date image - not too reliable.

Since the shapes of fields irrigated with a center pivot system are more distinct than those using other forms of irrigation methods, the accuracy of these results is thought to be better than the accuracy of identifying all forms of irrigated lands.

Data source examination From a review of the INRC permit system and all other available sources, it was learned that the average size of permitted land in Harrison and Monona Counties is 81 and 93 hectares, respectively. The estimated irrigated area from different sources in Table 17 was divided by average sizes in order to calculate the estimated number of irrigated land parcels in Harrison and Monona Counties. About 65 percent of the irrigated land in Harrison County and about 80 percent in Monona County have center pivot irrigation systems. About 81 and 84 percent of the permitted lands in Harrison and Monona Counties, respectively, are in the flood plain of the Missouri River. All center pivot systems in both counties are in the flood plain zone.[1] From this information, a new version of Table 19 is Table 23. Data given in this table are adjusted for 1977 (the irrigation permits in 1977 were about 95 percent of those in 1978) and are used to check the results from the 1977 LANDSAT image analysis.

Numbers in Table 23 indicate that the LANDSAT results are much closer to the data from source "A" than any other sources. For Harrison County, the reported number of center pivot systems is 51 and on the image it was counted to be 46. The reported number for Monona County is 95, and the counted number is 81. Data from other sources differ drastically from the actual numbers and are not reliable.

---

[1]Personal communication with county extension agents and interpretation of LANDSAT images.

Table 23. Number of irrigated farms during growing season of 1977

Source	Harrison			Monona		
	All types		Center pivot	All types		Center pivot
	County	Floodplain		County	Floodplain	
A	79	64	51	118	99	95
B	38	31	25	54	46	43
C	117	95	76	297	250	238
D	203	165	132	307	258	246
INRC:						
1977	215	174	140	312	261	250
1976	125	101	81	166	145	133
LANDSAT	71[a]		46	101[a]		81

[a]Calculated by dividing the number of center pivot systems observed on LANDSAT by the ratio of center pivot to other irrigated land.

Crop Identification

Observation techniques

To measure the reflectivity of different crops in near-infrared region of spectrum, a microdensitometer scan line was run over the low altitude aerial photo slide of farms north of Ames, Iowa (Figure 45(A)). The direction of the scan line is shown in Figure 46(B), a schematic diagram of the scene. Results of the scanning are shown in the form of a graph in Figure 46. As it appears from this graph, and also by visual observation of the actual scene in Figure 45, the corn has a higher reflectivity than soybeans at this stage of growth. The date of the photograph was

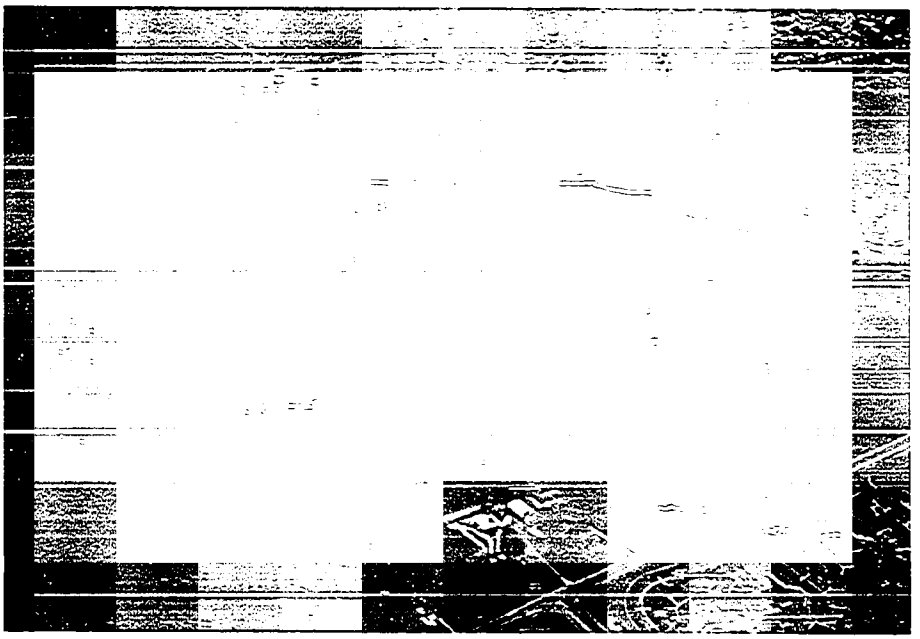

A

Figure 45. A) Low altitude aerial photo of farms at north Ames, Iowa

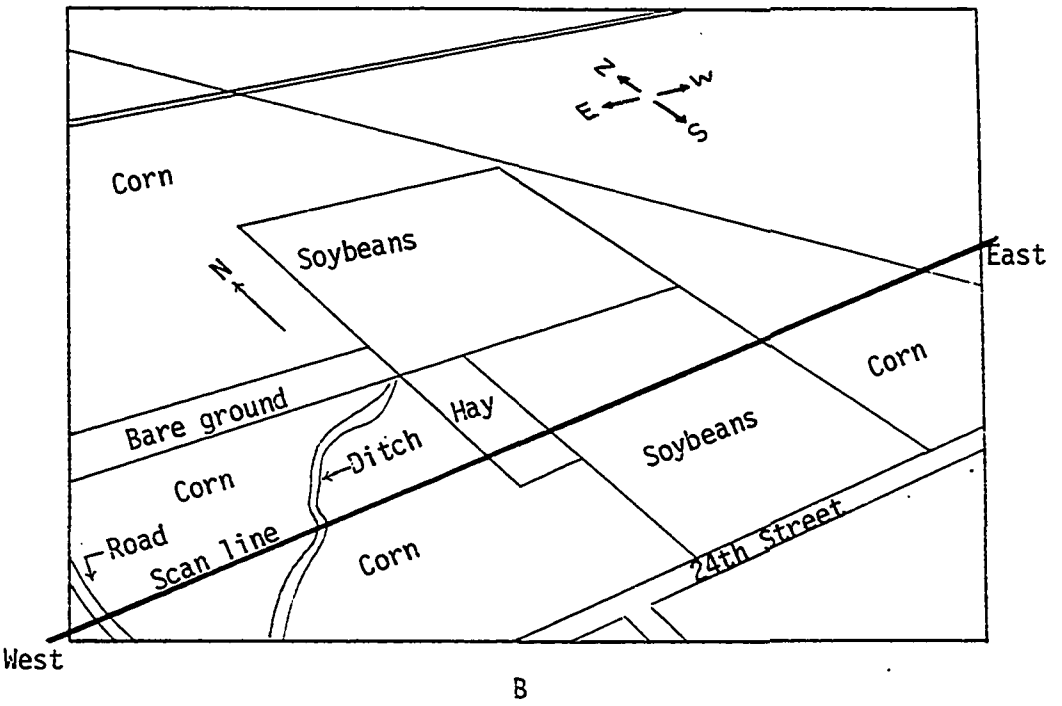

Figure 45. (Continued)

B) Scanning direction, east to west

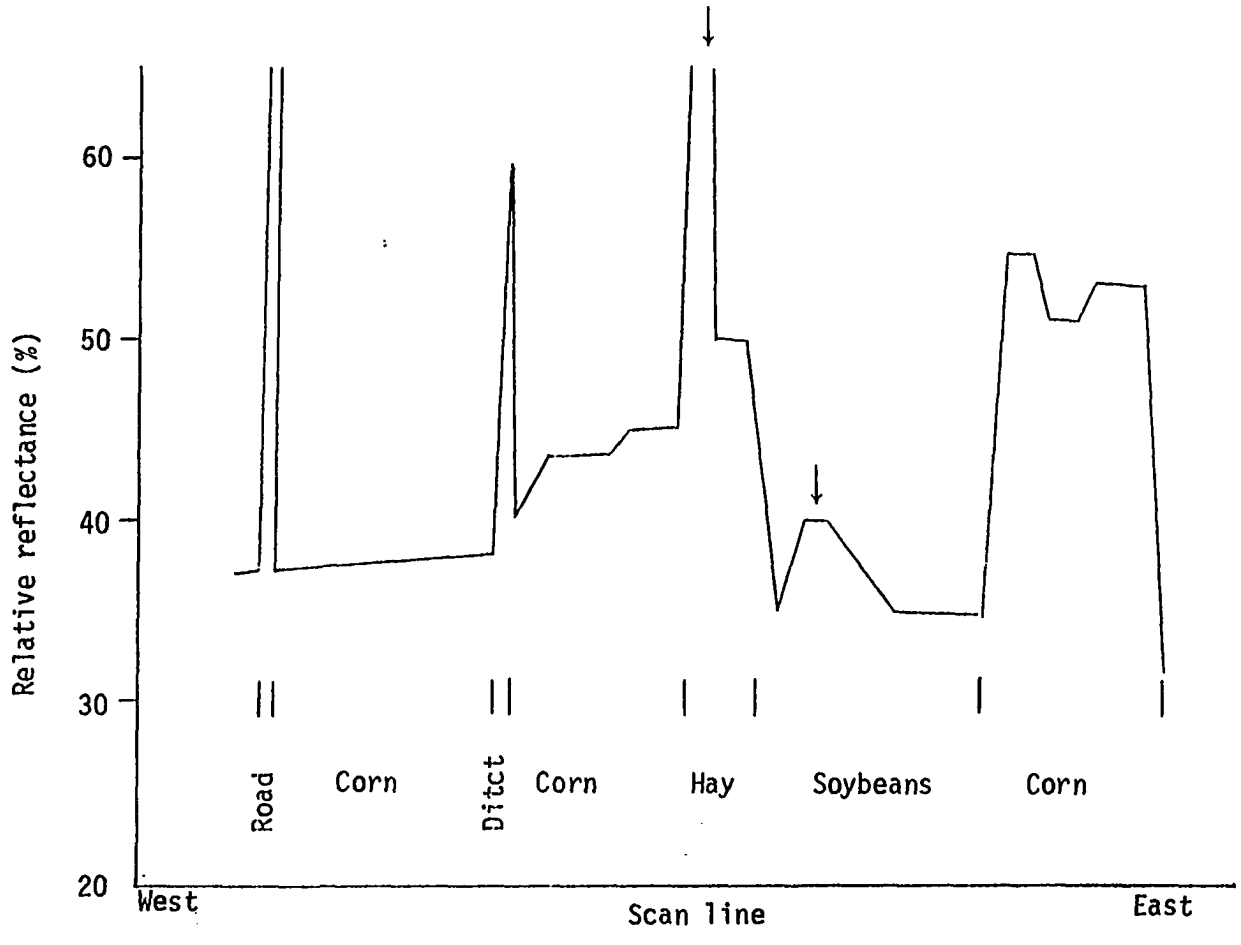

Figure 46. Recorded relative reflectivity from scanning slide shown in Figure 45

August 25, 1980. From the same graph, it can be observed that hay also has a higher reflectivity than soybeans. The east half of the land with hay shows lower reflectivity than the west half. A ground truth observation of the scene indicated that the parcel on the east had higher soil moisture while the hay on the west was under moisture stress. This represents the fact that, even among the same crops, different degrees of reflectivities exist due to various levels of soil moisture or stages of growth. Different levels of growth can also be observed in Figure 45, where soybeans on the north show different values or shades from those at the southern section of the image. The field on the north had been planted about 2 weeks earlier than the one on the south. It is recommended that the interpreter study such low-altitude photographs to increase his experience. Such experiences contribute to his accuracy in LANDSAT image interpretation. The use of multispectral channels as a means for distinguishing between different materials is shown in Figure 47. This figure represents a generalized differentiation between soil and grass, though it contains no detailed information about any specific type of soil or grass.

The value of multispectral photography in discovering crop diseases has already proven to be great. A study by Colwell (1956) showed that sufficiently early discovery of agricultural diseases will permit control measures to be taken before significant damage is done. Figure 48 shows the reflectance characteristics of healthy and diseased wheat and oats. At the early stage of plant development, it is hard or almost impossible to do tonal separation of healthy crops. In contrast, however, diseased plants give more light reflectance than the healthy plants in the range

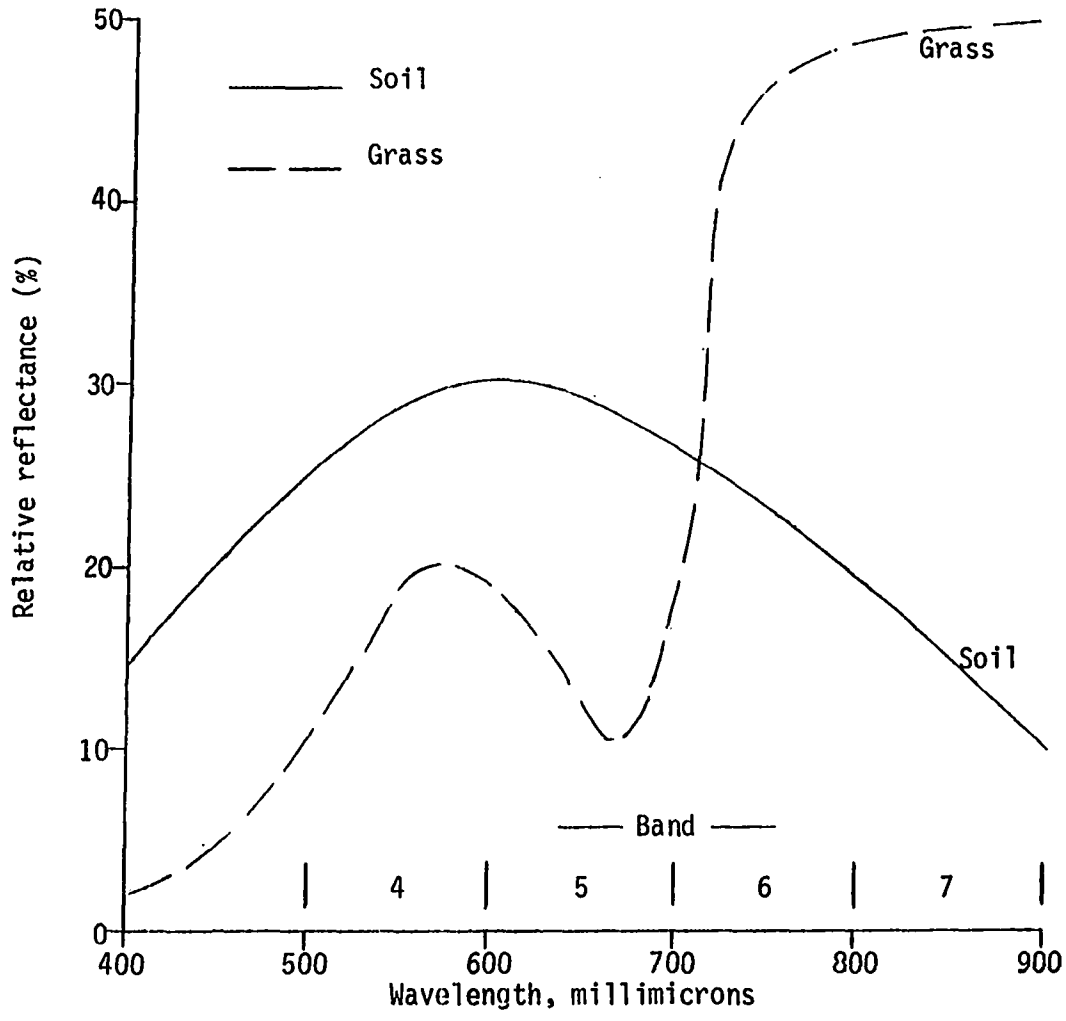

Figure 47. Generalized differentiation between soil and grass in different bands

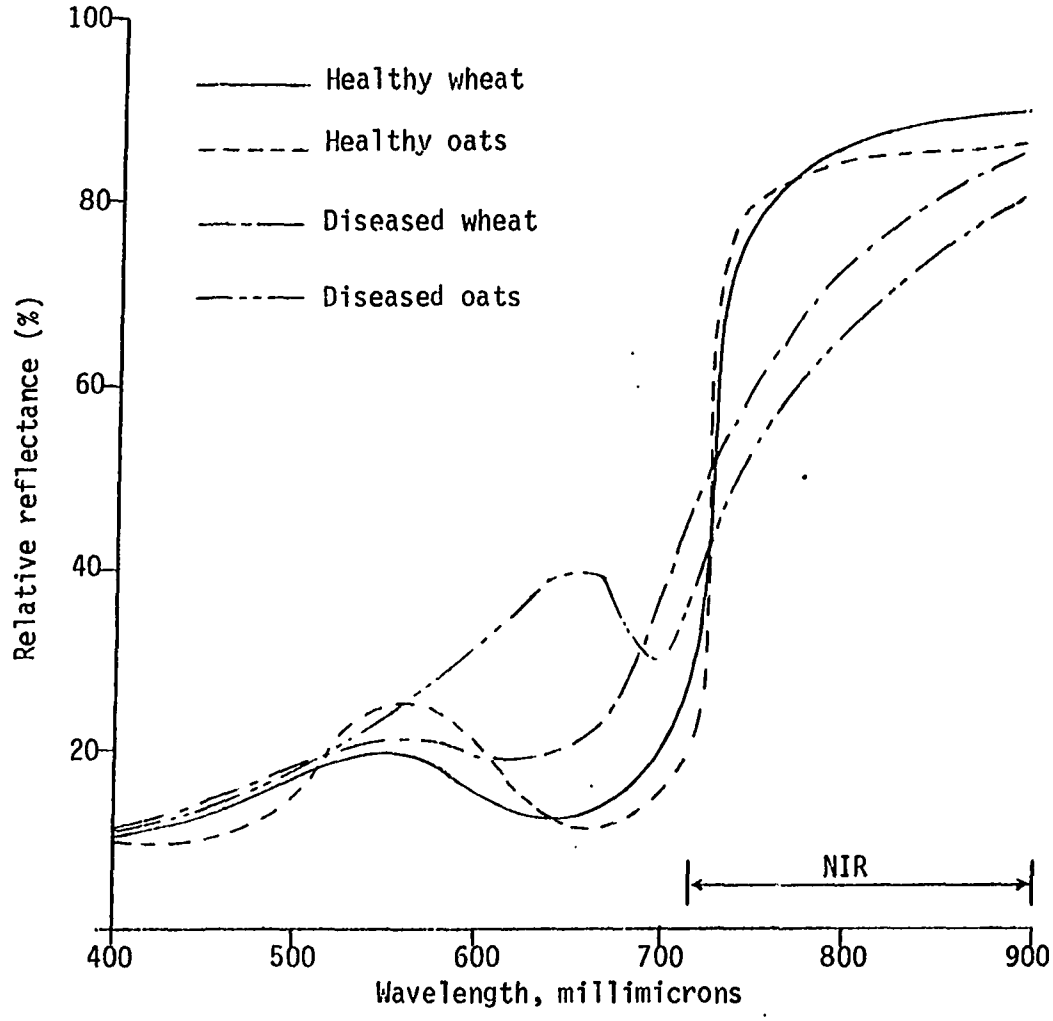

Figure 48. Reflectance characteristics of healthy and diseased wheat and oats in different ranges of wavelength

600 to 700 millimicrons and less light reflectance in the range 700 to 900 millimicrons. In oats, the differences between healthy and diseased plants in both bands are significant, but for wheat, the difference is significant only in the range of 700 to 900 millimicrons. Thus, in band 600 to 700 millimicrons diseased oats appear lighter than healthy oats, while healthy wheat and diseased wheat both appear dark in tone. In the band 700 to 900 millimicrons, both healthy wheat and healthy oats appear lighter in tone than diseased wheat and diseased oats. In times of moisture stress, these differences in reflectivity would help to identify diseased wheat and oats.

The degree of maturity and yield for a given crop influence the reflectance at any stage of growth. This maturity and yield can be assessed as the history of any crop is traced in terms of its changing reflectances. When a crop is diseased or seriously damaged, its reflectances decrease, particularly in the infrared, allowing the presence of crop stress to be recognized. Lack of available moisture also stresses a crop, which effect again shows up as a reduction of reflected light intensity in the infrared, usually as a drop in reflectance in the green MSS band (4), and as a rise in the red MSS band (5). In grasses, bush, and other forage vegetation of the range land, the amount of feed available (or biomass) also can be estimated by measurments of relative radiance levels.

Growing crops appear in various shades of pink to red in false color composites. Young plants tend to appear pinkish while many fully matured crops are bright red. In general, all leafy vegetation by itself has a similar reflectance spectrum regardless of plant or crop species.

The differences among crops, by which they are separated and identified, result from degree of maturity, percent of canopy cover, and differences in soil type and soil moisture. When data from all four channels of the MSS are used, there are usually enough subtle differences in reflectance from one crop to the next to distinguish them. Also, if certain crops are not separable at one time of the year, they are normally separable at another time due to the differences in planting, maturing, and harvesting dates. For these reasons, it is necessary to consider the seasonal development of the major crops of the region under study. Figures 49 and 50 show such seasonal development for corn and soybeans in Iowa. Note that the stage of growth changes from year to year, and, to avoid an error in judgement, the average seasonal growth for at least the last 5 preceding years should be used.

Two main difficulties in identifying crop types are overlapping growth periods and complex cropping patterns. Growth period is important because the same crop planted at two different times will give two different reflectivities which may confuse the interpreter. Soil background also affects the seasonal reflectance patterns of crops. In the floodplain areas of Monona County, croplands that are located on the west side showed higher reflectance on the image than those on the east side. The soils on the west side of the floodplain are lighter in texture and contain less organic materials than the soils on the west side (see LANDSAT image in Figure 23).

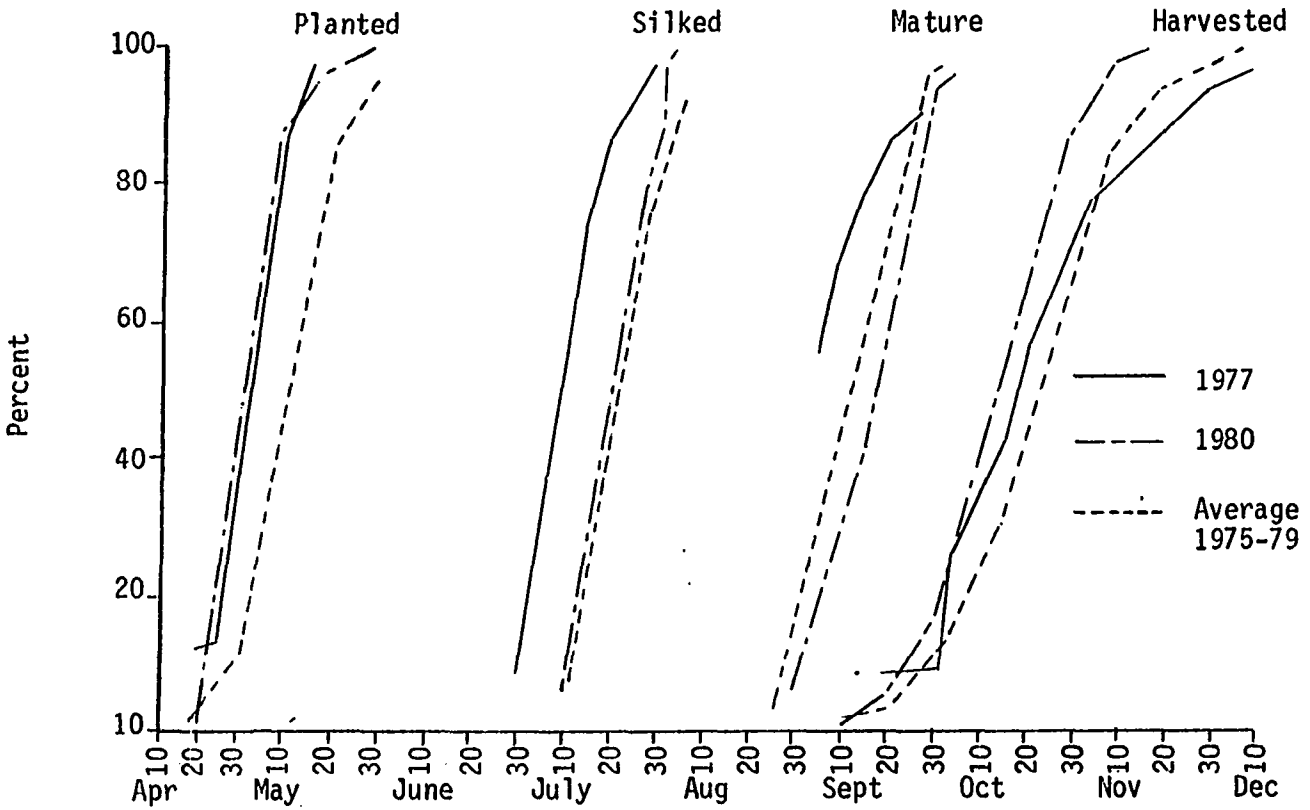

Figure 49. Corn growth calendar (Iowa Department of Agriculture, Des Moines, Iowa)

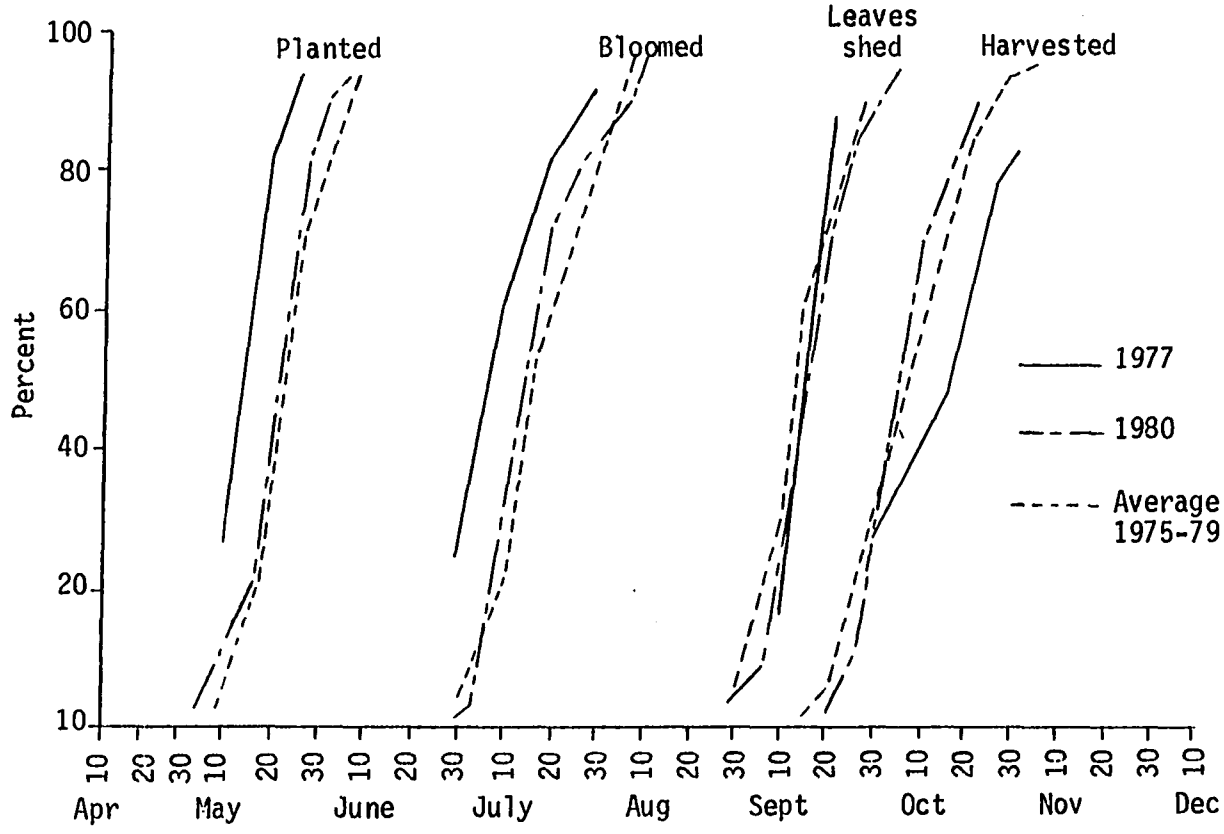

Figure 50. Soybean growth calendar (Iowa Department of Agriculture, Des Moines, Iowa)

Analysis of the experiment

Crop information for the years 1972 through 1980 was obtained from the Iowa Department of Agriculture to verify the accuracy of the interpretation methods. More complete crop data for eight townships of Monona County were also collected for the years 1973 through 1979 from yearly annual farm census reports. These eight townships are in the floodplain area of the county. Selected information is listed in Tables I and II of Appendix C. Not all of these data can be directly used in interpretation, but they can provide background knowledge and, thus, a sense of confidence for the interpreter. Out of the eight townships, Sherman Township was selected for the field-by-field verification of the results of interpretation, derived from images, by comparing them to the farm data. The same field-by-field comparison was made on the same areas as the irrigated areas analysis.

Table 24 shows the number of land parcels under corn and soybeans in Sherman Township as they are reported in the Iowa Annual Farm Census. From contacts with the extension agent in Monona County and from contact with randomly-selected farmers, the reliability of these data were checked for years 1976 through 1979.

Table 24. Number of land parcels under corn and soybeans in Sherman Township from 1976 through 1979[a]

Year	Crop			Number of farms
	Corn	Soybeans	Others	
1976	43	39		44
1977	41	39		42
1978	41	39		42
1979	42	41		43

[a]Source: Iowa Department of Agriculture.

After the interpretation of the images was conducted using the method explained above, their results were compared with the numbers given in Table 24. For the interpretation, the two images of August 29, 1976, and August 19, 1978, were selected for analysis. Study of crop calendars for corn and soybeans along with the degree of reflectivity of each crop in the respective stage of growth (from the crop calendar) indicated that soybeans should appear in uniform light red (pinkish) and corn should appear in a nonuniform-textured dark red. Other crops, such as hay and alfalfa, should appear in the shades of green. The results are summarized below.

Date of image	Uniform light red	Nonuniform dark red	Green
	Number of land parcels		
August 29, 1976	45	47	8
August 19, 1978	44	45	9

Combining the above results with numbers in Table 24, the values below were constructed to show the accuracy of the remote sensing.

	1976		1978	
	Corn	Soybeans	Corn	Soybeans
Interpretation results	47	45	45	44
Farm Census data	43	39	41	39

As the numbers above indicate, the accuracy of the measurements is encouraging. The accuracy of corn identification was about 91 percent on both the 1976 and 1978 images. For soybeans, it was 87 and 89 percent, respectively. The lower accuracy in soybean identification can be attributed to

the fact that some of the adjacent lands may have been blended in the view due to very uniform texture of the soybean image.

OVERVIEW

Information obtained from LANDSAT imagery is of value to many disciplines of water resources. A review of remote sensing application has been presented in this thesis. In the field of water resources, one of the important questions is the availability of water for different users. Water availability is a function of several dynamic processes at the earth's surface. Water resource allocation is better achieved if more accurate and up to date data were provided to the water managers and decision makers. In the absence of repetitive data over long periods, the water resource planner is confronted with a problem of making a decision with incomplete data on the changing environment.

To resolve this water resources problem, it is necessary to determine the amount of water being used for various beneficial uses and where it is being applied. In general, a unified goal about how to manage the water resources in a region is hard to reach where there is no agreement among the different estimates of data by various agencies who are involved. One example is the lack of realistic irrigation data which creates many difficulties for water resources planners. Differences in the estimate of water use and availability is highly related to the lack of knowledge about the area of irrigated lands. One reason for the wide ranges in the estimates is that those lands nominally considered irrigated land by certain agencies may not necessarily have been irrigated.

Many of the water resources features are detectible with satellite sensors. Strong light absorbancy of water in the near-infrared region

provides the opportunity to observe it by near-infrared bands of LANDSAT scanners. This research has examined the ability of LANDSAT to monitor the factors which affect the water consumption by irrigation in western Iowa. These factors are soil moisture, areas under irrigation, and crop types. The amount of water needed for irrigation is largely determined by precipitation and soil moisture, plant physiology and crop type, and the area of lands under the irrigation.

Using average precipitation and water use data during season for each major crop, the calculated water use for selected crops (Table 25) indicates that corn uses 3.8 centimeters more water than falls as precipitation during the growing season and soybeans uses 5.5 centimeters more. The deficit must be supplied either by soil moisture reverses or supplementary irrigation.

Once the monitoring system of irrigated land has been established, the amount of water withdrawn for the supplementary irrigation can be estimated. The Iowa Natural Resources Council specifies the limit of water that can be withdrawn by each permitee. Table 26 shows the trend of the total permitted water withdrawal, by the sources since 1972 for Harrison and Monona Counties. Combining information given in this table with the area of irrigated land estimated from the LANDSAT images, the amount of water withdrawn for irrigation can be estimated (Figure 51). Since the irrigation in Iowa is supplementary to the soil moisture and precipitation, the water withdrawal is 100 percent consumptive use and is out of the water resource system of the basin.

Table 25. Excess (+) or deficiency (-) of precipitation to estimated water use for major crops in central IOwa, in centimeters (Iowa Natural Resources Council, 1978)

Crop	March	April	May	June	July	August	September	October	Total
Corn			+4.3	+4.0	-7.3	-5.3	-0.3	+0.8	-3.8
Soybeans			+2.3	+5.8	-6.5	-6.0	-1.3	+0.2	-5.5
Sorghum			+2.5	+6.0	-4.3	-7.3	-1.5	+1.3	-3.3
Alfalfa		+1.8	+1.0	+7.0	-4.5	-2.5	-3.3	+1.3	-5.5
Oats	+1.0	+1.0	+1.3	+0.0	+0.2	+3.5			+8.0

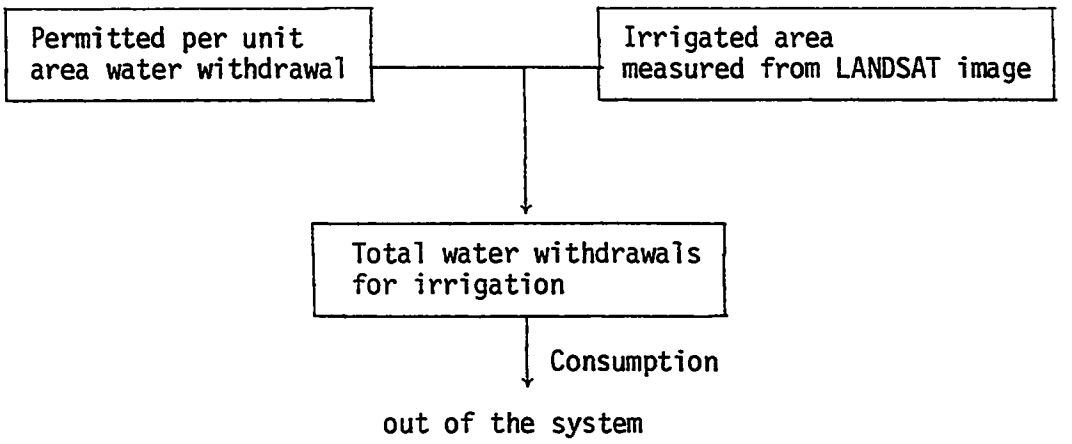

Figure 51. A model to apply the LANDSAT information in estimating the amount of water withdrawals for irrigation

Table 26. Trends of the permitted water withdrawal for Harrison and Monona Counties[a]

Year	No. of permits		Area (ha)		Permitted water withdrawals, million cubic meters per year							
					Well		Reservoir		Stream		Total	
	Harrison	Monona	Harrison	Monona	Harrison	Monona	Harrison	Monona	Harrison	Monona	Harrison	Monona
1972	77	115	5475	9685	16.57	35.60	0.49	0.59	1.00	0.84	18.06	37.03
1973	83	111	5918	9714	17.83	35.74	0.49	0.59	1.00	0.80	19.32	37.13
1974	81	108	5993	9350	18.45	34.63	0.49	0.59	1.00	0.80	19.94	36.02
1975	102	127	7613	11455	23.79	42.78	0.73	0.59	1.25	3.02	25.77	46.39
1976	125	166	9348	14863	29.56	54.80	0.73	0.59	1.25	3.02	31.54	58.41
1977	215	312	16854	30056	53.54	106.31	0.73	0.59	1.25	3.02	55.52	109.92
1978	218	321	17304	31096	55.41	108.99	0.59	0.59	0.92	4.17	56.92	113.75
1979	222	324	17700	31222	56.57	109.37	1.29	0.59	1.37	4.17	59.23	114.13
1980	211	306	17204	310149	54.82	104.99	1.29	0.39	1.31	4.17	57.42	109.55

[a]Source: Iowa Natural Resources Council, Des Moines, Iowa.

SUMMARY

Examination of the methods introduced in this study showed that the manual interpretation of LANDSAT images is a low cost and easy approach to monitor the irrigated areas and the crop types. The results of visual measurement of image density values as a technique for monitoring soil moisture showed it to be very tedious and not reliable. Thus, any further effort to apply this method in soil moisture measurement is not recommended. The results of the monitoring of generalized soil moisture using the micro-densitometer were more promising, yet more research is needed before it can be recommended. However, it is expected that in the near future, when better quality images with higher resolution are available, this method may become a useful tool to the water resource planner.

Factors which affect the quality of image interpretation have been discussed in this thesis. Special attention was paid to the background sources and data to prevent misinterpretation. Also, the state of the art in remote sensing application to the water resources has been reviewed and many aspects of related research have been presented and explained so the reader will be able to find the possible application of remote sensing to the area of his interest.

The following recommendations have been made for proper selection of LANDSAT images, based on this study:

- Band 6 of MSS has little value in crop, soil and water studies;
- Band 7 is suitable for drainage area and drainage density measurement, if the image is selected at the right time of the year. For Iowa, the best time is early in spring when the young vegetation is actively

growing and crops have not emerged. This vegetation along the stream and river channels is viewed much darker in contrast to the image background, making the interpretation easy. This band is also suitable for studying rivers and lakes. To measure fluctuation in reservoir levels, this band is recommended.

- Band 5 is recommended for use in areas which are mostly under crops during summer. Irrigated lands can be recognized using band 5. This band is also suitable for monitoring the general soil moisture condition.

The major advantage of the methods of interpretation discussed in this study is that they do not require special expertise or expensive special equipment and they are not beyond the reach of many potential users. These methods will provide the planning agencies an economical procedure for collecting supplemental data on land use, irrigation and soil moisture. However, these methods will not completely replace the need for field data collection. Field data are necessary to insure proper interpretation of LANDSAT images.

RECOMMENDATIONS FOR FUTURE RESEARCH

This study was limited by several problems which have affected the accuracy of its results. These problems were basically due to two factors. The first factor was the limited funds available for obtaining LANDSAT images. The second one was the absence of enough experience in LANDSAT interpretation by the author. However, valuable experience was gained by the author by doing this research. If a similar study were to be conducted again, there would be several new ideas which should be incorporated in advance. Methods and techniques presented in this thesis are considered to be reliable approaches to the study of the subjects under study and have already shown their applicabilities.

The following suggestions cover the problems associated with the imagery selection. The remainder of these suggestions will provide a ground for conducting a more accurate interpretation of LANDSAT images.

Images of band 5 are most suitable for use in areas which are under crop cultivation during summer months. Irrigated lands can also be recognized using this band. Similar shapes, such as farmlands, on black and white transparencies of band 5 are not easily differentiable when projected onto a screen with an overhead projector. Thus, LANDSAT band 5 black and white transparencies are not recommended for studies of this nature.

When measuring image reflectivity for any purpose, one should remember that soil type and its condition affect the ground reflectivity. Another important factor which affects the reflectivity is vegetation. The reflectivity not only varies with the type of cover, but also changes due

to the stem and leaf angle, height, and stage of the growth.

In monitoring both irrigated lands and crop types, the contrast between the lands is an essential factor in image analysis. Since the images which have been taken right after a heavy precipitation have a more uniform and darker background tone, their contrast is much lower than those taken during a dry period. For monitoring the soil moisture, images belonging to both wet and dry periods are invaluable and provide a better differentiation.

In crop type identification, the best images to use are false color composite. Most of the time, these types of images are not readily available to the user. If the cost is not a limiting factor, the EROS data center can provide, by special order, most of the false color composite, but at a much higher price (currently about five times more expensive). The multidate images throughout the growing season are required if higher accuracy is to be expected in crop type recognition.

The black and white prints which were used in visual quantification of surface reflectivity should have the same image characteristics as those of the film negatives used in the density measurements using the microdensitometer; i.e., they should have the same scene identification number (see Table 9 and Figure 23). Providing this requirement, the results from the visual observation and microdensitometer measurement could be compared, and, thus, a more conclusive judgement could be made. However, the author is in favor of using microdensitometry procedure only and rejects the idea of visual measurement as a very tedious and inaccurate method. The time and the money spent for the visual interpretation of soil moisture could be used for more in-depth and detail study by microdensitometer.

Although cloud-free images are most suitable pictures to be used in the remote sensing project, in order to not lose desirable dates, images with up to 10 percent cloud cover should also be considered. It is possible that the area of interest is not covered by the clouds.

It is more convenient and accurate to use the largest available scale of LANDSAT imagery, i.e., the print with the scale of 1:250,000. The size of areas are seen four times greater at this scale than those on the prints with the scale of 1:500,000.

Ground truth data are required for comparison with remote sensing data to establish the validity of findings. Knowing that the data from existing satellite systems are available only periodically, every 18 days from LANDSAT, the value of ground truth data is more realized. If one is going to work on remote sensing projects, he must carefully plan the ground data sampling program ahead of time such that it would match the dates when the images are recorded. The LANDSAT overpasses are calendared and they can be predicted.

Soil moisture data should be collected not only for different years, but also more often in shorter intervals throughout each given year. This will reduce the errors due to interpolation of longer interval data. By doing so, it is then possible to analyze the relation between the reflectivity and soil moisture data within each year as well as for different years.

More direct contact with the farmers in the study area is encouraged if the higher accuracy is desired in monitoring the irrigated lands or crop types. One way of collecting information is by questionnaires sent to the farmers, explaining the nature of the investigation and requesting them to

provide data on water use and crop type. Some researchers have used this method of communication and have received good responses from the farmers.

The results of interpretation will be more accurate if the interpretation is being done at least by two persons who work simultaneously on similar images. The interpreters should not be aware of the results obtained by the other parties. Knowing each other's results may influence the state of interpretation and the results could become biased.

In the manual interpretation of the LANDSAT images, access to a Zoom Transfer Scope is a great advantage. This instrument facilitates the investigation and helps the researcher to locate the area under study by superimposing the image over existing maps of the same region.

If the above requirements are met, then it would be expected that there would be a relatively higher accuracy of the results for both irrigated areas measurement and crop type recognition. In this study, the accuracy of the results for these parts was about 90 percent. No estimated accuracy for the results of monitoring soil moisture can be given at this point until more in-depth study, based on the recommendations made here, is conducted.

Based on the above recommendations, a step-by-step procedure, to be used in future studies, has been outlined below:

A. General preparation

   1. Select the area under study and define the problems which are to be reviewed in this area, e.g., soil moisture, irrigated areas, and crop types.
   2. The area under study can be as large as a county. Monona County was about the right size for this study.

3. Collect and compile all available information from various sources about this area and also about the subjects under study. This information includes farm and crop statistics, irrigation permit records, soil moisture data, precipitation data, general road map, and soil association map.
4. Obtain a Worldwide Reference System (WRS) map from EROS data center and locate the nominal scene center over the study area. The LANDSAT Data Type print out (see Figure 23) for the same scene center can also be obtained from the EROS data center. After reviewing the information given in the printout, select a most recent high-quality cloud-free image taken during the growing season and order a black and white print of band 5 with scale of 1:250,000.
5. Using a Zoom Transfer Scope, impose the LANDSAT image over the county road map and locate all important features on the image. Study the scene and become familiar with the location on the image.

After these primary steps are taken, then more specific procedures can be followed for each subject.

B. Soil moisture

1. Past soil moisture data need to be collected since 1972 (when first LANDSAT started its operation). In the event no soil moisture data are available in the study area, a soil moisture monitoring program will be necessary. Soil moisture sampling should be done every 18 days at the time of LANDSAT overpass,

beginning in late April and continuing until mid November. Several samples (5 at least) should be taken during each sampling time along a straight line over a distance of about 20 kilometers. Two years of soil moisture data will be needed for statistical analysis.

These data will provide a more realistic knowledge about the soil moisture condition and variation along the scan line. The scanning of the images then can be done over the same line where the soil moisture data are obtained. Only near surface soil samples are needed

2. Inspect the lands along the scanning line on the ground while sampling and make a record of any changes on the ground which may affect the reflectivity, such as changes in soil type, vegetation, etc.
3. From the LANDSAT Data Type printout, select the images taken during growing season since 1972. Select all available images taken at the same time as the soil moisture data. For scanning purposes, the image type should be negative slides of band 5.
4. Images for any purpose can be selected among those with the cloud cover of 10 percent or less. There is a chance that the area under observation is not covered by the clouds.
5. After scanning is completed, statistical analysis can be done to infer the relation between the soil moisture data and ground reflectivity for both within each year and between different years.

6. If the soil type and color changes drastically along the sampling line, the data for locations with different soil type and color should be treated separately.

C. Irrigated areas and crop types

1. Based on the existing irrigation and crop data, select at least 2 townships with the largest number of farms and irrigated lands.
2. The farmers in these townships should be contacted to determine information about their past and present agricultural practices, i.e., crop types, crop rotation and irrigation frequency. Additional field data on crop type and irrigation practices may be needed for a period of five years in order to obtain accurate data in the study area.
3. Review all LANDSAT images at the EROS archive and select at least for two years when the most ground data and good quality images are available.
4. For monitoring irrigated lands, black and white prints of band 5 with the scale of 1:250,000 are recommended for easy interpretation. For crop type identification, false color composite transparencies (or prints with the scale of 1:250,000) are needed.
5. For monitoring irrigated lands, images taken right after heavy precipitation should not be used.

It is hoped that the future satellite systems with more capability and more advanced technology will produce better images with higher resolution which, in turn, make the interpretation simpler and more reliable.

LITERATURE CITED

Akers, J. P. 1964. Geology and groundwater in the central part of Apache County, Arizona. U.S. Geological Survey Water Supply Paper 521-A.

Akhavi, M. S. 1980. Water resources investigations in West Central Iran using LANDSAT data. Water Resources 16:987-995.

Allen, R. F., R. D. Jackson and P. J. Pinter. 1980. To relate LANDSAT data to U.S. agriculture. Agricultural Engineering 61:12-14.

American Society of Photogrammetry. 1975. Manual of Remote Sensing. American Society of Photogrammetry, Falls Church, Virginia.

Anderson, J. R., E. E. Hardy, J. T. Roach and R. E. Witmer. 1976. A land use and land cover classification system for use with remote sensor data. U.S. Geological Survey Professional Paper 964.

Anderson, R. R., B. E. Hoyer and J. V. Taranik. 1974. Guide to aerial imagery of Iowa. Iowa Geological Survey, Iowa City, Iowa.

Anderson, W. H. 1978. Flood damage assessment using computer-assisted analysis of color infrared photography. Journal of Soil and Water Conservation 33:283-286.

Anuta, P. E., S. J. Kristof, D. W. Levandowski, T. L. Phillips and R. B. MacDonald. 1971. Crop, soil, and geological mapping from digitized multispectral satellite photography. LARS INformation Note No. 061371. Purdue University, Lafayette, Indiana.

Askari, F. and N. L. Faust. 1981. Automated classification of runoff coefficients from LANDSAT multispectral data. *In* Technical Papers of the American Society of Photogrammetry. 47th Annual Meeting, Washington, D.C. American Society of Photogrammetry, Falls Church, VA.

Barr, B. F. and E. A. Martinko. 1978. The application of remote sensing to resource management and environmental quality programs in Kansas. NASA:N78-27484.

Barr, B. G. and E. A. Martinko. 1979. The application of remote sensing to resource management and environmental quality programs in Kansas. NASA:N79-30605.

Barrett, E. C. and L. F. Curtis, eds. 1972. Environmental remote sensing: Application and achievements. Edward Arnold, Ltd., London.

Bausch and Lomb. 1975. Zoom Transfer Scope instruction manual. Bausch and Lomb, Rochester, New York.

Beck, R. H. 1975. Spectral characteristics of soil related to the interaction of soil moisture, organic carbon and clay content. M.S. Thesis. Purdue University, West Lafayette, Indiana.

Becker, D. 1979. The need for identification of irrigated lands in the Missouri River Basin. *In* Symposium Proceedings of Identifying Irrigated Lands Using Remote Sensing Techniques: State of the Art, Sioux Falls, S.D. Missouri River Basin Commission, Omaha, Nebraska.

Bernstein, R. 1974. Scene correction of ERTS data using digital image processing techniques. Third Earth Resources Technology Satellite-1 Symposium. NASA SP-351.

Best, R. B. and D. G. Moore. 1977. Inventory of wetland habitat using remote sensing for the proposed Oahe irrigation unit in eastern South Dakota. NASA:N77-30568.

Blanchard, B. J. 1977. Demonstration to characterize watershed runoff potential by microwave techniques. NASA-CR-151426.

Blanchard, B. J. and G. A. Gander. 1972. Remote sensing in hydrology. Agricultural Research Service, U.S. Department of Agriculture, Chickasha, Oklahoma.

Bock, P. 1974. Approaches to earth survey problems through use of space techniques. Akademie-Verlag, Berlin.

Brera, A. M. and F. Shahrokhi. 1978. Application of LANDSAT data to monitor desert spreading in the Sahara region. *In* Proceedings of the twelfth International Symposium on Remote Sensing of Environment, Ann Arbor, Michigan. Environmental Research Institute, Ann Arbor, Mich.

Bruns, P. E., G. G. Coppelman, W. B. Beck and K. J. Peterson. 1976. Dover, New Hampshire land use as portrayed by aerial photography and LANDSAT data. *In* Remote Sensing of Earth Resources. Vol. V. Fifth Annual Remote Sensing of Earth Resources Conference, Tullahoma, Tennessee. University of Tennessee, Tullahoma, Tenn.

Bushnell, T. M. 1929. Aerial photographs of Jennings County. Proceedings of Indiana Academy of Science 39:229-230.

Byers, H. R. 1974. General meteorology. McGraw-Hill Book Co., New York.

Campbell, J. B. and F. M. Henderson. 1981. Comparisons of land cover classifications from selected remote sensing systems. *In* Technical Papers of the American Society of Photogrammetry. 47th Annual Meeting, Washington, D.C. American Society of Photogrammetry, Falls Church, Virginia.

Carlson, M. P. and P. M. Seevers. 1976. Application of LANDSAT imagery in land use inventory and classification in Nebraska. NASA:N77-16400.

Carneggie, D. M., S. D. DeGloria and R. N. Colwell. 1975. Usefulness of LANDSAT data for monitoring plant development and range conditions in California's annual grassland. *In* Proceedings of the NASA Earth Resources Survey Symposium, Houston, Texas. NASA.

Carter, W. D. and R. W. Paulson. 1978. Introduction to monitoring dynamic environmental phenomena of the world using satellite data collection system. U.S. Geological Survey Circular 803.

Castruccio, P. A., H. L. Loats, Jr., T. R. Fowler and S. L. Frech. 1975. The application of remote sensing to the development and formulation of hydrologic models. NASA-CR-144078.

Chesnutwood, C. M. 1976. Detection of episodic phenomena on LANDSAT imagery. NASA:N79-13462.

Colwell, R. N. 1956. Determining the prevalence of certain cereal crop diseases by means of aerial photography. Hilgardin 26:223-286.

Colwell, R. N. 1961. Some practical applications of multiband spectral reconnaissance. American Scientist 49:9-36.

Colwell, R. N. 1977a. Determining the usefulness of remote sensing for estimating agricultural water demand in California. NASA:N77-30551.

Colwell, R. N. 1977b. An inventory of irrigated lands for selected counties within the state of California based on LANDSAT and supporting aircraft data. NASA:N77-31576.

Condit, C. D. and P. S. Chavez, Jr. 1979. Basic concepts of computerized digital image processing for geologists. Geological Survey Bulletin 1462.

Dominiques, O. A. 1960. A comparative analysis of black and white aerial photographs as aids in the mapping of soils in wild land area. pp. 398-402. *In* Manual of Photographic Interpretation. American Society of Photogrammetry, Washington, D.C.

Dozier, J., J. E. Estes and D. S. Simoneti. 1978. Remote sensing applications to hydrologic modeling in the Southern Sierra Nevada and portions of the San Joagrin Valley. NASA:N78-23503.

Draeger, W. C. 1976. Monitoring irrigated land acreage using LANDSAT imagery: An application example. USGS Sioux Falls. Open File Report No. 76-630. 23 pp.

Draeger, W. C., J. D. Nichols, A. S. Benson, D. G. Larrabee, W. M. Senkus and C. M. Hay. 1974. Regional agriculture surveys using ERTS-1 data. Third Earth Resources Technology Satellite-1 Symposium. Vol. I. NASA SP-351.

El Kassas, I. A. 1977. Potential application of remote sensing in locating and tracking of antarctic icebergs. Nuclear Material Corporation, Cairo, Egypt.

El Shazly, E. M., M. A. Abdel Hady and I. A. El Kassas. 1977. Delineation of land features in Egypt by LANDSAT satellite images. *In* Remote Sensing of Earth Resources. Vol. VI. Sixth Annual Remote Sensing of Earth Resources Conference, Tullahoma, Tennessee. University of Tennessee, Tullahoma, Tennessee.

Engman, E. T. and J. R. Annett. 1977. Remote sensing application to a partial area model. NASA:N78-23501.

Erb, B. R. 1974. The utility of ERTS-1 data for applications in agriculture and forestry. Third Earth Resources Technology Satellite Symposium. Vol. I. NASA SP-351.

Ernst-Dottavio, C. L., R. M. Hoffer and R. P. Mroczynski. 1981. Spectral characteristics of wetland habitats. Photgrammetric Engineering and Remote Sensing. American Society of Photogrammetry 47:223-227.

Fischer, W. A. 1971. Uses of applications satellites for inventorying and monitoring the Earth's resources. U.S. Geological Survey, Washington, D.C.

Foster, K. E., R. A. Schowengerdt and C. E. Glass. 1980. The use of LANDSAT imagery in ground water exploration. Water Resources Bulletin 16:934-937.

Fritz, N. L. 1968. Optimum methods for using infrared-sensitive color films. Photogrammetry Engineering 34:1128.

Gangstad, E. O., ed. 1980. Weed control methods for public health application. CRC Press, Inc., Boca Raton, Florida.

Garvin, L. E. and R. F. Pascucci. 1973. Remote sensing and analysis of soils and vegetation in the California desert. *In* Proceedings of Convention in Applied Remote Sensing of Arid Lands. University of Arizona, Tucson, Arizona.

Gates, D. M. 1970. Physical and physiological properties of plants. p. 224-252. *In* Remote sensing. National Academy of Science, Washington, D.C.

General Electric Co., Space Division. 1972. ERTS data users handbook. General Electric Co., Beltsville, Maryland.

General Electric Co., Space Division. 1976. Image 100 user manual. General Electric Co., Daytona Beach, Florida.

Goldberg, M. C. and Weiner, E. R. 1972. Applications of spectroscopy to remote determinations of water quality. NASA report MSC-05937.

Graigoryev, Al. A. and V. B. Lipatov. 1977. Dust storms in the coastal regions of the Aral Sea from space imagery. *In* Remote sensing of Earth resources. Vol. VI. Sixth Annual Remote Sensing of Earth Resources Conference, Tullahoma, Tennessee. University of Tennessee, Tullahoma, Tennessee.

Hammack, J. C. 1977. Hydrographic application of LANDSAT - present and future capabilities. *In* Proceedings of the American Society of Photogrammetry, Little Rock, Arkansas. American Society of Photogrammetry, Falls Church, Virginia.

Hardy, E. E. and R. L. Shelton. 1975. Inventorying New York land use and natural resources. New York's Food and Life Science 3:4-7.

Hardy, R. L. 1977. Least square prediction. Photogrammetric Engineering and Remote Sensing 43:475-491.

Harnage, J. and D. Landgrebe, eds. 1975. LANDSAT-D trematic mapper technical working group. Final report. JSC-09797 NASA.

Heaslip, G. B. 1975. Environmental data handling. John Wiley and Sons, New York.

Hinkle, R. E. 1976. An environmental analysis of LANDSAT-1 multispectral imagery of a possible power plant site employing digital image processing. *In* Remote sensing of Earth resources. Vol. V. Fifth Annual Remote Sensing of Earth Resources Conference, Tullahoma, Tennessee. University of Tennessee, Tullahoma, Tennessee.

Hoffer, R. M. 1967. Interpretation of remote multispectral imagery of agricultural crops. LARS Research Bulletin No. 831. Purdue University, Lafayette, Indiana.

Hoffer, R. M. 1972. Land utilization and water resources inventories over extended test sites. LARS, Purdue University, Lafayette, Indiana.

Horton, M. L. and J. L. Heilman. 1973. Crop identification using ERTS imagery. Symposium on Significant Results Obtained from the Earth Resources Technology Satellite-1. NASA SP-327.

Howard, J. A. 1976. Satellite remote sensing of agricultural resources for developing countries, present and future. An international perspective. *In* Remote sensing of the terrestrial environment. Butterworths, London.

International Astronautical Federation. 1974. Grand Systems for receiving, analyzing and disseminating Earth resources satellite data. International Astronautical Federation, Paris, France.

Iowa Department of Agriculture. 1972-1981. Various issues. Iowa Agricultural Statistics. Iowa Department of Agriculture, Des Moines, Iowa.

Iowa Natural Resources Council. 1978. Iowa water plan '78: Framework study main report. Iowa Natural Resources Council, Des Moines, Iowa.

Jansen, I. J. and T. E. Fenton. 1978. Computer processing of soil survey information. J. Soil and Water Cons. 33:188-190.

Johannsen, C. J. and T. W. Barney. 1981. Remote sensing applications for resource management. J. Soil and Water Cons. 36:128-131.

Kalensky, Z. D., W. C. Moore and L. R. Scherk. 1979. Flood mapping by LANDSAT. *In* Satellite hydrology. Proceedings of fifth annual William T. Pecora Memorial Symposium, Sioux Falls, S. D. AWRA, Minneapolis, Minnesota.

Kalush, R. J., Jr. 1979. The problem of resolution in the LANDSAT imagery. Remote Sensing Quaterly 1(1):

Kamat, D. S., A. K. Kandya, K. L. Majunder and V. L. Swaminathan. 1977. Mapping of forest region from LANDSAT imagery by computer: A case study of East Baster region. *In* Remote sensing of Earth resources. Vol. VI. Sixth Annual Remote Sensing of Earth Resources Conference, Tullahoma, Tennessee. University of Tennessee, Tullahoma, Tennessee.

Khorram, S. and E. F. Katibah. 1981. Use of LANDSAT multispectral scanner data in vegetation mapping of a forested area. *In* Technical Papers of the American Society of Photogrammetry, 47th annual meeting, Washington, D.C. American Society of Photogrammetry, Falls Church, Virginia.

Kirschner, F. R., S. A. Kaminsky, R. A. Weismiller, H. R. Sinclair and E. J. Hinzel. 1977. Soil map unit composition and assessment by digital LANDSAT data. Information Note 092377. Laboratory for Application of Remote Sensing, West Lafayette, Indiana.

Koch, D. L. and P. J. Horick. 1976. Irrigation in Iowa. Iowa Geological Survey, Iowa City, Iowa.

Krinsley, D. B. 1974. The utilization of ERTS-1 generated images in the evaluation of some Iranian playas as sites for economic and engineering development. U.S. Geological Survey, Reston, Virginia.

Kunde, V. G., B. J. Conrath, R. A. Manel, W. C. McGuire, C. Prabhakara, and V. Salomonson. 1974. The Nimbus 4 infrared spectroscopy experiment 2. Journal of Geophysical Research 79:777-784.

Land Use Laboratory. 1973. A land classification method for land use planning. Office for Planning and Programming, Iowa State University, Ames, Iowa.

Lang, R. and A. Armour. 1980. Environmental planning resource book. Lands Directorate, Environment Canada, Montreal, Canada.

Lapp, R. E. and H. L. Andrews. 1954. Nuclear radiation physics. Prentice-Hall, Englewood Cliffs, New Jersey.

LARS. 1968. Automatic classification of green vegetation, soil and water. Purdue Agricultural Experiment Station Research Progress Report 310.

LARS. 1971. Annual report. Laboratory for Agricultural Remote Sensing. Purdue University, Lafayette, Indiana.

Lee Williams, T. H. and J. Poracsky. 1979. Mapping irrigated lands from LANDSAT. *In* Satellite hydrology. Proceedings of fifth Annual William T. Pecora Memorial Symposium, Sioux Falls, S. D. AWRA, Minneapolis, Minnesota.

Lee Williams, T. H. 1977. The role of ground troth data and an approach to its collection. *In* Remote sensing of Earth resources. Vol. VI. Sixth annual Remote Sensing of Earth Resources Conference, Tullahoma, Tennessee. University of Tennessee, Tullahoma, Tennessee.

Lillesant, T. M. and R. W. Kiefer. 1979. Remote sensing and image interpretation. John Wiley and Sons, New York.

Lintz, J., Jr. and D. S. Simonett, eds. 1976. Remote sensing of environment. Addison-Wesley Publication Company, Inc., London.

MacDonald, H. C. and W. P. Waite. 1971. Soil moisture detection with imaging radars. Water Resources Research 7:100-110.

MacDonald, H. C. and W. P. Waite. 1977. LANDSAT change detection can aid in water quality monitoring. *In* Proceedings of the American Society of Photogrammetry, Little Rock, Arkansas. American Society of Photogrammetry, Falls Church, Virginia.

MacDowall, J. 1972. Simulation studies of ERTS-A & B data for hydrologic studies in the Lake Ontario basin. Annual Earth Resources Program Review, Manned Spacecraft Center, Houston, Texas 4:17-21.

Matson, M. and C. P. Berg. 1981. Satellite detection of seiches in Great Salt Lake, Utah. Water Resources Bulletin 17:122-128.

Mausel, P. W. and L. Guernsey. 1977. Machine Processing of LANDSAT multispectral data for low cost development of regional land cover information in Indiana. *In* Remote sensing of Earth resources. Vol. VI. Sixth Annual Remote Sensing of Earth Resources Conference, Tullahoma, Tennessee. University of Tennesse, Tullahoma, Tennessee.

McAdams, M. P. 1979. Quantitative analysis of LANDSAT flood mapping capabilities. *In* Satellite hydrology. Proceedings of Fifth Annual William T. Pecora Memorial Symposium, Sioux Falls, S.D. AWRA, Minneapolis, Minnesota.

McCloy, K. R., K. J. Shepherd and G. F. McIntosh. 1977. Water utilization, evapotranspiration and soil moisture monitoring in the South-East region of South Australia. NASA:N78-11447.

McGinnis, D. F., Jr., M. Matson and D. R. Wiesent. 1978. Selected hydrologic applications of LANDSAT-2 data: An evaluation. NASA:N79-32603.

McKim, H. L., T. L. Marlar and D. M. Anderson. 1972. The use of ERTS-1 imagery in the national program for the inspection of dams. Corps of Engineers, U.S. Army, Hanover, New Hampshire.

McNair, A. J., H. L. Heydt, Ta Liang and G. Levine. 1976. Engineering analysis of LANDSAT-1 data for Southeast Asian agriculture. NASA: N77-16411.

Mercanti, E. P. 1974. Widening ERTS application. Astronautics and Aeronautics 5:28-39.

Moore, G. K. 1978. Satellite surveillance of physical water-quality characteristics. U.S. Geological Survey. Sioux Falls, South Dakota.

Morain, S. A. and D. L. Williams. 1975. Wheat production estimates using satellite images. Agronomy Journal. American Society of Agronomy 67:361-364.

Morgan, K. M., G. B. Lee, R. W. Kiefer, T. C. Daniel, G. D. Bubenzer and J. T. Murdock. 1978. Prediction of soil loss on cropland with remote sensing. Journal of Soil and Water Conservation 33:291-293.

Mower, R. D. and M. L. Heinrich. 1977. A computer processed (LANDSAT) land cover map of North Dakota. *In* Remote sensing of Earth resources. Vol. VI. Sixth Annual Remote Sensing of Earth Resources Conference, Tullahoma, Tennessee. University of Tennessee, Tullahoma, Tennessee.

Mower, R. D. and G. E. Johnson. 1976. The application of LANDSAT data to regional land use problems in The Devils Lake basin, North Dakota. *In* Remote sensing of Earth resources. Vol. V. Fifth Annual Remote Sensing of Earth Resources Conference, Tullahoma, Tennessee. University of Tennessee, Tullahoma, Tennessee.

Nalepka, R. F., J. Colwell and D. P. Rice. 1977a. Wheat productivity estimates using LANDSAT data. NASA:N78-10534.

Nalepka, R. F., W. A. Malila and J. M. Gleason. 1977b. Investigations of spectral separability of small grains, early season wheat detection, and multicrop inventory planning. NASA:N78-13499.

NASA. 1979. LANDSAT data users handbook. U.S. Geological Survey, Arlington, Virginia.

Norwood, V. T. 1974. Multispectral scanner (MSS) improved resolution study. NASA Contract NAS5-21935. Hughes Aircraft Co., Culver City, California.

OWRT. 1978. Water well location by fracture trace mapping. Technology Transfer Office of Water Research and Technology, University Park, Pennsylvania.

Parada, N. J. 1977. Surface hydrodynamical models through synoptic interpretation of LANDSAT MSS images in logoonal and coastal waters. NASA:N78-31487.

Parry, J. T., W. R. Cowan and J. A. Hegenbottom. 1969. Soil studies using color photos. Photogrametric Engineering 35:44-56.

Paulson, R. W. 1978. Use of Earth satellites for automation of hydrologic data collection. U.S. Geological Survey Circular 756.

Perry, R. M., J. E. Rutledge and D. A. Morra. 1974. Remote sensing environmental and geotechnical application. Dams and Moore Engineering Bulletin 45.

Peters, L. J. 1978. Application of aerial photographic interpretation for the prediction of groundwater potential at Early, Iowa. Department of Civil Engineering, Iowa State University, Ames, Iowa.

Pettry, D. E., N. L. Powell and M. E. Newhouse. 1974. Use of remote sensing in agriculture. NASA:N74-26876.

Pluhowski, E. J. 1972. Hydrologic interpretations based on infrared imagery of Long Island, New York. Geological Survey Water-Supply Paper 2009-B.

Poracsky, J. and T. H. Lee Williams. 1979. Irrigation mapping in Western Kansas using LANDSAT. *In* Symposium proceedings of identifying irrigated lands using remote sensing techniques: State of the art, Sioux Falls, S.D. Missouri River Basin Commission, Omaha, Nebraska.

Pouquet, J. 1974. Earth sciences in the age of the satellite. D. Reidel Publication Company, Boston.

Prosser, W. J., Jr. 1980. Case histories in the use of remote sensing tools in engineering, geologic, and hydrogeologic applications. ACSM-ASP Convention, St. Louis, Missouri: American Society of Photogrammetry 46th Annual Meeting. American Society of Photogrammetry, Falls Church, Virginia.

Ragan, R. M. and V. V. Salomonson. 1978. The definition of hydrologic model parameters using remote sensing techniques. *In* Proceedings of the twelfth International Symposium on Remote Sensing of Environment, Ann Arbor, Michigan. Environmental Research Institute, Ann Arbor, Michigan.

Ragan, R. M. and R. J. Jackson. 1976. Hydrograph synthesis using LANDSAT remote sensing and the SCS models. NASA TM-X-913-76-161, Goddard Space Flight Center.

Rango, A., J. Foster and V. V. Salomonson. 1975. Extraction and utilization of space acquired physiographic data for water resources development. Water Resources Bulletin 11:1245-1255.

Reeves, C. C. 1973. Dynamics of Playa lakes in the Texas high plains. *In* Symposium on significant results obtained from ERTS-1. Vol. 1. NASA SP-327.

Rogers, R. 1979. Remotely sensed data processing techniques, present and future. *In* Symposium proceedings of identifying irrigated lands using remote sensing techniques: State of the Art, Sioux Falls, S.D. Missouri River Basin Commission, Omaha, Nebraska.

Rosenberg, N. J. 1974. Microclimate: The biological environment. John Wiley and Sons, New York.

Rudd, R. D. 1974. Remote sensing: A better view. Duxbury Press, Belmont, California.

Ruff, J. F. 1974. Clarks Fork Yellowstone River remote sensing study. Journal of Hydraulic Division, American Society of Civil Engineering 100:106-111.

Sabins, F. F., Jr. 1978. Remote sensing principles and interpretation. W. H. Freeman and Company, San Francisco, California.

Schmugge, T. J., J. M. Meneely, A. Rango and R. Neff. 1977. Satellite microwave observations of soil moisture variations. Water Resources Bulletin 13:265-281.

Schubert, J. S. and N. H. MacLeod. 1973. Digital analysis of Potomac River Basin from ERTS imagery. *In* Symposium on Significant Results Obtained from ERTS-1, Vol. 2, NASA SP-327.

Sharber, L. A. and F. Shahrokhi. 1977. The application of satellite data in monitoring strip mines. *In* Remote sensing of Earth resources. Vol. VI. Sixth annual Remote Sensing of Earth Resources Conference, Tullahoma, Tennessee. University of Tennessee, Tullahoma, Tennessee.

Shepherd, W. G. 1978. A study of Minnesota land and water resources using remote sensing. NASA:N78-26513.

Shih, S. F. and J. C. Gervin. 1980. Ridge regression techniques applied to LANDSAT investigation of water quality in Lake Okeechobee. Water Resources Bulletin 16:790-796.

Short, N. M. 1973. Mineral resources, geological structures and land form surveys. Third Earth Resources Technology Satellite Symposium. Vol. III, NASA.

Short, N. M., P. D. Lowman, Jr., S. C. Feden and W. A. Finch, Jr. 1976. Mission to earth: Landsat views earth. NASA, SP-360.

Shuchman, R., P. Jackson, F. Ruskey and H. Wagner. 1976. Geological reconnaisance of an oil shale region by remote sensing techniques. *In* Remote sensing of Earth resources. Vol. V. Fifth annual Remote Sensing of Earth Resources Conference, Tullahoma, Tennessee. University of Tennessee, Tullahoma, Tennessee.

Siegal, B. S. and A. R. Gillespie. 1980. Remote sensing in geology. John Wiley and Sons, New York.

Slack, R. B. and R. Welch. 1980. Soil conservation service runoff curve number estimates from LANDSAT data. Water Resources Bulletin 16: 887-893.

Smith, R. F. 1981. Extending the range of optical systems photographically. American Laboratory 1981:47-50.

Soil Conservation Service. 1972. National engineering handbook section 4: Hydrology. SCS-USDA, Washington, D.C.

Stow, D. A. and J. E. Estes. 1981. LANDSAT and digital terrain data for country-level resources management. Photogrammetric Engineering and Remote Sensing. American Society of Photogrammetry 47:215-222.

Swain, P. H. and S. M. Davis, eds. 1978. Remote sensing: The quantitative approach. McGraw-Hill, Inc., New York.

Taranik, J. V. and J. R. Lucas. 1979. LANDSAT multispectral data system characteristics. *In* Satellite hydrology, proceedings of fifth annual William T. Pecora Symposium. Sioux Falls, S. D. AWRA, Minneapolis, Minnesota.

Thamann, R. R. 1974. Remote sensing of agricultural resources. *In* J. E. Estes and L. W. Senger (eds.) Remote sensing techniques for environmental analysis. Hamilton Publication Co., Reno, Nevada.

Theis, J. B. 1977. An all-purpose change-detection and recording system. *In* Remote sensing of Earth resources. Vol. VI. Sixth annual Remote Sensing of Earth Resources Conference, Tullahoma, Tennessee. University of Tennessee, Tullahoma, Tennessee.

United Stated Department of Agriculture - Soil Conservation Service. 1959. Soil survey: Monona County, Iowa. United States Department of Agriculture, Washington, D. C.

Valley, S. L., ed. 1965. Handbook of geophysics and space environment. Cambridge Research Laboratory, Bedford, Mass.

Vickers, R. S. and A. J. Blanchard. 1973. Rapid measurements of soil moisture and water table depth by a monocycle radar. Department of Electrical Engineering, Colorado State University, Fort Collins, CO.

Wehde, M. E., K. J. Dalsted and B. K. Worcester. 1980. Resource applications of computerized data processing: The AREAS example. J. Soil and Water Cons. 35:36-40.

Weismiller, R. A. and S. A. Kaminsky. 1978. Application of remote sensing technology to soil survey research. J. Soil and Water Cons. 33:287-289.

Weismiller, R. A., I. D. Persinger and O. L. Montgomery. 1977. Soil inventory prepared from digital analysis of satellite multispectral scanner data and digitized topographic data. Soil Science Society of America Journal 4:1116-1170.

Westin, F. C. 1973. ERTS-1 imagery: A tool for identifying soil associations. *In* Proceedings Earth Survey Problems through the Use of Space Techniques. General Assembly, Committee on Space Research, Ronstang, W. Germany.

Westin, F. C. and C. J. Frazee. 1976. LANDSAT data, its use in a soil survey program. Soil Science Society of America Journal 40:81-89.

Whiting, J. M. 1979. Determination of groundwater inflow to prairie lakes using remote sensing. Saskatchewan Research Council, Saskatoon, Saskatchewan, Canada.

Wiesnet, D. R., D. F. McGinnis and M. Matson. 1977. Evaluation of LANDSAT-2 data for selected hydrologic application. NASA:N77-16404.

Williams, A. R. and R. P. C. Morgan. 1976. Geomorphological mapping applied to soil erosion evaluation. J. Soil and Water Cons. 31:164-167.

Wilson, J. R., Jr., C. Blackman and G. W. Spann. 1976. Land use change detection using LANDSAT data. *In* Remote sensing of Earth resources. Vol. V. Fifth annual Remote Sensing of Earth Resources Conference, Tullahoma, Tennessee. University of Tennessee, Tullahoma, Tennessee.

ACKNOWLEDGEMENTS

Deepest appreciation is extended to my major professor, Dr. T. Al Austin, whose guidance, knowledge, and friendship, as well as the fine example he has set, will always mean a great deal to me. Thanks also go to the members of my committee, Drs. R. W. Buchmann, C. E. Beer, H. P. Johnson, and R. A. Lohnes, for their interest in this project.

I am grateful for the data supplied by James F. Wiegand of the Iowa Natural Resources Council, and by T. W. Lowe, of the Missouri River Basin Commission. Those data were necessary for the completion of this project.

I also wish to thank Mrs. Donna Gladon for her care in typing this manuscript.

A special thank you goes to my wife, Olya, for her patience, understanding, and support during the course of this endeavor.

At this point, I would like to commemorate the late Dr. Merwin D. Dougal, who had been a member of my graduate committee. The example of excellence in his work and his great contributions to the area of water resources will long be remembered.

APPENDIX A.

DENSITY VALUES OF LANDSAT IMAGES:

VISUAL MEASUREMENT

Table I-A. Density values of LANDSAT images: Visual measurement. August 8, 1975 image

Grid[a] number	Shade[b]							Grid[c] density
	B20	D16	MG10	G8	LG6	VLG4	WO	
	Percent							
A1				50	50			7
2				50	50			7
3				60	40			7.2
4			40	30	30			8.2
5			50	30	20			8.6
6				50	50			7
B1			50	30	20			8.6
2			40	30	30			8.2
3				50	50			7
4				50	50			7
5			20	40	40			7.6
6				50	50			7
C1			70	20	10			9.2
2				50	50			7
3				50	50			7
4			20	40	40			7.6
5				50	50			7
6				50	50			7
D1			40	30	30			8.2
2			30	40	30			8
3				50	50			7
4				50	50			7
5				50	50			7
6				50	50			7
E1			60	20	20			8.8
2			30	40	30			8
3			40	30	30			6.2
4				50	50			7
5				50	50			7
6				50	50			7

[a]See Figure 26.

[b]See Table 11.

[c]Sum of the product of density value of a given shade and the percentage of that shade within the grid, e.g., for grid number E1, the grid density is calculated as follows: 10*0.60+8*0.20+6*0.20 = 8.8.

Table I-A. *Continued*

Grid[a] number	Shade[b]							Grid[c] density
	B20	D16	MG10	G8	LG6	VLG4	WO	
	Percent							
F1			40	30	30			8.2
2				50	50			7
3				50	50			7
4				50	50			7
5				50	50			7
6				50	50			7
							Total	266.6
							Mean	7.4

Table II-A. Density values of LANDSAT images: Visual measurement. July 30, 1975 image

Grid number	Shade							Grid density
	B20	D16	MG10	G8	LG6	VLG4	WO	
	Percent							
A1			40	30	30			8.2
2			60	20	20			8.8
3			70	20	10			9.2
4			60	40				9.2
5			40	60				8.8
6			20	80				8.4
B1			70	30				9.4
2			30	30	40			7.8
3			30	40	30			8.0
4			30	70				8.6
5			30	70				8.6
6			60	40				8.2
C1			20	30	50			7.4
2			10	30	60			7.0
3			10	30	60			7.0
4			10	30	60			7.0
5			10		40	50		3.6
6			10		40	50		3.6
D1				50	50			7.0
2				50	50			7.0
3			50	50				4.0
4			20	40	40			7.6
5				50	50			7.0
6				40	60			6.8
E1			40	40	20			8.4
2			30	40	30			8.0
3			20	80				8.4
4			20	80				8.4
5			10	50	40			7.4
6			20	70	10			8.2

Table II-A. *Continued*

Grid number	Shade							Grid density
	B20	D16	MG10	G8	LG6	VLG4	WO	
	Percent							
F1			30	40		30		7.4
2				50	50			7.0
3				50	50			7.0
4				50	50			7.0
5				50	50			7.0
6				50	50			7.0
							Total	272.4
							Mean	7.6

Table III-A. Density values of LANDSAT images: visual measurement. August 14, 1972 image

Grid number	Shade							Grid density
	B20	D16	MG10	G8	LG6	VLG4	WO	
	Percent							
A1			30	70				8.6
2			30	70				8.6
3			40	50		10		8.4
4			40	60				8.8
5			30	70				8.6
6			10	90				8.2
B1			50	50				9.0
2			30	70				8.6
3			40	50		10		8.4
4			10	90				8.2
5			10	90				8.2
6			10	90			8.2	
C1			40	60				8.8
2			10	90			8.2	
3		10		90				8.8
4		20	20	60				10.0
5			10	80				8.4
6				100				8.0
D1				100				8.0
2				100				8.0
3		20		80				9.6
4		20		80				9.6
5				100				8.0
6				100				8.0
E1		20		50		30		8.4
2		20		80				9.6
3		10		90				8.8
4			20	80				8.4
5				100				8.0
6				100				8.0

Table III-A. *Continued*

Grid number	Shade							Grid density
	B20	D16	MG10	G8	LG6	VLG4	WO	
	Percent							
F1		20	30	50				10.2
2				100				8.0
3				100				8.0
4				100				8.0
5				100				8.0
6				100				8.0
							Total	288.4
							Mean	8.0

Table IV-A. Density values of LANDSAT images: visual measurement. July 16, 1977 image

Grid number	Shade							Grid density
	B20	D16	MG10	G8	LG6	VLG4	WO	
	Percent							
A1		20	40	20	20			10.0
2		10	80	10				10.6
3		30	60	10				11.6
4		30	60	10				11.6
5			30	40	30			8.0
6			10	40	50			9.2
B1		10	70	10	10			10.0
2		10	30	40	10	10		8.8
3		20	50	30				10.6
4		20	20	50			10	9.2
5			40	50	10			8.6
6		10	80			10		10.0
C1			80	20				9.6
2			40	60				8.8
3		10	50	30		10		9.4
4			50	50				9.0
5			40	40		20		8.0
6			50	50				9.0
D1			30	50		20		7.8
2			50	50				9.0
3			30	50	10		10	7.6
4		10	30	40	20			9.0
5			40	40	20			8.4
6			40	40	20			8.4
E1		20	40	20			20	8.8
2			40	50	10			8.6
3			30	70				8.6
4			20	80				8.4
5			20	80				8.4
6			60	40				9.2

Table IV-A. *Continued*

Grid number	Shape							Grid density
	B20	D16	MG10	G8	LG6	VLG4	WO	
	Percent							
F1		50	40	10				12.8
2		40	30	20	10			11.0
3			40	60				8.8
4			40	60				8.8
5				50	50			9.0
6			50	50				9.0
						Total		333.6
						Mean		9.3

Table V-A. Density values of LANDSAT images: visual measurement. August 21, 1977 image

Grid number	Shape							Grid density
	B20	D16	MG10	G8	LG6	VLG4	WO	
	Percent							
A1			90	10				9.8
2			80	20				9.6
3		10	80	10				10.4
4		10	80	10				10.4
5			70		20	10		8.6
6			40	40	20			8.4
B1			70		20	10		8.6
1			60	40				9.2
3		30	60	10				11.6
4		20	70	10				11.0
5		30	60		10			11.4
6			90	10				9.8
C1			80	10	10			7.4
2			70	20	10			9.2
3		20	60			20		10.0
4		30	40		30			10.6
5		10	40	40	10			9.4
6		10	40	40	10			9.4
D1				90	10			7.8
2			40	50	10			8.6
3		30	50	20				11.4
4		40	40	20				10.4
5			30	50	20			8.4
6			40	50	10			8.6
E1		40	60					12.4
2		40	50		10			12.0
3		20	50		30			10.0
4			40	40	20			8.4
5		20	60	20				10.8
6			90	10				9.8

Table V-A. *Continued*

Grid number	Shape							Grid density
	B20	D16	MG10	G8	LG6	VLG4	WO	
	Percent							
F1		70	30					14.2
2			50	50				9.0
3			30	70				8.6
4			50	50				9.0
5			50	50				9.0
6			60	40				9.2
							Total	354.4
							Mean	9.8

Table VI-A. Density values of LANDSAT images: visual measurement. June 24, 1980 image

Grid number	Shape							Grid density
	B20	D16	MG10	G8	LG6	VLG4	WO	
	Percent							
A1		60		25			15	12.8
2		25		40			35	7.2
3		20	70				10	10.2
4		20	75			5		19.0
5	5	20	25	30	5	5	10	9.6
6			30	60		10		8.2
B1		75		15			10	13.2
2			80	15			5	9.2
3		20	75			5		10.9
4		20	60			20		10.0
5	5	15	70			10		10.8
6		80				20		13.6
C1		20	60			20		10.0
2		30	60			10		11.2
3		35	55		5	5		11.6
4	5	15	75			5		11.1
5		40	50		5	5		11.9
6		10	80		10			10.2
D1		10	75		10	5		9.9
2	5	10	75		10			10.7
3	20	10	50		20			11.8
4		80	10		10			15.0
4		20	70				10	10.2
6		10	85				5	10.1
E1	10	40	40		10			13.0
2	20	20	50		5	5		12.7
3	30	30	10		20	5	5	13.2
4		40	50			10		11.8
5	20	10	20	50				11.6
6		10	80			10		10.0

Table VI-A. *Continued*

Grid number	Shape							Grid density
	B20	D16	MG10	G8	LG6	VLG4	WO	
	Percent							
F1	70	20		10				18.0
2	20	60	10		5		5	16.1
3		20	50	20		5	5	10.0
4				70		10	20	6.0
5			40	30		30		7.6
6		20	70	10				11.0
						Total		413.1
						Mean		11.5

APPENDIX B.

RECORDED RELATIVE REFLECTIVITY

Table I-B. Recorded relative reflectivity from east to west scanning by microdensitometer. August 20, 1976 image

Distance on the chart record (mm)	Measured reflectivity (%)	Distance on the chart record (mm)	Measured reflectivity (%)
2	70	72	50
4	50	74	30
6	35	76	35
8	40	78	30
10	60	80	30
12	60	82	50
14	50	84	75
16	40	86	75
18	40	88	65
20	40	90	40
22	30	92	50
24	50	94	70
26	45	96	40
28	50	98	85
30	40	100	80
32	50	102	55
34	75	104	100
36	30	106	90
38	40	108	60
40	30	110	70
42	40	112	90
44	30	114	75
46	45	116	60
48	50	118	75
50	35	120	80
52	50	122	55
54	40	124	50
56	45	126	75
58	35	128	55
60	45	130	55
62	30	132	70
64	35	134	45
66	35	136	60
68	20	138	45
70	35	140	85
		Mean	52

Table II-B. Recorded relative reflectivity from east to west scanning by microdensitometer. June 29, 1974 image

Distance on the chart record (mm)	Measured reflectivity (%)	Distance on the chart record (mm)	Measured reflectivity (%)
2	60	72	55
4	55	74	55
6	50	76	35
8	65	78	35
10	65	80	55
12	75	82	30
14	50	84	25
16	45	86	25
18	45	88	45
20	50	90	50
22	65	92	55
24	75	94	55
26	75	96	35
28	70	98	80
30	55	100	75
32	40	102	70
34	45	104	65
36	30	106	50
38	35	108	35
40	40	110	35
42	40	112	35
44	40	114	50
36	30	116	60
48	30	118	40
50	30	120	40
52	60	122	50
54	60	124	60
56	60	126	60
58	45	128	40
60	60	130	45
62	60	132	50
64	45	134	50
66	45	136	50
68	60	138	50
70	65	140	50
		Mean	50

Table III-B. Recorded relative reflectivity from east to west scanning by microdensitometer. September 1975 image

Distance on the chart record (mm)	Measured reflectivity (%)	Distance on the chart record (mm)	Measured reflectivity (%)
2	75	72	40
4	65	74	35
6	55	76	55
8	40	78	60
10	60	80	35
12	35	82	35
14	50	84	35
16	45	86	30
18	40	88	30
20	35	90	40
22	55	92	55
24	65	94	30
26	60	96	30
28	60	98	35
30	50	100	40
32	40	102	40
34	45	104	50
36	55	106	35
38	65	108	35
40	70	110	50
42	45	112	50
44	40	114	50
46	40	116	35
48	40	118	50
50	50	120	65
52	45	122	55
54	50	124	55
56	30	126	55
58	30	128	35
60	30	130	35
62	45	132	40
64	45	134	60
66	40	136	45
68	40	138	40
70	40	140	50
		Mean	45

Table IV-B. Recorded relative reflectivity from east to west scanning by microdensitometer. September 28, 1979 image

Distance on the chart record (mm)	Measured reflectivity (%)	Distance on the chart record (mm)	Measured reflectivity (%)
2	35	72	40
4	40	74	40
6	40	76	40
8	40	78	30
10	35	80	35
12	30	82	40
14	50	84	50
16	45	86	45
18	35	88	35
20	35	90	35
22	35	92	35
24	30	94	40
26	35	96	40
28	35	98	40
30	40	100	35
32	35	102	35
34	35	104	40
36	40	106	40
38	35	108	40
40	30	110	35
42	40	112	40
44	45	114	60
46	40	116	55
48	55	118	45
50	35	120	45
52	35	122	45
54	40	124	40
56	40	126	25
58	50	128	30
60	35	130	25
62	35	132	30
64	35	134	40
66	35	136	40
68	50	138	30
70	45	140	25
		Mean	39

Table V-B. Recorded relative reflectivity from east to west scanning by microdensitometer. June 8, 1978 image

Distance on the chart record (mm)	Measured reflectivity (%)	Distance on the chart record (mm)	Measured reflectivity (%)
2	30	72	25
4	40	74	25
6	55	76	20
8	55	78	25
10	55	80	35
12	60	82	15
14	55	84	15
16	55	86	20
18	55	88	25
20	50	90	40
22	25	92	35
24	40	94	25
26	50	96	15
28	30	98	15
30	35	100	15
32	35	102	15
34	40	104	15
36	35	106	25
38	25	108	35
40	35	110	35
42	30	112	30
44	25	114	25
46	45	116	40
48	25	118	15
50	45	120	20
52	55	122	20
54	55	124	20
56	80	126	20
58	20	128	20
60	25	130	20
62	40	132	20
64	30	134	25
66	20	136	70
68	25	138	50
70	25	140	25
		Mean	33

Table VI-B. Recorded inverse relative reflectivity from north to south scanning (reading every 2 millimeter on chart record). June 8, 1978 image

1	2	3	4	5	6	7	8	9	10
100	55	80	45	75	25	70	55	60	45
100	60	100	55	30	55	100	100	100	100
40	90	85	90	25	25	95	100	80	100
35	95	70	95	30	90	100	100	100	100
25	90	55	40	80	100	100	50	100	60
30	65	90	50	65	100	100	90	90	60
45	50	100	75	60	100	95	65	100	75
30	75	80	70	55	75	90	100	85	50
45	80	60	100	40	80	100	100	50	100
30	85	45	60	25	100	100	90	100	40
30	70	65	30	55	80	70	80	100	70
65	100	80	55	100	95	65	100	55	50
25	70	70	55	60	85	80	100	100	100
65	70	80	50	85	75	80	100	50	50
25	95	35	45	95	100	100	70	100	45
65	55	70	30	35	90	100	100	70	100
100	50	100	65	100	85	70	85	100	50
100	55	75	90	80	100	100	95	100	60
100	45	95	60	100	90	100	55	95	40
100	85	70	80	100	85	90	75	100	60
45	60	100	100	60	100	60	55	100	90
50	50	100	100	100	100	100	45	50	50
35	55	30	35	100	80	85	100	65	50
50	60	35	95	80	100	60	80	75	85

Table VII-B. Recorded inverse relative reflectivity from north to south scanning (reading every 2 millimeters on chart record). August 20, 1976 image

1	2	3	4	5	6	7	8	9	10
80	75	40	45	55	35	30	55	30	50
50	65	50	50	30	35	35	55	45	70
55	65	70	30	55	25	45	60	50	40
60	45	30	35	45	60	25	70	35	85
70	30	50	40	35	45	40	50	50	80
60	35	50	40	55	65	25	35	40	55
50	65	90	40	40	30	40	40	45	100
35	50	50	35	45	35	35	60	35	90
40	95	50	35	25	45	30	60	45	60
35	85	30	40	60	50	40	50	30	70
30	60	30	50	30	70	45	40	35	90
35	50	30	35	60	60	40	40	35	75
50	85	30	55	55	60	45	40	20	60
45	55	35	70	50	30	25	30	35	75
50	75	35	55	50	40	45	50	50	80
60	50	45	45	45	40	35	45	30	55
65	60	60	40	45	40	45	50	35	50
55	85	30	35	45	45	40	40	30	75
100	50	30	35	45	40	30	50	30	55
35	45	50	45	50	55	30	75	50	55
75	80	30	50	35	35	35	30	75	70
65	40	30	40	55	35	45	40	75	45
70	50	30	30	60	40	25	30	65	60
45	60	35	50	30	35	25	40	40	45

APPENDIX C.

CROP INFORMATION

Table I-C. Crop information for eight townships in the floodplain area of Monona County

Township	Twshp. code	No. of farms	Farmland (ha)	Average farm size (ha)	Total cropland (ha)	Ratio of land (%) Cropland	Other	Corn (ha)	Soybeans (ha)	Farm unit corn + soybeans
					1973					
Ashton	1	51	9233	181	7850	85	15	4426	3274	
Fairview	5	33	6151	187	5135	83.5	16.5	2585	2172	
Franklin	6	62	10602	171	9299	87.7	12.3	5226	3792	
Lake	10	44	6108	139	5260	86.1	13.9	2654	2285	
Lincoln	11	58	10516	181	8325	79.2	20.8	4897	2956	
Sherman	14	49	11364	232	9530	83.9	16.1	5303	3725	
West Fork	18	39	12061	309	10646	88.3	11.7	7372	3109	
MONONA	133	982	163139	166	110051	67.5	32.5	69003	31200	
					1975					
Ashton	1	41	8185	200	7402	90.4	9.6	4229	2823	
Fairview	5	27	4523	168	4015	88.8	11.2	1881	1741	
Franklin	6	62	11450	185	10479	91.5	8.5	5664	4333	
Lake	10	41	6250	153	5823	93.2	6.8	3162	2381	
Lincoln	11	55	8948	163	7250	81	19	4340	2586	
Sherman	14	46	11213	244	10113	90	10	5304	3984	
West Fork	18	36	11477	319	10624	92.6	7.4	6963	2990	
Onawa	22	6	1036	173	917	88.6	12.4	469	399	
MONONA	133	890	156020	175	11824	71.7	28.2	69379	30627	

Table I-C. *Continued*

Township	Twshp. code	No. of farms	Farmland (ha)	Average farm size (ha)	Total cropland (ha)	Ratio of land (%) Cropland	Ratio of land (%) Other	Corn (ha)	Soybeans (ha)	Farm unit: corn + soybeans
					1976					
Ashton	1	42	8246	196	7634	92.6	7.4	4384	2875	39 + 36
Fairview	5	26	5300	204	4820	90.9	8.1	2445	1759	26 + 25
Franklin	6	58	9627	166	9099	94.5	5.5	4840	3601	58 + 54
Lake	10	37	5484	148	5063	92.3	6.7	2939	1845	37 + 33
Lincoln	11	50	8780	176	7296	83.1	16.9	4363	2466	49 + 47
Sherman	14	44	9668	220	8920	92.7	7.7	4348	3607	43 + 39
West Fork	18	37	11723	317	10668	91	9	7230	2892	37 + 31
Onawa	22	5	1068	214	1015	95.1	4.9	667	292	5 + 4
MONONA	133	800	143987	180	107562	74.7	25.3	67072	27416	779 + 566
					1977					
Ashton	1	36	7712	214	7208	93.5	6.5	3853	2981	34 + 35
Fairview	5	25	5166	207	4724	91.4	8.6	2258	1878	25 + 24
Franklin	6	50	9382	188	8781	93.6	6.4	4805	3289	50 + 48
Lake	10	38	5579	147	5241	93.9	6.1	2804	2203	38 + 35
Lincoln	11	49	8698	178	7148	82.2	17.8	4053	2538	48 + 43
Sherman	14	42	10072	240	9306	92.4	7.6	4504	3842	41 + 39
West Fork	18	41	12227	298	10790	88.3	11.7	6724	3617	41 + 38
Onawa	22	5	1115	223	1083	97.1	2.9	654	395	5 + 5
MONONA	133	790	145542	184	107546	73.9	26.1	64592	30383	767 + 575

Table I-C. *Continued*

Township	Twshp. code	No. of farms	Farmland (ha)	Average farm size (ha)	Total cropland (ha)	Ratio of land (%) Cropland	Other	Corn (ha)	Soybeans (ha)	Farm unit: corn + soybeans
					1978					
Ashton	1	34	7219	212	6555	90.8	9.2	3272	3104	32 + 33
Fairview	5	25	4765	191	4305	90.3	9.7	2115	2106	25 + 25
Franklin	6	53	10513	198	9162	87.2	12.8	5013	3898	53 + 52
Lake	10	40	6637	166	6099	91.9	8.1	3302	2298	39 + 36
Lincoln	11	51	8740	171	7368	84.3	15.7	4426	2819	48 + 46
Sherman	14	42	9645	129	8349	86.6	13.4	4088	4003	41 + 39
West Fork	18	41	11410	278	10541	92.4	7.6	6329	4168	41 + 39
Onawa	22	4	905	226	855	94.5	5.5	444	391	4 + 3
MONONA	133	787	144627	184	102898	71.1	28.9	62469	32877	761 + 574
					1979					
Ashton	1	36	7774	216	7163	92.1	7.9	3707	3338	34 + 35
Fairview	5	24	5101	212	4805	94.2	5.8	2232	2444	23 + 24
Franklin	6	50	10328	206	9510	92.1	7.9	5023	4169	50 + 49
Lake	10	44	2816	178	7453	95.4	4.6	3915	3106	42 + 40
Lincoln	11	47	8088	172	6923	85.6	14.4	3773	3038	44 + 43
Sherman	14	43	9636	224	8591	89.2	10.8	4122	4036	42 + 41
West Fork	18	42	12124	289	11181	92.2	7.8	6625	4504	41 + 39
Onawa	22	3	448	149	270	60.3	39.7	187	48	3 + 2
MONONA	133	757	142765	189	105052	73.6	26.4	62950	34706	726 + 552

Table II-C. Area of different crop in Harrison and Monona Counties for the years 1972 to 1980 in hectares (Iowa Department of Agriculture)

Year	Corn		Soybeans		Hay and alfalfa		Wheat, oats, sorghum	
	Monona	Harrison	Monona	Harrison	Monona	Harrison	Monona	Harrison
1972	62450	60790	23960	21930	--[a]	--	--	--
1973	69370	70500	32250	30230	7930	10930	6350	6760
1974	75310	76200	32050	30390	8460	11010	6600	8780
1975	70660	69000	31610	32900	--	--	--	--
1976	73610	73130	29870	30310	7890	10360	9550	12550
1977	69930	71270	34360	33750	8420	10970	10440	13440
1978	64350	67990	36020	38850	7970	11130	6720	8700
1979	68390	70420	39260	44680	7610	11660	5870	7330
1980	74460	71230	40590	44360	7410	11940	6190	7080

[a]Data not available.